ELUCIDATING THE CELLULAR INJURY MECHANISMS IN A SPINAL MODEL OF NEUROMYELITIS OPTICA

Büşra Selin Kenet

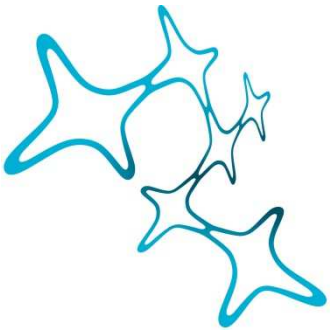

Graduate School of
Systemic Neurosciences
LMU Munich

Dissertation at the
Graduate School of Systemic Neurosciences
Ludwig-Maximilians-Universität München

May 2021

Supervisor
Prof. Thomas Misgeld
Institute of Neuronal Cell Biology
Technical University of Munich

First Reviewer: Prof. Thomas Misgeld
Second Reviewer: Dr. Florence Bareyre
External Reviewer: Prof. Bruno Weber

Date of Submission: 10 May 2021
Date of Defense: 2 December 2021

Table of Contents

List of Abbreviations

A1	Neurotoxic astrocyte
A2	Neuroprotective astrocyte
aCSF	Artifical cerebrospinal fluid
ADCC	Antibody-dependent cellular cytotoxicity
Aldh1L1	Aldehyde dehydrogenase 1 family member L1
AQP	Aquaporin
ATP	Adenosine triphosphate
BBB	Blood brain barrier
C1q	Complement component 1q
C3a, C5a	Anaphylatoxins
C3b, C4b	Opsonins
Ca^{2+}	Calcium ions
CAG	CMV immediate early enhancer and chicken beta actin
CD46	Membrane cofactor protein
CD55	Complement decay-accelerating factor
CDC	Complement-dependent cellular toxicity
CFP	Cyan fluorescent protein
CFS	Cerebrospinal fluid
CNS	Central nervous system
Cre	Cre recombinase
Cx	Connexin
DMSO	Dimethylsulfoxide
EAAT2	Excitatory amino acid transporter 2
EAE	Experimental autoimmune encephalomyelitis
EM	Electron microscopy
EpoB	Epothilone B
EtHD	Ethidium homodimer
FAD	Focal axonal degeneration
Fc	Fragment crystallizable region
FRET	Förster resonance energy transfer
GaAsP	Gallium arsenide phosphide
GECI	Genetically encoded Ca^{2+} indicator
GFAP	Glial fibrillary acidic protein
GFP	Green fluorescent protein
h	Hour
hCD59	Human CD59, MAC inhibitor protein
HE	Heterozygous
HO	Homozygous
i.p.	Intraperitoneal
IgG, IgM	Immunoglobulin G, M
IRES	Internal ribosome entry site
M1	AQP4 long isoform

M23	AQP4 short isoform
MAC	Membrane attack complex, C5b-C9
MAG	Myelin associated glycoprotein
MBP	Myelin basic protein
MMF	Medetomidine-midazolam-fentanyl
MOG	Myelin oligodendrocyte glycoprotein
MOGAD	MOG antibody-associated disorder
MS	Multiple sclerosis
NA	Numerical aperture
Na^+	Sodium ions
NMO	Neuromyelitis optica
NMOSD	Neuromyelitis optica spectrum disorders
OAP	Orthogonal array of particles
PEG	Polyethylene glycol
PFA	Paraformaldehyde
PLP	Proteolipid protein 1
ROS	Reactive oxygen species
s.c.	Subcutaneous
SARM	Sterile Alpha and TIR Motif
SEM	Standard error of the mean
Thy1	Thymus cell antigen 1
TTX	Tetrodotoxin
µm	Micrometer
WT	Wildtype
YFP	Yellow fluorescent protein

Abstract

Neuromyelitis optica spectrum disorder (NMOSD) is an neuroinflammatory disease of the central nervous system (CNS), causing demyelinating lesions characterized in the optic nerve, spinal cord and brain stem that result in severe disability presents with paralysis or blindness. Astrocytes are the primary target of autoimmune response in the majority of NMOSD patients, and they undergo complement-dependent lysis mediated by aquaporin-4 specific antibodies (AQP4-IgG) that are present in the serum and cerebrospinal fluid. In addition, subset of AQP4-IgG seronegative patients have antibodies against the myelin oligodendrocyte glycoprotein (MOG-IgG), rendering a direct injury on CNS myelin. Although the initial glial attack primarily starts in the astrocytic endfeet in AQP4-positive NMO, there is a rapid spread of cellular pathology described with the damage of surrounding cells, including the neurons and oligodendrocytes. Even though initial cellular targets of the disease and the immunopathological features of NMOSD lesions are well defined, mechanisms underlying secondary injury following the initial antibody-attack remain elusive.

In order to elucidate possible injury mechanisms that drive NMO-related pathology in axons and oligodendrocytes, I utilized in vivo imaging to follow the induction phase of experimental lesions in a mouse model of AQP4-IgG mediated NMO. By the help of time-lapse imaging experiments performed with genetic and pharmacological interventions, I could define the instant changes in morphological characteristics and intracellular calcium dynamics of the glial cells – astrocytes, oligodendrocytes - and axons. Our findings implicated that AQP4-IgG mediated astrocyte lysis leads to acute axonal beading that is driven by cytoskeletal disruptions, particularly in thin caliber axons; and cellular mechanism underlying formation of such beadings is distinct from axon injury pathways previously described in MS- or trauma-related models. With the survival surgery approach that I developed to study the fate of beaded axons on the following day of NMO lesion induction, I could also demonstrate that axonal beading state was persistent for a certain period without displaying apparent signs of neurodegeneration. Additionally, a rapid antibody-independent membrane attack complex (MAC)-mediated oligodendrocyte injury develops consequently to AQP4-IgG mediated astrocyte loss, implicating the contribution of complement related off-target effects in the spread of NMO pathology.

Overall, the data presented in my thesis improves the current understanding on the time course of cellular events involved in the NMO lesion induction, as well as mechanisms of injury that mediates NMO-related pathology spread from astrocytes to other CNS cells. Notably, our findings provided candidates for acute therapeutic treatments that can help with diminishing development of permanent neurological deficits.

1 Introduction

1.1 Astrocytes in health & disease

Astrocytes are the most abundant glial cell type, comprising ~30% of the cells in CNS (Liddelow and Barres, 2017). Astrocytes were initially considered as archetypical glia ('brain glue') and hence 'passive' counterparts of neurons that provide only structural support. However, over the last decades there have been advances in understanding the role of astrocytes in development and function of the nervous system (Sofroniew and Vinters, 2010; Allen and Lyons, 2018), as well as their contribution to the initiation, progression and resolution of different pathological conditions (Sofroniew, 2015; Linnerbauer et al., 2020; Han et al., 2021).

Astrocytes comprise of a heterogeneous glial cell population concerning morphology, gene expression profile and physiological characteristics – which depend amongst other factors on anatomical location, developmental stage and 'activation' status in response to the local micro-milieu. The fine 'star'-like processes, which gave astrocytes their name result in a complex cellular morphology that enables interaction with blood vessels, neurons and other glial cells in the CNS. Such interactions allow astrocytes to play a wide variety of roles in molecular, cellular and structural support (Sofroniew and Vinters, 2010; Verkhratsky et al., 2012).

Astrocytic end-feet form the glia limitans, which sheaths the perivascular spaces and lies directly below the pia mater (Liu et al., 2013). These end-feet contribute to neurovascular coupling where astrocytes are involved in regulating activity-dependent adjustments in local blood flow (Attwell et al., 2010). The glia limitans also helps maintaining the blood-brain barrier (BBB), which shields the CNS parenchyma from invasion of peripheral immune cells, as well as from non-selective influx of soluble factors, such as serum-derived proteins (Abbott et al., 2006; Daneman and Prat, 2015). Following pathological insults that induce astrocyte dysfunction or loss, such as trauma, ischemia or neuroinflammation, the integrity of the glia limitans can be compromised. The resulting immune cell recruitment and immune signaling in the CNS can then further aggravate the pathology, but might also contribute to repair processes (Sofroniew, 2015).

Indeed, during development, astrocytes play essential tropic roles for neurons. For instance, astrocytes are required for neuronal survival and migration (Lemke, 2001), they promote formation of functional synapses via release of factors such as thrombospondin or cholesterol, and together with microglia contribute to synapse pruning, using engulfment receptors such as

the mammalian Draper homologue (Stevens et al., 2007; Chung et al., 2015). Once synapses are mature, astrocytes are involved in neurotransmitter biosynthesis and turnover, and regulate the homeostasis of the CNS extracellular milieu (e.g. by buffering ions such as potassium that accumulate extracellularly during neuronal firing, regulating water and pH balance) (Verkhratsky and Nedergaard, 2018). Astrocytes maintain a local energy store via glycogen granules and can provide metabolic support to neurons via delivery of the energy substrate, lactate (Magistretti and Allaman, 2018; Verkhratsky and Nedergaard, 2018). In addition, astrocytes are embedded in various further metabolic task-sharing and detoxification networks with neurons, e.g. for glutamate or lipid substrates (Rosenberg and Aizenman, 1989; Anderson and Swanson, 2000).

Beyond links via the extracellular milieu, astrocytes are also cytoplasmically coupled amongst themselves and with other glial cells. Astrocytes express connexin (Cx) proteins, which form gap junctions with neighboring astrocytes and oligodendrocytes. Such glial coupling enables long distance intercellular signaling, exchange of ions (e.g. during propagation of astrocytic calcium waves or potassium buffering of astrocytes), metabolites and neurotransmitters (e.g. glutamate, ATP, D-serine) (Giaume et al., 2013). This glial gap junction coupling obtains specificity by cell-type specific expression of hemichannel subtypes, such as Cx30/43 in astrocytes and Cx32/47 in oligodendrocytes (Orthmann-Murphy et al., 2007).

This broad set of roles of astrocytes and the cellular networks, in which they are embedded, already implies possible contributions of this cell type in a wide variety of disease processes. Indeed, astrocytes actively responds to injury or disease via a process called ‘reactive astrogliosis’ (Pekny and Pekna, 2014). Astrogliosis can involve proliferative or non-proliferative states and involves structural and molecular changes that result in gain or loss of certain astrocytic functions (Sofroniew, 2020). Such changes can result in BBB permeability, metabolic stress and synaptic dysfunction that can contribute to a wide variety of neurological diseases, ranging from trauma, neuroinflammation or neurodegeneration (Phatnani and Maniatis, 2015; Pekny et al., 2016). Importantly, however, astrogliosis does not necessarily have only detrimental effects on neuronal survival and function. Indeed, the net impact of astrocytic changes on disease outcome likely depends on timing and the overall cellular context of a given CNS pathology (Rothhammer and Quintana, 2015; Sofroniew, 2015). One concept that has been put forward is the polarization of reactive astrocytes into more neurotoxic (‘A1’) and neuroprotective (‘A2’) phenotypes. These were implicated to play differential roles in neuroinflammatory and neurodegenerative diseases, but also following ischemia or during

aging (Liddelow et al., 2017; Clarke et al., 2018). However, a recently defined consensus on astrocyte reactivity and gliosis aims to go beyond such a simplified polarized classification, as typically only a mixed set of A1- or A2-related transcripts were upregulated in different disease settings and do not suffice to neatly categorize the possible phenotypic diversity into only two classes (Escartin et al., 2021). Instead, multiple variables of reactivity should be taken into account together with transcriptomic profiles (e.g. proliferation, morphological and functional state of astrocytes). Such astrogliosis definition cover the spectrum of variable reactivity states that occur in response to CNS perturbations of different severity (Escartin et al., 2021).

1.2 Neuromyelitis optica spectrum disorders – definition, clinical picture & diagnostic criteria

Neuromyelitis optica (NMO; originally called Devic's disease, Devic & Gault, 1894; (Jarius and Wildemann, 2013)), is an autoimmune disease of the central nervous system mostly characterized by simultaneous presentation of transverse myelitis and optic neuritis, and to a lesser extent with brain involvement (Wingerchuk et al., 2015). While NMO was initially described as a monophasic disease, most patients show relapses without intermittent disease progression (Jarius et al., 2020), characterized by motor (paralysis), sensory deficits (visual loss, pain) and fatigue. Vomiting and nausea, as well as intractable hiccups are reported in the cases with cerebral involvement (Wingerchuk et al., 2015; Jarius et al., 2020). NMO was regarded as a variant of multiple sclerosis until the discovery of a NMO-specific serum antibody against aquaporin-4 (AQP4), which can be used as an entity-defining diagnostic marker (Lennon et al., 2004; Lennon et al., 2005). The majority of NMO patients (~80%) is seropositive for AQP4-IgG (Lennon et al., 2004; Levy et al., 2021), but also there is a considerable number of AQP4-IgG seronegative patients. Many of these patients have antibodies against the CNS myelin surface antigen, myelin oligodendrocyte glycoprotein (MOG-IgG) (Mader et al., 2011; Kitley et al., 2012; Probstel et al., 2015), but a small subset of patients lacks a currently discernible antibody, and would be considered 'idiopathic' (Jarius et al., 2020). MOG-IgG-positive patients show distinct disease characteristics (Kitley et al., 2012; Kitley et al., 2014; Sato et al., 2014) including a lower number of relapses, earlier disease onset and a higher males-to-female ratio compared to AQP4-IgG-positive NMO, which affects females more frequently (female:male ≈ 10:1) (Hor et al., 2020; Jarius et al., 2020). This distinct clinical presentation of AQP4- and MOG-IgG-positive patients, as well as variability

among patients in the initial clinical syndromes that may present with brainstem involvement, have resulted in a broadened diagnostic criteria and gave rise to the term 'neuromyelitis optica spectrum disorders', NMOSD (Wingerchuk et al., 2007; Fujihara, 2019). However, 'NMOSD' is inconsistently used in the literature, and recently the suggestion has been made to subsume MOG-IgG-positive patients under a distinct entity of 'MOG antibody-associated disorder' (MOGAD) (Hoftberger et al., 2020). For the purpose of this thesis, I will use the term 'NMO' or 'NMO-related' for AQP4-IgG-associated pathology, while I will refer to 'NMOSD', when broader autoantibody-mediated glial pathology is meant.

Current diagnostic criteria for NMO/NMOSD/MOGAD include serological status, radiological findings and clinical presentation with certain core characteristics, including optic neuritis, acute myelitis, or area postrema syndrome (Wingerchuk et al., 2015). Using such definitions, the prevalence of NMOSD range between 0.5 -1:100.000 across the globe, being more common in East-Asians (Hor et al., 2020).

In addition to the discovery of biomarkers and the resulting ongoing reclassifications, there has also been substantial progress in understanding the neuropathological and pathomechanistic underpinnings of NMSOD, as well as in the neurobiology of aquaporins, which I will describe in the following sections.

1.3 NMOSD neuropathology

Neuropathological investigations of AQP4-IgG seropositive NMO lesions mostly revealed AQP4 or GFAP loss. Additionally, perivascular deposition of immunoglobulins and complement proteins is apparent (Misu et al., 2007; Roemer et al., 2007). Depending on the stage of these lesions, demyelination, axonal damage and immune cell infiltration are also apparent, sometimes resulting in necrotic lesions that bear hallmarks of secondary tissue destruction (Misu et al., 2013; Lucchinetti et al., 2014). Immune infiltrates contain predominantly macrophages/activated microglia and granulocyte, but also the presence of cells of the adaptive immune system (T cells) have been reported (Lucchinetti et al., 2002; Misu et al., 2013). Additionally, sub-pial pathology with AQP4 loss, complement deposition and microglial reactivity was described (Guo et al., 2017). Notably, the absence of AQP4 immunoreactivity does not always indicate complete loss of astrocytes. Indeed, there have been reports of IgG-induced AQP4 internalization leading to loss of surface AQP4 without astrocyte necrosis (Hinson et al., 2008; Hinson et al., 2012). Despite the destructive quality that advanced

NMO lesions often display, signs of tissue repair can also be found: For instance, signs of astrocyte repopulation and remyelination have been noted (Parratt and Prineas, 2010; Bruck et al., 2012; Guo et al., 2017). Most of these neuropathological descriptions refer to NMO, and in comparison, less is known about the neuropathology of MOGAD. A primary characteristic here appears to be demyelination with predominant MOG loss compared to other myelin proteins, such as MBP and MAG. As in NMO, complement deposition and macrophage infiltration is apparent within demyelinating lesions (Takai et al., 2020). Interestingly, despite primary demyelination, axons and oligodendrocytes are relatively preserved (Weber et al., 2018; Hoftberger et al., 2020; Takai et al., 2020), without any astrocyte or AQP4 loss (Weber et al., 2018; Takai et al., 2020).

1.4 Animal models of NMOSD, and current understanding on NMOSD pathogenesis

An important driver of progress in our pathomechanistic understanding of NMOSD has been the development of animal models of the disease. The discovery of AQP4-IgG as a disease marker and likely initiating factor of NMO (Lennon et al., 2004; Lennon et al., 2005), many efforts have been undertaken to develop experimental models of NMO in order to study the pathogenesis of the disease and to investigate new candidate approaches to therapy. However, establishing AQP4 autoimmunity in rodents has been challenging, as deletional immune tolerance seems to be strong in rodents (Vogel et al., 2017). Only recently, AQP4-mimotopes have been reported to induce production of AQP4 autoantibodies in rats (Tsymala et al., 2020). Instead, for the last decade, passive transfer of NMO-related autoantibodies was the prevailing approach to model NMO lesions in rodents. For this, AQP4 antibodies (in many instances, together with human complement) were transferred to mice or rats via a range of delivery techniques, including local or systemic injection. Such models confirmed the potential pathogenicity of AQP4-IgGs and successfully represented characteristics of human NMO, which aided the study of disease pathogenesis and progression in rodent brain, optic nerve and spinal cord (Duan and Verkman, 2020).

Early transfer models combined transfer of NMO-related IgG with rat models of experimental autoimmune encephalomyelitis (EAE), which induces neuroinflammation and compromises the BBB. Intraperitoneal delivery of AQP4-IgGs to EAE-primed rodents resulted in CNS entry of antibodies, which triggered AQP4 and GFAP loss, together with perivascular deposition of

complement proteins and immune cell infiltration into the CNS (Bradl et al., 2009; Kinoshita et al., 2009; Wrzos et al., 2014). However, these EAE/NMO passive transfer models mostly lack substantial demyelination and axon pathology, which are found in human NMO lesions (Bennett et al., 2009; Bradl et al., 2009; Kinoshita et al., 2009). In order to improve recapitulation of human NMO pathology, and avoid the use of EAE, various passive transfer NMO models using experimental naïve rodents have been established. Delivery of patient derived or recombinant AQP4-IgGs, together with human complement directly to CNS tissue induced experimental NMO lesions. Astrocyte loss in these models was antibody-titer dependent and mediated by complement-dependent cell (CDC) toxicity (Saadoun et al., 2010; Ratelade et al., 2013; Wrzos et al., 2014; Herwerth et al., 2016). CDC mediates a direct injury on astrocytes via the coupling of complement protein C1q to antigen-antibody complexes. This activates the classical complement cascade with sequential enzymatic conversion of complement proteins and insertion of the membrane attack complex (MAC) into the plasma membrane of astrocytes - causing the osmolytic death of these cells (see section 1.6). While secondary axonal injury (Saadoun et al., 2010; Herwerth et al., 2016), as well as demyelination and oligodendrocyte loss was described in these models (Saadoun et al., 2010; Wrzos et al., 2014), the exact mechanisms of such 'off-target' injury still remain to be determined. Several reports from in vitro and in vivo studies by the Verkman lab have suggested a complement-mediated bystander injury on oligodendrocytes and neurons. Following activation of complement proteins, neighboring cells within the range of 100 µm to astrocytes might be targeted via diffusion of soluble components forming MAC, causing MAC insertion on oligodendrocyte and axon membranes (Tradtrantip et al., 2017; Duan et al., 2018) – even though these cells do not express AQP4 and are hence not directly targeted by NMO antibodies. In addition to such complement-mediated bystander cell targeting, there have been reports of antibody-dependent cellular cytotoxicity (ADCC) as the result of AQP4-IgG binding based on the use of differentially de-functionalized recombinant IgGs for transfer. In this setting, an effector cell type – e.g. nature killer cells - recognizes the Fc regions of AQP4-IgG on astrocytes and target these cells via cytotoxic degranulation and phagocytosis independently of complement activation (Ratelade et al., 2012; Ratelade et al., 2013; Duan et al., 2019).

Notably, in contrast to AQP4-IgGs, the pathogenicity of MOG-IgGs in transfer experiments to rodents has been reported to be independent of complement activation or immune cell infiltration (Saadoun et al., 2014). While one day after MOG-IgG/complement delivery, there were structural changes to myelin and axons, these changes were reversible within two weeks

and there was no indication of astrocyte, neuronal or oligodendrocyte loss as seen with AQP4-IgG-mediated injury. The exact mode of MOG-IgG-mediated injury remains elusive, but the authors suggested an antibody-mediated MOG internalization, which might hinder C1q-mediated complement activation (Saadoun et al., 2014).

Thus, while the potential pathogenicity of AQP4-IgG for intracerebral lesion formation is now largely undisputed and the complemented-mediated lysis of astrocytes appears to drive formation of destructive lesions (Saadoun et al., 2010; Wrzos et al., 2014), many questions remain open. For instance, it is unknown, whether bystander injury to axons and oligodendrocytes happens in vivo. In addition, which cell injury programs are triggered in axons and oligodendrocytes is unresolved, which has important translational implications that might guide efforts of neuroprotection, myelin preservation or repair. These questions are at the center of my thesis. Ultimately, transfer models of NMOSD cannot elucidate how the autoantibody responses against glial antigens are induced in NMOSD patients, and how peripheral IgGs initially enter the CNS. For the latter, possible entry routes involve CNS sites such as area postrema (Popescu et al., 2011), or blood-CSF barrier (Guo et al., 2017). However, the elucidation of the earlier steps in NMOSD pathogenesis will have to await the development of more realistic models of disease initiation in rodents, and co-aligned studies on the immune pathogenesis of NMOSD in humans.

1.5 Role of aquaporins in NMO

As AQP4 appears to be the primary target of IgG-mediated autoimmunity in NMO, the question arises whether the pathophysiology of NMO is solely explained by the ensuing complement-mediated lysis of glial cells, or whether loss of AQP4 function per se might contribute. AQPs are osmotically driven, bidirectional water channel proteins that regulate cellular water and osmotic homeostasis. Two members of the AQP gene family - AQP1 and AQP4 - are expressed in the CNS (Papadopoulos and Verkman, 2013). AQP4 is primarily located on ependymal cells and astrocytes, especially on the pial end-feet at the glia limitans and around vessels (Frigeri et al., 1995). In the periphery, AQP4 is expressed in skeletal muscle, kidney, stomach and lung tissue (Frigeri et al., 1995; Frigeri et al., 1998). AQP4 monomers consist of six membrane-spanning helical domains, although each monomer can function as a water transport unit itself; AQP4s are found in tetramers on the plasma membranes (Papadopoulos and Verkman, 2013). Two isoforms of AQP4, long ‘M1’ and short

'M23' are expressed; and only the latter one is found in orthogonal arrays of particles (OAPs), in which AQP4 M1 and M23 monomers further aggregate to supramolecular assemblies, which appear to be the primary targets of AQP4-IgGs in NMO (Nicchia et al., 2009; Phuan et al., 2012).

Binding of AQP4-IgG to its target antigen triggers at least two processes. First, internalization and degradation of AQP4 protein, putatively together with other interacting membrane proteins, such as the astrocytic glutamate transporter, EAAT2 (Hinson et al., 2008; Hinson et al., 2012) – which together result in water dyshomeostasis and cellular edema (Hinson et al., 2012), or glutamate excitotoxicity (Wrzos et al., 2014; Marignier et al., 2016). Second, AQP4-IgG can also activate the complement cascade, eventually resulting in MAC assembly and lytic death of astrocytes (Ratelade et al., 2013; Herwerth et al., 2016). Notably, this outcome might be promoted by the relatively low expression level of complement inhibitors, such as CD59, on the surface of astrocytes (Wang et al., 2017). The internalization of AQP4 vs. astrocyte lysis might arise from isoform-related effects: It has been suggested that M1 isoform of AQP4 is preferentially internalized following IgG binding, while M23 isoform can resist internalization and rather triggers complement activation (Hinson et al., 2012). However, these hypotheses are still under debate, as contradictory results have been reported on preferential internalization of these isoforms or AQP4 following IgG binding (Ratelade et al., 2011; Rossi et al., 2012).

1.6 Complement system and its role in NMO

The complement system is part of the innate immune system and compromise more than 50 plasma and membrane-bound proteins (Dunkelberger and Song, 2010; Kanmogne and Klein, 2021). Upon activation, complement proteins mediate responses against pathogens, but is also involved in the tissue responses after sterile injury via interacting receptors on T cells, B cells and dendritic cells (Dunkelberger and Song, 2010; Dalakas et al., 2020). Complement activation involves sequential proteolytic activation of complement proteins, which eventually result in formation of activated C3 and C5 convertases. These activated proteases mediate production of complement effectors, such as anaphylatoxins (C3a, C5a), opsonins (C3b, C4b) and the membrane attack complex (MAC, C5b-9) (Dunkelberger and Song, 2010; Dalakas et al., 2020).

Three major pathways of complement activation have been described: The classical, the lectin and the alternative pathways. The classical complement cascade is initiated by recognition of

surface pathogens or antibody-antigen complexes via the C1 complex, which binds to the Fc region of complement-fixing antibodies IgG or IgM and in turn, activates C1r/C1s to cleave C4 and C2. The resulting cleavage products mediate C3a and C3b release, with the latter activating C5 convertase that generates C5a and C5b. While the anaphylatoxins C3a and C5a recruit more immune cells to the activation site, C3b and C4b act as opsonins that tag cells for phagocytic clearance (Dunkelberger and Song, 2010). Activated C5b sequentially binds to C6 and C7 proteins and initiates MAC formation without further proteolytic steps. Following conformational changes that generate a lipophilic membrane-binding site, the C5b-7 complex is anchored to the plasma membrane surface. Subsequent C8 incorporation promotes penetration of the C5b-8 complex into the plasma membrane (Bayly-Jones et al., 2017). This complex, organizes C9 oligomerization, which results in a non-selective 11nm pore in the target cell's or pathogen's membrane (Farkas et al., 2002; Tegla et al., 2011; Bayly-Jones et al., 2017). Such membrane pores allow ion and water flux, eventually leading osmolytic death of the target. The lectin pathway is analogous to the classical complement cascade, except that it is initiated by association of a mannose-binding lectin to sugar monomers on the pathogen surface (Dunkelberger and Song, 2010). The alternative pathway refers to spontaneous activation of the complement cascade resulting in C3a and C3b generation. This pathway is continuously active at a low level, and amplifies C3b and C5 convertase activity in the classical and lectin pathways (Dunkelberger and Song, 2010).

Notably, in the CNS, complement does not only regulate responses to pathogens or other bona fide inflammatory processes (Dalakas et al., 2020; Kanmogne and Klein, 2021; Propson et al., 2021). Specific complement components are also implicated in circuit remodeling, e.g. by removal of cell corpses or elimination of synapses during development (Stephan et al., 2012). Microglia-mediated pruning of synapses is mediated by the C1q and C3 components of the classical complement cascade, e.g. in the developing visual circuits in cortex or motor circuits in the spinal cord (Stevens et al., 2007; Schafer et al., 2012; Bialas and Stevens, 2013; Vukojicic et al., 2019). The same complement proteins might also modulate synaptic plasticity during aging (Stephan et al., 2013; Shi et al., 2015), and mediate synapse loss during neurodegeneration or neuroinflammation (Propson et al., 2021). Additionally, C1q can also act as a neuroprotective signaling factor without the need for complement activation (Benoit and Tenner, 2011).

As expected for a powerful and potentially destructive host defense system, complement activity is controlled by several layers of regulation. Membrane-bound complement regulators

can be expressed on potential target cells to inhibit complement activation in a cell-autonomous fashion. This includes the trans-membrane proteins CD46 and CD55, which prevent early amplification steps of complement activation, or the glycosylphosphatidylinositol (GPI)-anchored protein CD59 that prevents MAC formation and insertion into the plasma membrane (Dunkelberger and Song, 2010). CD59 binds to the C8 and C9 components of the MAC, interferes with C8-C9 interaction and oligomerization of C9, which is essential for terminal pore formation and lytic activity of MAC (Farkas et al., 2002; Kimberley et al., 2007). CD59 can also block the reported ion channel function of 'leaky' C5b-8/9 complexes that precede full-fledged MAC pores (Farkas et al., 2002).

In addition to blocking specific steps along the complement activation and execution cascades, nucleated cells can also resist MAC action by removal of the C5b-9 complex from the membrane by endocytosis or vesicular shedding (Scolding et al., 1989b; Moskovich and Fishelson, 2007). In such cases, MAC can still exert sub-lytic activation of intercellular signaling cascades that are either dependent on pore activity (e.g. ion or metabolite fluxes), or pore-independent (e.g. where MAC proteins trigger second messenger signaling) (Xie et al., 2020). Such signaling can initiate various cell death pathways (Ziporen et al., 2009; Lusthaus et al., 2018), but also pro-inflammatory (Triantafilou et al., 2013) or pro-survival signaling (Soane et al., 1999; Cudrici et al., 2006).

The complement systems plays a central role in a number of diseases, including NMOSD, where it mediated AQP4-IgG and MOG-IgG-targeted injury. IgG antibodies can interact with C1q upon their binding to their target antigens and appear to initiate the classical complement cascade (Hinson et al., 2007; Mader et al., 2011). In NMO, for instance, perivascular deposition of AQP4-IgGs and activated complement proteins is apparent within lesions (Lucchinetti et al., 2002; Misu et al., 2007; Roemer et al., 2007; Misu et al., 2013). Accordingly, rodent NMO models based on transfer of AQP4-IgG also support the role of complement activation in disease pathogenesis. Typically, human complement needs to be co-transferred with IgGs to induce full-fledged pathology. This induces antibody-mediated deposition of lytic MAC pore on astrocytic membranes and their osmo-ionic lysis (Saadoun et al., 2010; Ratelade et al., 2013; Wrzos et al., 2014; Herwerth et al., 2016). This pathology was prevented by C1 inhibitors, targeting C1q with antibodies or following depletion of C1q from the transferred human complement (Saadoun et al., 2010; Phuan et al., 2013; Herwerth et al., 2016). Similarly, in MOGAD, complement deposition is present in demyelinating lesions, again arguing for a contribution of complement in pathogenesis (Takai et al., 2020).

While thus the role for complement in NMOSD pathogenesis is largely undisputed, the extent and specificity of this role is less clear. First, there are hints towards complement independent roles of the autoantibodies, by either interfering with the target antigens function (see above, Section 1.5) or by targeting cell-mediated immune attacks towards the target glial cell (Ratelade et al., 2012). Second, activated complement can cause 'bystander' injury on cells that do not express the target antigens of the auto-antibody, likely especially in settings where two cell types are in close proximity as astrocytes are to oligodendrocytes or neurons (e.g. at nodes of Ranvier or synapses, respectively). In experimental NMO models, such bystander injury was proposed because MAC proteins and their putative insertion on neurons and oligodendrocytes was observed by immunofluorescence staining, while initial complement cascade activator, C1q component was only bound to astrocytes (Tradtrantip et al., 2017; Duan et al., 2018). These results were interpreted as indicative of a special vulnerability of neurons and oligodendrocytes to a 'bystander' complement attack, as these cells express low levels of complement regulator proteins, such as CD59. Indeed, such bystander killing could be modeled in cell culture systems of complement-mediated astrocyte lysis (Tradtrantip et al., 2017; Duan et al., 2018). Notably, even tissues that express AQP4 outside the CNS (such as kidney, skeletal muscle, stomach and lungs) do not show signs of an autoimmune attack in NMOSD patients (Jarius et al., 2020). This has been mostly attributed to high expression of complement regulatory proteins (e.g. CD46, CD5, CD59) in peripheral tissues compared to the CNS (Saadoun and Papadopoulos, 2015; Wang et al., 2017), supporting the notion that protection against complement attack might be as much a determinant of which cells are targeted, as the specificity of the initial antibody binding. In line with this notion, CD59 knock-out rats developed kidney and skeletal muscle injury following passive transfer of AQP4-IgGs, which was prevented by treatment with a complement inhibitor (Yao and Verkman, 2017a).

1.7 Mouse models of in vivo spinal cord imaging

While in vitro and ex vivo studies have helped elucidate many fundamental concepts in neurobiology, the mammalian nervous system is difficult to model outside of its in vivo context– this problem also applies to neurological disease modeling, especially for conditions that require the interaction of different organ systems as in neuroinflammation. Therefore, in vivo imaging is particularly important for studying the CNS and its disorders, and many pioneering technical developments in in vivo imaging where devised to study the CNS. For the spinal cord, both widefield (Kerschensteiner et al., 2005; Misgeld et al., 2007) or multi-photon

microscopy techniques (Davalos et al., 2008; Johannssen and Helmchen, 2010) have been applied. While the former is simpler, cheaper and uses less light, the latter provides optical sectioning for 3D reconstructions, can resolve denser labeling and allows deeper tissue penetration, even though in the white matter tracts of the spinal cord even two-photon imaging is restricted to relatively superficial areas (<100µm) likely due to scattering effects of myelin. Combined with an ever evolving combination of structural, functional and subcellular labeling approaches (Romanelli et al., 2013; Rose et al., 2014; Lin and Schnitzer, 2016) that can be transgenically or virally delivered (Deverman et al., 2016; Chan et al., 2017; Ravindra Kumar et al., 2020), spinal in vivo imaging has allowed studying neuro-immune and neuro-glia interactions, neuronal activity and subcellular dynamics under homeostatic and disease conditions (Akassoglou et al., 2017; Nelson et al., 2019; Schumacher et al., 2019). In the disease context, spinal in vivo imaging was used to characterize axonal pathology following models of spinal injury (Kerschensteiner et al., 2005; Williams et al., 2014; Lorenzana et al., 2015), or multiple sclerosis-related neuroinflammation (Nikic et al., 2011; Witte et al., 2019), as well as investigating glial pathology (Davalos et al., 2005; Nimmerjahn et al., 2005; Farrar et al., 2012; Romanelli et al., 2016) and vascular changes (Davalos et al., 2008), but also to explore pain signaling (Chen et al., 2018; Yoshihara et al., 2018).

One limitation of the original approach to spinal in vivo imaging was the lack of a stable chronic window preparation and the need for long anesthesia (Kerschensteiner et al., 2005; Misgeld et al., 2007). Implantation of chronic windows on the spinal cord is anatomically more challenging compared to cortex, given the mobility of the spine and the absence of a stable bony surface for attaching the window. Still, there have been advances in developing chronic spinal windows based on spinal adaptors that fuse a few segments and can allow repetitive observations over weeks or even months (Farrar et al., 2012; Fenrich et al., 2012). Additionally, wearable miniature-scope versions of such windows have been explored to study spinal micro-circuits in awake behaving animals (Sekiguchi et al., 2016; Nelson et al., 2019). While usage of such approaches can overcome the limitations of repeated surgery and anesthesia-related physiological artifacts, they still provide comparatively limited optical depth penetration and spatial resolution compared to conventional imaging setups, thus have not overcome the problem of the consistently observed chronic inflammatory response to the chronic window, which is a special concern when modeling chronic neuroinflammatory diseases.

Thus, for neuroinflammatory disease models, acute imaging remains an important approach to study the early stages of lesion development (Nikic et al., 2011; Sorbara et al., 2014). For

NMOSD, we have previously established an in vivo imaging approach using an acute experimental mouse model of NMO-related injury. This involves a laminectomy and local application of patient-derived or recombinant AQP4-IgGs together with human complement to spinal cord (Herwerth et al., 2016). Our model was the first in vivo imaging model to study the induction of acute experimental NMO-related lesions, with the ability of performing time-lapse recordings for up to 8 hours. Combined with transgenic labeling of neuronal and glial cell populations, this model can be used to assess the spread of pathology from the primary astrocytic target to secondarily affected cells types (Herwerth et al., 2016) – and underpins the studies that I performed for this thesis.

1.8 Aims of the thesis

My PhD research has focused on identifying the possible injury mechanisms that drive NMO-related pathology. Therefore, I have addressed the following objectives by taking advantage of our AQP4-IgG/complement-mediated spinal NMO mouse model (Herwerth et al., 2016) that is suitable for performing time-lapse in vivo imaging (Figure 1):

- Defining the temporal sequence of axon and oligodendrocyte injury in regard to astrocyte loss during the induction phase of experimental NMO (Section 2)
- Implicating the early hallmarks of glial and axonal injury, and identifying intracellular cascades promoting cell damage and loss (Section 2)
- Elucidating activated complement vulnerabilities of cells that are not primarily targeted by NMO-IgGs, and whether such vulnerability takes part in progression of experimental NMO (e.g. for oligodendrocytes, Section 2.2)
- Establishing a survival surgery approach compatible with our AQP4-IgG/complement mediated NMO model to investigate the long-term fate of injured cells following induction of astrocyte depletion (e.g. for axons, Section 2.1)

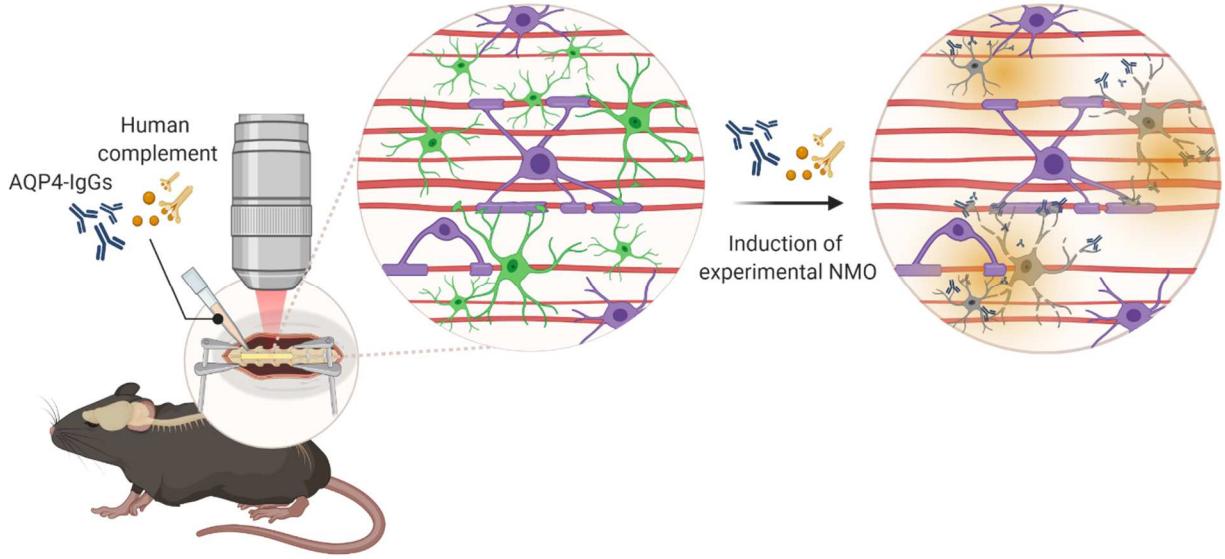

Figure 1. In vivo imaging of cellular injury mechanisms in a mouse model of spinal NMO

Transgenic mouse lines that express cell-specific, genetically encoded fluorescent proteins or calcium sensors were used to image NMO-related cellular pathology. Following laminectomy surgery, a dura-free imaging window was prepared to allow AQP4-IgG/complement application over the dorsal spinal cord to induce astrocyte (green, left) loss. Consequent to astrocyte damage (gray, right), we have investigated intracellular events and the morphological changes in axons (red) and oligodendrocytes (purple) by performing in vivo time-lapse imaging experiments. (Figure was created with BioRender.com)

2 Results

Manuscript I

A new form of axonal pathology in a spinal model of neuromyelitis optica

Marina Herwerth[1, 2, †, ‡], Selin Kenet[1, 3†], Martina Schifferer[4, 5], Anne Winkler[6], Melanie Weber[1, §], Nicolas Snaidero[1], Jeffrey L. Bennett[7], Christine Stadelmann[6], Bernhard Hemmer[2, 5], Thomas Misgeld[1, 4, 5, *]

Manuscript ready for submission

Contribution to the manuscript: I established the survival surgery approach compatible with our acute NMO model, and conducted and analyzed all the survival NMO experiments presented in the manuscript. Together with Marina Herwerth and Thomas Misgeld, I drafted and edited the manuscript, and the figures with the input from other authors.

A new form of axonal pathology in a spinal model of neuromyelitis optica

Marina Herwerth[1, 2, †, ‡], Selin Kenet[1, 3†], Martina Schifferer[4, 5], Anne Winkler[6], Melanie Weber[1, §], Nicolas Snaidero[1], Jeffrey L. Bennett[7], Christine Stadelmann[6], Bernhard Hemmer[2, 5], Thomas Misgeld[1, 4, 5, *]

[1]Institute of Neuronal Cell Biology, Technische Universität München, Munich, Germany.

[2]Department of Neurology, Klinikum rechts der Isar, Technical University of Munich, Germany.

[3]Graduate School of Systemic Neurosciences, Ludwig-Maximilians University, Munich, Germany.

[4]German Center for Neurodegenerative Diseases (DZNE), Munich, Germany.

[5]Munich Cluster of Systems Neurology (SyNergy), Munich, Germany.

[6]Institute of Neuropathology, University Medical Center Göttingen, Germany.

[7]Departments of Neurology and Ophthalmology, Programs in Neuroscience and Immunology, University of Colorado School of Medicine, Aurora USA.

†Equal first authors

‡ Present address: Institute of Pharmacology and Toxicology, University of Zurich, Zurich, Switzerland.

§ Present address: Department of Cardiovascular Surgery, German Heart Center Munich, Technical University of Munich, Germany.

*Corresponding author: thomas.misgeld@tum.de (T.M.)

One Sentence Summary:

Herwerth et al. reveal a cytoskeletal axon injury mechanism triggered by autoimmune astrocyte lysis in neuromyelitis optica.

Abstract

Neuromyelitis optica (NMO) is a chronic neuroinflammatory disease, which primarily targets astrocytes and often results in severe axon injury of unknown mechanism. NMO patients harbor autoantibodies against the astrocytic water channel protein, aquaporin-4 (AQP4-IgG), which induce complement-mediated astrocyte lysis. Using in vivo imaging in a mouse model of spinal AQP4-IgG induced lesions; we explored the mechanism of axon injury that followed astrocyte loss. In particular, small caliber axons showed a swift and morphologically distinct 'pearls-on-string' transformation independent of myelination. Such beaded axons were also readily detectable in NMO lesions. Functional imaging revealed that calcium homeostasis was initially preserved in this 'acute axonal beading' state ruling out disruption of the axonal membrane, which is unique compared to previously described forms of traumatic and inflammatory axon injury. Pharmacological, genetic and morphological analyses revealed that AQP4-IgG induced axon injury involved osmotic stress and ionic overload, as axonal beading could be partly prevented by raising extracellular osmolarity and by blocking sodium channels. Remodeling of the axonal cytoskeleton including loss of microtubules was observed in the beaded axons. Treatment with the microtubule stabilizer epothilone B, a therapy in development for traumatic and degenerative axonopathies, prevented axonal beading, indicating a potential role in the acute treatment of NMO attacks. Our results reveal a new form of immune-mediated axon pathology distinct from known cascades of posttraumatic and inflammatory axon loss, and propose new strategies for neuroprotection in NMO and related diseases.

Introduction

In many neurological diseases, damage to axons plays a central role in pathology. In some conditions, such as neurodegeneration or multiple sclerosis (MS), axon injury is insidious and slowly progressive. In others diseases, e.g. trauma and stroke, axons are damaged in a cataclysmic event. While in the former conditions, the optimal strategy to prevent axon injury is early disease modulation, while acute neuroprotection and neuroregeneration need to be prioritized in the latter.

Neuromyelitis optica (NMO), which is part of a spectrum of antibody-mediated autoimmune CNS disorders (Wingerchuk et al., 2015; Fujihara, 2019), presents a blend of these disease dynamics. In NMO patients, astrocytes are the primary target of aquaporin-4 specific autoantibodies (AQP4-IgGs) (Lennon et al., 2004; Lennon et al., 2005; Hinson et al., 2007) astrocyte injury is swiftly followed by demyelination and neuronal pathology (Roemer et al., 2007; Misu et al., 2013). The resulting disease is characterized by relapses, and unlike in MS, disease progression is rarely observed between attacks (Wingerchuk et al., 2007; Combes et al., 2017). Instead, even the first inflammatory lesions typically inflict irreparable damage to axons in the eponymous fiber tracts of spinal cord and optic nerve. Thus, devising early neuroprotective interventions would be an important addition to emerging immunomodulatory therapies (Jarius et al., 2020; Levy et al., 2021), which only allow blunting further damage once the diagnosis is established and the initial damage has occurred. In addition to these specific therapeutic needs, AQP4-IgG-positive NMO also represents a paradigmatic example of an 'astrocytopathy' (Lucchinetti et al., 2014; Bennett and Owens, 2017). As astrocyte damage is increasingly implicated in more common neuroinflammatory and neurodegenerative diseases (Brosnan and Raine, 2013; Booth et al., 2017; Liddelow et al., 2017; Rothhammer et al., 2018; Yun et al., 2018; Prineas and Lee, 2019; Linnerbauer et al., 2020), understanding how axon injury emerges as a consequence of astrocyte dysfunction is of general importance.

Thus far, the mechanisms of axon injury in NMO have mostly been inferred from neuropathological analysis (Kawachi and Lassmann, 2017). Possible mechanisms of axon injury in NMO include inflammatory bystander damage via complement (Duan et al., 2018), as well as ionic, ischemic or excitotoxic mechanisms driven by astrocytic loss (Kawachi and Lassmann, 2017). In addition, previously established programs of axon degeneration, such as Wallerian-like degeneration or focal axonal degeneration (Nikic et al., 2011; Witte et al., 2019; Coleman and Hoke, 2020) have been implicated in NMO (Misu et al., 2013; Hokari et al., 2016; Cai et al., 2017), suggesting shared axon destruction pathways between NMO and

neurodegeneration or MS. Still, no clear-cut axon injury program that could represent a suitable down-stream target for neuroprotective interventions in NMO has been revealed.

We have previously established two-photon in vivo imaging of the mouse spinal cord as a suitable approach to model the dynamics of cellular injury in AQP4-IgG-induced lesions in mice (Herwerth et al., 2016). In this model, astrocytes undergo lytic cell death after local application of NMO patient-derived AQP4-IgG and human complement to dorsal white matter tracts. Direct in vivo observation then reveals the quick spread of pathology to other cell types, including neurons and their axons. We now explored the mechanisms of such axon injury and demonstrate that these changes—which closely mimics the axon pathology seen in NMO — are neither due to the known axon destruction programs, such as Wallerian-like axon loss or MS-related focal axonal degeneration, nor involve bystander injury via complement pores. Instead, axons in acute astrocytopathic lesions undergo a 'beading' phenomenon that thus far has not been characterized in vivo, which could largely be prevented by microtubule stabilization, a therapy strategy previously investigated in traumatic spinal cord injury (Ruschel et al., 2015) — suggesting a potential new target for neuroprotective intervention in NMO-related pathology.

Results

Axonal beading occurs in early NMO lesions

Previously, we had observed by in vivo two photon imaging of the exposed mouse spinal cord, that topical AQP4-IgG/complement application induces almost complete loss of local subpial astrocytes in white matter tracts, followed by swift axon injury characterized by a 'pearls-on-string' pattern (Herwerth et al., 2016). First, we confirmed that the axonal beading pattern in our NMO model is indeed also found in acute NMO lesions, where astrocyte loss, demyelination, immune infiltration and reduced axonal density have been previously described (Lucchinetti et al., 2014). To characterize axonal pathology, we identified seven early NMO lesions (5/9 screened biopsies, 2/9 autopsies; **Table 1**) that contained MRP14-positive macrophages – a marker for early stage lesions (Bruck et al., 1995b) and suitable axon orientation to score beading by either neurofilament staining or Bielschowsky silver impregnation (**Fig. 1A, B**). Axonal beading was readily apparent in NMO lesions and greatly increased compared to perilesional white matter and control tissues (5 biopsies/ 4 autopsies of unrelated pathologies; for details, see **Table 2**, **Fig. 1C**). Thus, 'pearls-on-string'-like axon

pathology is a pervasive feature in early NMO, suggesting that our spinal NMO mouse model (Herwerth et al., 2016) is suitable to investigate the mechanisms of NMO-related axon injury.

Axonal beading precedes calcium dyshomeostasis in experimental NMO lesions

In many neuropathological settings, axonal pathology (such as spheroid formation) is preceded by calcium overload in the cytoplasm (Coleman, 2005; Friese et al., 2014), either derived from intracellular stores (Orem et al., 2020), or from influx of extracellular calcium via ion channels (Friese et al., 2007; Schattling et al., 2012) or non-specific membrane disruptions (Williams et al., 2014; Witte et al., 2019). While sometimes reversible (Williams et al., 2014), such calcium overload can cause activation of destructive intracellular signaling cascades that eventually result in irreversible axon degeneration (Coleman, 2005). Thus, we tested whether in our experimental NMO model, intra-axonal calcium elevation precedes axonal beading. We used *Thy1*:TNXXL transgenic mice, which express a fluorescence resonance energy transfer (FRET)-based calcium sensor in neurons (Mank et al., 2008). As in our previous experiments (Herwerth et al., 2016), application of complement together with NMO patient-derived AQP4-IgG or recombinant (r) AQP4-IgG induced fast and progressive beading of many axons within a 6-hour observation period (**Fig. 1D-E**; astrocyte survival for patient-derived AQP4-IgG at 3h measured in *Aldh1l1*:GFPx*Thy1*:OFP3 mice, mean±SEM: NMO 3.8 ± 2.5%, n = 6). Such axonal damage was largely absent after application of complement with IgG from healthy donor or recombinant control-IgG (**Fig. 1D-E**). In contrast to other models of neuroinflammation or trauma (Nikic et al., 2011; Williams et al., 2014), no axons progressed or recovered from beading during the imaging period, suggesting a relatively stable state of axon injury.

Unexpectedly, we found that most beaded axons did not show an increase in calcium level during the first 6 hours of astrocyte ablation (**Fig. 1D, E**). Moreover, the minority of axons in which calcium increases showed this increase with substantial delay, and no axon showed a detectable calcium increase before axonal beading started (**Fig. 1F**). Even in the subset of axons that did show a calcium increase, there was no fixed temporal relationship between the onset of axonal beading and of the calcium rise (**Fig. 1G**). Altogether, these data suggest that AQP4-IgG mediated astrocyte loss induces a distinct form of axon pathology, which is calcium-independent at onset and subsequently leads to an impairment of axonal calcium homeostasis. This cascade thus reverses the sequence of events found in most previously described forms of

axonal injury (Coleman, 2005; Friese et al., 2014), including neuroinflammation (Schattling et al., 2012; Witte et al., 2019).

Experimental NMO lesions lead to persistent axonal beading

We next explored, whether beading was a transient or lasting pathology. As acute in vivo two-photon imaging only allowed us to follow early axonal injury within a 6-hour time window, we turned to a survival surgery approach to assay chronic axonal changes after initiation of experimental NMO lesions (Kerschensteiner et al., 2005; Williams et al., 2014) (**Fig. 2**). For this, we exposed the dorsal spinal cords of *Aldh1l1*:GFPx*Thy1*:OFP3 mice with rAQP4- or rCtrl-IgG plus human complement. One day after surgical closure of the laminectomy, the animals were perfused and the spinal cords were examined by confocal microscopy (for details, see Methods). Application of rAQP4-IgG, compared to rCtrl-IgG, induced a pronounced reduction in astrocyte density in many areas of the spinal cord (**Fig. 2A-C**). Analysis of axonal beading showed that while a subset of axons also had caliber variations in rCtrl-IgG-treated spinal cords (most likely due to the opening of the dura required for IgG application), astrocyte ablation by AQP4-IgG induced a significantly higher fraction of beaded axons (**Fig. 2D**), suggesting that NMO-related axonal beading is a persistent phenomenon. We did not observe any axon fragments, which typically last for days in the spinal cord (Kerschensteiner et al., 2005), suggesting that axonal beading represents a stable dysmorphic state that can persist for days.

Beading predominantly affects small caliber axons independently of myelination

In addition to astrocyte loss, demyelination is another hallmark of NMO lesion pathology (Parratt and Prineas, 2010; Bruck et al., 2012). Axonal beading could be the immediate consequence of myelin pathology (Weil et al., 2016). This would predict that only myelinated axons would undergo beading after AQP4-IgG induced astrocyte loss. As myelination requires a target axon above a threshold diameter (Waxman and Bennett, 1972), large caliber axons would be expected to be most vulnerable to beading, if myelin was a central contributor. However, when we compared the axon caliber of the beaded vs. the non-beaded axons in *Thy1*:TNXXL mice, thinner axons were more vulnerable to develop beading (**Fig. 3A**). Based on this observation, we assumed that unmyelinated axons might also develop beading due to astrocyte loss. Due to limitations in resolution in light microscopy and in differentiation between myelinated and unmyelinated axons, we examined the morphology of myelinated and unmyelinated axons in mouse NMO lesions via serial section electron microscopy (EM; **Fig.**

3B-E). This approach revealed that in addition to myelinated axons, also non-myelinated axons showed the beading phenomenon (mean±SEM: NMO n_{myel} = 47.4 ± 10.4%, n_{unmyel} = 74.1 ± 4.4%; n=3 mice **Fig. 3F**). Notably, also control unmyelinated axons showed caliber variations (mean±SEM: control n_{unmyel} = control: 30.5 ± 11.3%; n=3 mice **Fig. 3F**), which can likely be explained by presynaptic varicosities (Greenberg et al., 1990), but the beading phenomenon could be clearly identified by a significant increase in swelling density induced in the experimental NMO lesions (**Fig. 3G**). Overall, the axonal injury following AQP4-IgG mediated astrocyte loss especially affects thin axons, whether they are myelinated or not, and therefore it is unlikely to be initiated by NMO-related myelin pathology.

Axonal beading involves local cytoskeletal remodeling driven by osmo-ionic overload

Another potential driver of axon shape changes is cytoskeletal remodeling, which in some cases can result in local organelle accumulations due to disrupted transport (Coleman, 2005; Beirowski et al., 2010). We used transmission EM to directly assess the cytoskeleton inside beaded axons and found that microtubules were unusually sparse and disorganized, in contrast to the well-organized cytoskeletal structures in control axons (**Fig. 4A**). In line with these ultrastructural results, confocal analysis of tubulin immunostainings (**Fig. 4B-C**) revealed local loss and reorganization of microtubules at the center of axonal beads compared to well-preserved parallel-running microtubule bundles outside the swellings or in control axons (**Fig. 4B**). We quantified βIII-tubulin immunofluorescence relative to a fluorescent protein (OFP) transgenically expressed in axons. Tubulin staining was reduced by >50% within axonal beads compared either to the interjacent axon segments in AQP4-IgG-induced lesions or to axons under control conditions (**Fig. 4C**). As cytoskeletal breakdown is known to occur during Wallerian degeneration and related processes (Beirowski et al., 2010; Coleman and Freeman, 2010), we explored whether deleting a central mediator of Wallerian-like degeneration, sterile alpha and TIR motif-containing protein 1 (SARM1) (Osterloh et al., 2012) would affect NMO-related axon beading. In SARM1-deficient mice, treatment with AQP4-IgG/complement resulted similar kinetics and extent of axon loss as in heterozygote $SARM1^{+/-}$ mice (fraction of surviving astrocytes after 3h, mean ± SEM: $SARM1^{-/-}$: 2.3 ± 1.9%; $SARM^{-/+}$: 2.4 ± 1.4%, n = 5 mice each), without a difference in the degree of axonal beading (**Fig. 4D**). Thus, Wallerian-like degeneration does not appear to play a key role in NMO-related axon injury.

Another notable ultrastructural feature of the axonal beads was that they typically showed few membranous organelles, in contrast to axonal swellings that result from ‘traffic jams’ of

organelle transport (Maday et al., 2014). As this scarcity in organellar content could indicate cytoplasmic expansion due to cellular edema and because astrocytes via AQP4 play a central role in water homeostasis (Papadopoulos and Verkman, 2013), we probed whether changing the osmotic milieu by applying a hyperosmolar (200% of the initial osmolarity) mannitol solution would affect acute axonal beading. Indeed, this delayed and significantly reduced the number of beaded axons during experimental NMO lesion formation (**Fig. 4E**). At the same time, astrocytes were still efficiently ablated by AQP4-IgG/complement treatment (fraction of surviving astrocytes after 3h, mean ± SEM: 1.5 ± 0.5%, n = 4). Similarly, reducing the sodium influx to axons using the voltage-gated sodium channel blocker tetrodotoxin (TTX, 1 µM), also significantly protected axons from beading (**Fig. 4F**) while astrocytes were still lysed (fraction of surviving astrocytes after 3h, mean ± SEM: 3.0 ± 2.3%, n = 6). These results imply that osmotic and ionic overload, likely due to astrocyte necrosis, together with calcium-independent cytoskeletal remodeling mediate the initial phase of acute axonal beading in our NMO model.

Microtubule stabilization prevents acute axonal beading in experimental NMO lesions

While microtubule loss is not an early or dominant feature in MS-related forms of axon degeneration (Sorbara et al., 2014), in some traumatic and neurodegenerative settings, microtubule alterations are a prominent feature in injured axons and might also contribute to the intrinsic inefficiency of CNS axon regeneration. Accordingly, microtubule stabilization using taxenes or related drugs (Hellal et al., 2011; Ruschel et al., 2015) has been explored as pro-regenerative interventions after axon transection. Whether such an approach could be used for axon protection in NMO-related pathology is unknown.

Local application of microtubule stabilizer epothilone B (epoB) during AQP4-IgG/complement treatment, greatly reduced the number of beaded axons was, while it did not affect astrocyte survival (Fig. **5A-C**). Similarly, as epoB is CNS-permeant, after intraperitoneal (i.p.) injection of epoB (Ruschel et al., 2015) 24 hours prior to local lesion induction also reduced axonal beading (**Fig. 5D**). Analysis of βIII-tubulin immunostainings confirmed microtubule stabilization after local epoB treatment by showing a significant preservation of microtubule content in axon beads (**Fig 5E**), but also in interjacent non-beaded axon segments (βIII-tub/OFP ratio after epoB: 1.66 ± 0.17, n = 65 axons vs. vehicle: 0.57 ± 0.05, n = 188, 5 mice each). Overall, these results imply that microtubule stabilization might be a suitable strategy to protect axons during early phases of NMO lesion formation.

Discussion

Astrocyte pathology—the structural hallmark of NMO—has been implicated in neuronal dystrophy associated with many neurodegenerative and neuroinflammatory diseases (Verkhratsky et al., 2012; Pekny et al., 2016; Liddelow et al., 2017). To date, these observations have been largely confined to the chronic phases of lesion formation and involved the slow development of reactive astrocyte phenotypes (Hokari et al., 2016; Kawachi and Lassmann, 2017). Often, the impact of such a neurotoxic polarization of astrocytes is mediated via indirect cellular signaling involving microglial crosstalk, e.g. in models of MS (Liddelow et al., 2017; Rothhammer et al., 2018), but also implicated recently in chronic NMO lesions (Chen et al., 2020). In contrast, the impact of acute astrocytic injury during the early phases of NMO lesion formation has received less attention, even though the swift development of lasting axonal injury and persistent neurological deficits are characteristic of this neuroinflammatory disease (Jarius et al., 2020). Understanding the underlying axon injury mechanisms is important, as in contrast to more common neuroinflammatory diseases—such as MS—, the first episode of NMO often already has devastating consequences that would need acute neuroprotective intervention, in addition to ameliorating relapse risk by immunomodulatory intervention (Tradtrantip et al., 2020).

Here we describe ‘acute axonal beading’ as the swift consequence of in vivo astrocyte loss and as the earliest observable axon injury in acute experimental NMO lesions. Acute axonal beading represents a new form of calcium-independent axonal pathology that is distinct from the mechanisms of axon injury previously described during MS-related neuroinflammation or trauma. We show that after lytic depletion of astrocytes, axonal microtubules are lost, accompanied by fast and lasting axon beading in a ‘pearls-on-string’ pattern that is evident in NMO lesions as well (**Fig. 1C**). These insights regarding the involvement of a specific axon loss mechanism (Coleman and Perry, 2002; Raff et al., 2002) are important, as they hint towards cytoskeletal stabilization as a possible intervention point for acute neuroprotection during destructive episodes of NMO.

Acute axonal beading has characteristics that set it apart from other pathways that hitherto have been implicated in axon pathology in general, and especially in axonal spheroid formation (Beirowski et al., 2010). One central feature that sets NMO-related acute axonal beading apart of most previously proposed axon injury cascades is the lack of initial calcium overload—indeed, in our observations, axonal beading was typically complete before signs of calcium overload appeared without any evident fixed time delay (range of delay: 10 to 250 min; **Fig.**

1F-G). In contrast, most other forms of axon injury show signs of calcium dysregulation before structural axon pathology becomes apparent, including MS-related neuroinflammation (Nitsch et al., 2004; Witte et al., 2019), trauma (Knoferle et al., 2010; Stirling et al., 2014; Williams et al., 2014) or hypoxia (Ouardouz et al., 2003; Stirling and Stys, 2010). These cascades are initiated by the spurious opening of calcium channels (Stys, 1998), release from internal stores (Orem et al., 2020) or the reversal of calcium-carrying membrane pumps (Yang et al., 2013), often as a consequence of sodium overload. In contrast, the axons in acute experimental NMO lesions do not seem to experience early calcium overload (**Fig. 1E**), even though TTX-sensitive voltage-gated sodium channels that act upstream of calcium in a range of axonal pathologies (Wolf et al., 2001; Waxman, 2006), appear relevant for the beading process (**Fig. 4F**). However, this role likely relates more to a sodium influx-related osmotic challenge than acting as a driver of secondary calcium influx (see below). Similarly, mitochondrial dysfunction is an early hallmark of many pathways that involve 'virtual hypoxia' induced by ionic overload (Trapp and Stys, 2009). In addition, our ultrastructural analysis did not show the characteristic mitochondrial pathology that can be found early e.g. in many neurodegenerative conditions in MS (Nikic et al., 2011; Court and Coleman, 2012) or chronic NMO lesions (Hokari et al., 2016).

The absence of early calcium influx also rules out a number of additional pathways of axon injury that have been suggested to drive neuroinflammatory axon loss. For instance, there could be a spurious attack by complement components that preassemble on astrocytes as part of the AQP4-mediated injury and spill over to nearby axonal membranes. Such 'bystander injury' has been invoked to explain the spread of cellular injuries in NMO in general (Tradtrantip et al., 2017), but also for neurons in particular (Duan et al., 2018). However, whether such a mechanism could also affect axons in white matter tracts directly is unknown (Bruck et al., 1995a). Our in vivo imaging data provide little support for this: The affected axons are mostly—albeit not all—myelinated, which would likely hinder access of a macromolecular attack complex such as complement (Serna et al., 2016), except at the nodes of Ranvier. However, we see little evidence for an onset of beading at nodes, in contrast to swellings that we previously described in a model of MS (Nikic et al., 2011). Moreover, from previous work involving in vivo dye loading and calcium imaging (Williams et al., 2014; Witte et al., 2019), we know that in vivo calcium imaging is sensitive to the presence of 10nm pores, as would be expected if the MAC assembled on axonal membranes (Serna et al., 2016). Thus, the late occurrence of calcium influx largely rules out the mechanisms of axonal bystander injury. The

same applies to the formation of membrane nanoruptures (Witte et al., 2019) observed during another well-established inflammatory axon degeneration pathway, focal axonal degeneration, which is characteristic of MS (Nikic et al., 2011; Witte et al., 2019), but has also been implicated in chronic NMO (Hokari et al., 2016). Finally, Wallerian-like degeneration, which is the best understood molecular cascade resulting in axon swelling and subsequent fragmentation (Kerschensteiner et al., 2005; Beirowski et al., 2010; Singh et al., 2017), also typically involves calcium influx (Vargas et al., 2015; Coleman and Hoke, 2020). In line with the absence of such calcium influx, deletion of SARM—the central endogenous mediator of Wallerian degeneration (Osterloh et al., 2012)—had no discernible effect on NMO-related lesions (**Fig. 4D**). Thus, our data suggest that an axon injury pathway distinct from those previously described in neuroinflammation and trauma underlies acute axonal beading induced by astrocyte lysis in NMO.

Our intravital, ultrastructural and histological investigations, point to important features of this unusual form of axonal pathology: (1) While many axons (76 ± 2,8% in the dorsal column of *Thy1:*TNXXL mice; **Fig. 3A-B**) undergo this change, thin-caliber axons are especially vulnerable (**Fig. 3A**). (2) This vulnerability does not strictly relate to myelination, as both myelinated and non-myelinated axons appear beaded in EM (**Fig. 3D-F**), making a geometrical or mechanical cause for the vulnerability of thin axons more likely. (3) The axonal beads show a striking reorganization of the cytoskeleton with local loss of microtubules (**Fig. 4B**). Together, this supports the view that cytoskeletal reorganization drives acute axonal beading, which further distinguishes NMO-related axon injury from other forms of inflammatory axon damage - cf. (Sorbara et al., 2014). The fact that acute axonal beading can be largely prevented by stabilizing microtubules (**Fig. 5**), but also by blunting hypo-osmotic impact (**Fig. 4E**), corroborates this notion—and points to a possible therapeutic target. Notably, the morphological and mechanistic features of NMO-related in vivo axon injury harbor parallels to a previously characterized ex vivo phenomenon of axonal beading, which is prominent in fixed and isolated PNS axons after stretch (Ochs et al., 1997), but can also be modeled in vitro using PNS axons exposed to osmotic shock (Pullarkat et al., 2006). Indeed, also in the ex vivo PNS stretch model, calcium was not required, myelinated, as well as non-myelinated axons were affected, and local cytoskeletal changes were observed (Ochs and Jersild, 1987; Ochs et al., 1997). In vitro, axoplasm-filled swellings were described that had a microtubular ‘core’ strikingly similar to the microtubular arrangements we observed in NMO-related injury - cf. Fig. 2 in (Datar et al., 2019) with our **Fig. 4B**). A modeling analysis of the beading

transformation (Datar et al., 2019) in vitro revealed that hyperosmotic shock disrupts the interplay of longitudinally running microtubules, sub-membranous actin and membrane surfaces tension resulting in a surface tension-driven shape destabilization that finally results in beading—again in line with our result that small caliber (and hence high surface-to-volume ratio) axons showed special vulnerability.

Targeting the microtubular cytoskeleton (e.g. by pharmacological stabilization using taxenes or epothilones; (Ruschel et al., 2015)) is currently a widely debated form of intervention in neurodegeneration (Ballatore et al., 2012; Zhang et al., 2012) and after neurotrauma (Curcio and Bradke, 2018; Griffin and Bradke, 2020). Such intervention has been proposed to stabilize degenerating axon ends, promote axon outgrowth and reduce scaring (Erturk et al., 2007; Hellal et al., 2011; Ruschel et al., 2015), but perhaps also to protect homeostatic function such as axonal transport (Fernandez-Valenzuela et al., 2020). However, in neuroinflammation, microtubule stabilization has not been seen as a promising target, on the one hand because hitherto microtubular changes were described as rather late changes in axon (Sorbara et al., 2014); cf. (Shriver and Dittel, 2006), but also because the immunosuppressive effects of microtubule-targeting drugs hamper analysis of direct axonal effects in chronic settings (O'Sullivan et al., 2013). Indeed, these immunosuppressive effects — as well as chronic neurotoxicity and the possibility of preventing physiological plasticity (Brill et al., 2016) — make the implementation of microtubule stabilizing therapies in traumatic settings challenging, both acutely and to support long-term recovery. In contrast, we now show that in our NMO model, epothilone (as well as hyperosmotic intervention using mannitol) can largely prevent beading during the acute phase. This result is in line with previously described pearling instability models of axons: when microtubules are disrupted, the threshold tension to form beadings is decreased, as the internal cytoskeletal elastic resistance is altered (Datar et al., 2019). The decrease in such elasticity, together with the presence of additional osmotic tension due to the release of the cytosolic components of lysed astrocytes or altered osmotic regulation due to lack of astrocyte end feet (Pullarkat et al., 2006; Datar et al., 2019), are likely drivers of acute axonal beading. Given the result that the beaded state is relatively long lived (**Fig. 2**), but is eventually followed by potentially destructive calcium dysregulation (**Fig. 1D-E**), a window of opportunity for protective intervention might exist. Given the time line of our model, microtubule stabilization here is very likely to act directly on axons, rather than the immune system. Moreover, in an NMO setting, also an acute anti-proliferative effect would be less of a problem, as a course of steroids is part of current standard relapse management anyway

(O'Sullivan et al., 2013). Therefore, in summary, our data suggest that acute disruption of the microtubular cytoskeleton might be a worthwhile target to explore as an acute axon-protective intervention point during a destructive NMO relapse.

Materials and Methods

Animals

To image astrocytes, we used 2- to 5-month old male and female *Aldh1l1*:GFP mice obtained from MMRRC (strain: Tg(Aldh1l1-EGFP)OFC789Gsat/Mmucd) and to image axons *Thy1*:OFP3 mice (Brill et al., 2011), courtesy of J. Lichtman, Harvard U., Cambridge, MA. The *Thy1*:TNXXL strain—courtesy of O. Griesbeck (Max Planck Institute of Neurobiology, Martinsried)—was used to measure axonal calcium levels as previously described (Mank et al., 2008; Williams et al., 2014). The SARM knockout mouse line was a courtesy of A. Ding (Cornell U., Ithaca, NY). Animal experiments were conducted in accordance with local regulations and were approved by the responsible regulatory agencies.

Patient sera, antibodies and complement source

AQP4-IgG-positive NMO sera were collected from patients treated in the Department of Neurology, Klinikum rechts der Isar, Technical University of Munich, Germany. Samples were stored in the biobank of the department, which is part of the Joint Biobank Munich in the framework of the German Biobank Node. Written informed consent was obtained from each participant. The study was approved by the ethics committee of the Technical University of Munich. All cases fulfilled the Wingerchuk diagnostic criteria for NMO (Wingerchuk et al., 2015). Healthy donor plasma was used as a control (Ctrl-IgGs) and three different sera of healthy subjects obtained from the 'blood bank' of the Bavarian Red Cross were pooled and served as complement source. AQP4-IgG-positive NMO and Ctrl-IgG samples were heat-inactivated. In some experiments, a human IgG1 recombinant antibody rAQP4-IgG (clone 7-5-53) reconstructed from a clonotypic plasma blast obtained from the CSF of an NMO patient was used (Bennett et al., 2009). The recombinant rCtrl-IgG (clone ICOS-5-2), a human IgG_1 antibody of unknown specificity from a meningitis patient, served as an isotype control.

Human tissue

To investigate axonal pathology, we screened formalin-fixed and paraffin-embedded biopsy and autopsy tissue from the archives of the Institute of Neuropathology at the University Medical Centre Göttingen. The study was approved by the local ethics committee. Of the 18

NMO patients with tissues available (9 biopsies and 9 autopsies), 7 lesions fulfilled the criteria for analysis, i.e. lesions localized in white matter tracts with longitudinally running axons. The samples were classified as early lesions, defined by the presence of recently infiltrated MRP14 positive macrophages (Bruck et al., 1995b; Winkler et al., 2021). Only biopsies from patients that were later tested to be AQP4-IgG-positive were included. The serological status was unknown in autopsied cases, as these NMO patients had died before AQP4-IgG testing was available. Neuropathologically, NMO was confirmed by the presence of inflammatory, demyelinating, macrophage-rich CNS-lesions with loss of GFAP- and AQP4-expressing astrocytes and relative axonal preservation (**Table 1**).

Table 1: Clinical data of NMO patients

Patient	B/A	Age/sex	Disease duration (years)	Serum AQP4-IgG	CNS region studied
1	B	37/f	9	positive	Occipital lobe
2	B	31/f	5	positive	Parietal lobe
3	B	57/m	10	positive	Parietal lobe
4	B	45/f	>2	positive	Spinal cord
5	B	42/m	10	positive	Frontal lobe
6	A	16/f	4	N/A	Pons
7	A	69/f	0.4	N/A	Pons

B=biopsy; A=autopsy; f=female; m=male; N/A=not available

Biopsies used as controls contained—besides diseased areas, which were not analyzed — neuro-pathologically normal white matter with axons that were assessable longitudinally. Except for one patient, autopsies showed no CNS pathology (**Table 2**).

Table 2: Clinical data of control patients

Patient	B/A	Age/sex	Neuropathological diagnosis	Cause of death	CNS region studied
1	B	76/m	Glioblastoma mult.	n/a	Frontal lobe
2	B	78/m	Vasculitis	n/a	Frontal lobe
3	B	81/m	Glioblastoma mult.	n/a	Temporal lobe
4	B	75/m	Multiple sclerosis	n/a	Corpus callosum
5	A	57/m	No CNS pathology	Cardiac arrest	Pons
6	A	57/f	No CNS pathology	Sepsis	Pons
7	A	39/f	No CNS pathology	Pulm. embolism	Pons
8	A	65/m	TBI	Trauma	Pons
9	A	38/f	No CNS pathology	Breast carcinoma	Pons

B=biopsy; A=autopsy; f=female; m=male; mult.= multifome; n/a=not applicablePulm.=Pulmonary; TBI=Traumatic brain injury

Formalin fixed paraffin embedded tissue was cut into 1-2 µm thick sections and used for histological and immunohistochemical stainings. To investigate astrocyte loss, immunohistochemistry was performed using antibodies directed against AQP4 (1:200, rabbit, Sigma Aldrich, #A5971) and GFAP (1:1000, rabbit, Dako, #A5971). LFB/PAS staining was

used to detect demyelination, while MRP14 immunohistochemistry (1:500, mouse, Acris, clone S36.48, #BM4026) served to detect recently infiltrated macrophages. Axonal pathology was investigated by Bielschowsky silver impregnation and immunohistochemistry for NF200 (1:400, mouse, clone N52, Sigma Aldrich, #N0142) for 'pearls-on-string' morphology at 400x magnification. Using Bielschowsky silver impregnation, axons with multiple swellings within NMO were counted and related to the lesion size measured with the software ImageJ/Fiji (Schindelin et al., 2012; Schneider et al., 2012). On the same slide, axons in a fixed area the adjacent non-lesioned white matter were evaluated. Additionally, neuropathologically normal white matter of control patients was analyzed. For NF200 immunohistochemistry, all beaded axons (also with single swellings) were quantified using a morphometric grid within the lesion, in the non-lesioned and in control white matter. All quantifications were performed at 400x magnification in at least 8 different fields of view and presented as counts per mm^2.

Mouse NMO model

Surgical procedures: Laminectomy surgery was performed as previously described (Nikic et al., 2011; Herwerth et al., 2016). In brief, mice were anesthetized by an intraperitoneal injection of meditomidin (0.5mg/kg), midazolam (5mg/kg) and fentanyl (0.05 mg/kg). Anesthesia was re-applied as needed. After a double dorsal laminectomy over the third lumbar (L3) and L4 segments, mice were suspended using compact spinal cord clamps (Davalos et al., 2008). An imaging window free from dura was established in the imaging area using a bent hypodermic needle. To allow superfusion with artificial cerebrospinal fluid (aCSF, in mM: 148.2 NaCl, 3.0 KCl, 0.8 Na_2HPO_4, 0.2 NaH_2PO_4, 1.4 $CaCl_2$ and 0.8 $MgCl_2$), a well around the opening was built using 2-3% agarose.

In vivo imaging: In vivo imaging of the lumbar spinal cord was performed as previously described (Nikic et al., 2011; Romanelli et al., 2013; Herwerth et al., 2016). Briefly, stacks were acquired using two-photon microscopes (Olympus FV1000 MPE or FVMPE-RS) tuned to 1000 nm to excite green and orange fluorescent proteins (GFP/OFP) at the same time. The systems were equipped with a x25/1.05 N.A water-dipping cone objective. Emission was first filtered through a 690 nm short-pass dichroic mirror; to separate the GFP and OFP channels, we used a G/R filter set (BA495-540, BA570-625) mounted in front of gallium arsenide phosphide (GaAsP) photomultiplier tubes. For FRET signal imaging in *Thy1:*TNXXL mice, the laser was tuned to 840 nm and a CFP/YFP cube (BA480/40, BA540/40) was positioned in front of GaAsP detectors to separate CFP and cpCitrine signals as previously described

(Williams et al., 2014). Time-lapse (xyzt) stacks were acquired at 10-minute intervals for 6 hours with the following parameters: 30-50 images (zoom 2.0; pixel size: 0.281 µm) at 1 µm z-step intervals.

Diluted recombinant antibodies (rAQP4-IgG vs rCtrl-IgG ICOS-5-2; 1,5µg/ml respectively) or heat-inactivated plasma (AQP4-IgG vs Ctrl-IgG; 150 µg/ml respectively) together with 20% of pooled healthy donor sera as a complement source was applied every 30 minutes for the first 2 hours; afterwards the solution was refreshed every 60 minutes. Under these experimental conditions, we have previously shown that phototoxicity and transgenic labeling does not significantly influence the health of spinal axons (Nikic et al., 2011; Romanelli et al., 2013; Williams et al., 2014; Herwerth et al., 2016). TTX (1 µM, Tocris) was washed in for 10 minutes before the start of the experiment. Mannitol (Sigma; 300 mM) was solved in aCSF and applied continuously throughout the experiment to achieve a stable hyperosmolar condition (200% of the initial osmolarity). Experiments with pharmacological manipulations were scored by a blinded observer.

FRET analysis: Data analysis was done as previously described (Williams et al., 2014). Time-lapse recordings were first inspected as z-projected image stacks and putative changes from low to high calcium were marked. Each such calcium transition was individually verified in unprocessed three-dimensional (3D) image stacks. Only axons that were observable at least 50 µm in length were included in the analysis. Local background was subtracted from each channel prior to calculating the cpCitrine/CFP ratio. Axons were scored as having elevated calcium levels if the cpCitrine/CFP ratio was 50% greater than at baseline cf. (Williams et al., 2014). Axonal caliber was measured as the diameter of individual axons in a representative area in unprocessed image stacks, using the Fiji plot profile plugin.

Epothilone B administration

For local administration, vehicle alone (PEG 300, Sigma) or epoB (Selleckchem, 5 µg/ml, dissolved in vehicle) was delivered during NMO experiment continuously via bath application from 30 minutes on until the end of the experiment (6 hours) in double transgenic *Aldh1l1:*GFP x *Thy1:*OFP3 mice. For systemic administration, mice were i.p. injected with 1.5 mg/kg BW epoB (dissolved in vehicle, 100 µl volume) or vehicle alone 24 hours prior to imaging experiments (Ruschel et al., 2015). No abnormal behavior or weight loss were observed in mice during this time-period.

Immunohistochemistry and confocal imaging

Mice were perfused transcardially with 4% paraformaldehyde (PFA) in 0.0.1M phosphate-buffered saline (1xPBS; in mM: 1.5 KH_2PO_4, 2.7 KCl, 8.1 Na_2HPO_4, and 137 NaCl), followed by an additional overnight fixation in 4% PFA. On the next days, whole mounts of lumbar spinal cord were extracted and kept in well-plates filled with 1xPBS for further staining procedures. Antibodies were diluted in 0.2% Triton X-100, 10% normal goat serum, and 1% bovine serum albumin in PBS. For tubulin staining, spinal cord tissue was incubated with Alexa Fluor 647-conjugated βIII-tubulin antibody (mouse; BioLegend, 1:200) for 6 days. Afterwards, the stained whole mounts of fixed spinal cords (2-4 spinal segments) were secured with the dorsal surface in contact with a cover glass in 2% agarose for imaging. Samples were scanned with an upright confocal microscope (Olympus FV1000) equipped with x20/ 0.8 N.A. and x60/1.42 N.A. oil-immersion objectives, as previously described (Williams et al., 2014; Herwerth et al., 2016). For quantification, regions of interest were drawn around beadings, then the mean gray values within and between the beadings were measured for each axon, and averaged for every channel. Background subtraction was applied to each single optical section, and the ratio of the mean gray values for the tubulin staining and the OFP3 signal were used to normalize for cytoplasmic content. The analysis of epoB experiments in *Aldh1l1:*GFP x *Thy1:*OFP mice was performed blinded to exclude observer bias.

Electron microscopy

Transmission electron microscopy (TEM): The animals used for the TEM experiment were perfused directly after the experiment with 5 mL HBSS, followed by 30 mL fixative (2.5% glutaraldehyde, 4% paraformaldehyde in phosphate buffer). The spinal cord at the laminectomy site was immersed in the same solution during the perfusion. After overnight fixation, the spinal cord was extracted and further post-fixed overnight at 4°C in the same fixative. The area below the laminectomy was collected and post-fixed with 2% OsO_4 and 1.5% ferricyanide (Science Services), dehydrated by ethanol, then acetone and finally Epon-embedded (Serva). 50 nm ultrathin sections from the area corresponding to the imaging site in the two-photon acute imaging experiment were contrasted with 4% uranyl acetate (Science Services) and lead citrate (Sigma). The imaging was done on a TEM JEM 1400plus (JEOL) equipped with an 8Mpixel camera (Ruby, JEOL). Large areas covering the first 20-30 micrometer from the dorsal pial surface of the spinal cord were imaged using the Shuttle-and-Find software at 8000 nm/pixel. Images were processed using the open-source image analysis software, Fiji.

Serial section electron microscopy using automated tape-collecting ultramicrotome (ATUM): we applied a standard rOTO en bloc staining protocol including a tannic acid incubation step. Spinal cord cross sections (0.5 mm thickness) were initially postfixed in 2% osmium tetroxide (EMS), 1.5% potassium ferricyanide (Sigma) in 0.1 M sodium cacodylate (Science Services) buffer (pH 7.4). After three washing steps in buffer and water, the staining was enhanced by reaction with 1% thiocarbohydrazide (Sigma) for 45 min at 40°C. The tissue was washed in water and incubated in 2% aqueous osmium tetroxide, washed and further contrasted by 0.2% tannic acid for 30 min. After overnight incubation in 1% aqueous uranyl acetate at 4°C and 2h at 50°C, Walton's lead aspartate treatment (L-aspartic acid, Sigma; lead nitrate, Alfa Aesar) was performed for 30 min at room temperature. The samples were dehydrated in an ascending ethanol series and infiltrated with Epon (medium hardness, Serva). In order to prevent folds, the dorsal part of the spinal cord cross section was supported by mouse cortex tissue (Hildebrand et al., 2017). The block was trimmed by 200 µm at a 90° angle on each side using a TRIM90 diamond knife (Diatome) on an ATUMtome (Powertome, RMC). Consecutive sections were taken with a 35° ultra-diamond knife (Diatome) at a nominal cutting thickness of 200 nm and collected on freshly plasma-treated (custom-built, based on Pelco easiGlow, adopted from M. Terasaki, U. Connecticut, CT), carbon-coated (R. Schalek, and J. Lichtman, Harvard U., Cambridge, MA.) Kapton tape (Kasthuri et al., 2015). Sections on Kapton were assembled onto adhesive carbon tape (Science Services) attached to 4-inch silicon wafers (Siegert Wafer). Kapton and silicon were connected by adhesive carbon tape strips (Science Services) for grounding. EM micrographs were acquired on a Crossbeam Gemini 340 SEM (Zeiss) with a four-quadrant backscatter detector at 8 kV. In ATLAS5 Array Tomography (Fibics), the whole wafer area was scanned at 8000 nm/pixel to generate an overview map. In total, 130-160 sections were selected and imaged at 200 x 200 x 200 nm^3 and a region at the dorsal spinal cord acquired at 20 x 20 x 200 nm^3. High resolution micrographs (3x3 nm^2) were taken from smaller regions on selected sections. The 20 x 20 x 200 nm^3 image stacks were aligned by a sequence of automatic and manual processing steps in Fiji TrakEM2 (Schindelin et al., 2012). VAST software was used for reconstructions (Berger et al., 2018). A region of 150 x 50 µm, in 50 µm distance from the middle dorsal vein, was used for quantification. The area of each numerated myelinated and unmyelinated axon was measured every 2 µm (10 slices) throughout the stack (130-160 slices). Only axons that could be followed by at least 70 slices were included. Given that the difference between control and mouse NMO experiments was obvious, we relinquished scoring the morphological axonal changes blindly. Axonal diameter changes were scored as swellings, if the diameter locally increased by least 50%.

Swellings that could not be followed completely were excluded from the analysis. The number of swellings per axon was referred to the measured length of axon to get a longitudinal density.

NMO survival surgeries

Mice were anaesthetized by i.p. injection of fentanyl (0.05 mg/kg), midazolam (5 mg/kg), meditomidin (0.5 mg/kg) (MMF). Anesthesia was re-applied when needed. After a double dorsal laminectomy over the L5 and L6 segments, the dura mater was punctured with the tip of a hypodermic needle to allow insertion of intrathecal catheter (ALZET® 0007743). The catheter was secured to surrounding tissues using 4-0 Ethilon sutures, and dorsal side was covered with 2% agarose in aCSF. Two additional punctures in the dura mater were made at the caudal end of the surgery site to avoid pressure increases during the superfusion. Recombinant antibodies rAQP4-IgG (7-5-53, 6µg/ml) or rCtrl-IgG (ICOS-5-2, 6µg/ml) with 20% of healthy donor serum, diluted in aCSF, were subdurally superfused for 90 minutes with a 150µl/h flow rate using a syringe pump. Afterwards, the catheter was removed and the surgical site was covered with 2% agarose in aCSF. The incision site was closed with wound clips, and mice were given post-surgery analgesia (Metacam, 2 mg/kg), followed by administration of Atipamezol (2.5 mg/kg), Flumazenil (0.5 mg/kg), Naloxon (1.2 mg/kg) to antagonize MMF. 0.9% NaCl solution was delivered s.c. for rehydration. Animals were kept on heating pads until fully recovered. Mice were sacrificed on the next day via isoflurane overdose and transcardially perfused with 1x PBS and 4% PFA. Tissues were fixed overnight with 4% PFA at 4°C. To define areas of substantial astrocyte depletion, whole-mounts of fixed spinal cords up to 4-5 segments in length were prepared. Tissues were embedded in 1% agarose in 1xPBS, with the dorsal surface facing a cover glass. These hanging drop preparations were scanned on an Olympus FV1000 confocal microscope with x20/0.8 N.A. and x60/1.42 N.A. oil-immersion objectives using z-steps of 1µm and 0.7µm, respectively. High-resolution images taken with an x60/1.42 N.A. objective were used for quantification. Only areas rostral to the surgical site were analyzed to avoid any surgery-related injuries. In rAQP4-IgG treated mice, only astrocyte depleted regions were included in the evaluation of axonal beading, which was performed blinded. Only the axons observable at least 50 µm in length were included in the analysis.

Image processing/representation

Images were processed using the open-source image analysis software Fiji and Adobe Creative Suite. For some figure representations, different channels of confocal image series

were combined using pseudo-color in Adobe Photoshop. In non-quantitative panels, gamma value was adjusted non-linearly to enhance visibility of low-intensity objects. Data sets were processed with Excel (Microsoft Corporation, Redmond, WA).

Data analysis

Results are presented as mean ± SEM. Statistical significance was analyzed with the GraphPad Prism 9 software (GraphPad Software, San Diego, California USA) using nonparametric t-tests followed by Mann-Whitney tests for comparing two groups and nonparametric ANOVA followed by Kruskal-Wallis tests for comparing more than two groups. P values < 0.05 were considered to be significant and indicated by "*", p values < 0.01 by "**" and <0.001 by "***".

References

Ballatore C, Brunden KR, Huryn DM, Trojanowski JQ, Lee VM, Smith AB, 3rd (2012) Microtubule stabilizing agents as potential treatment for Alzheimer's disease and related neurodegenerative tauopathies. J Med Chem 55:8979-8996.

Beirowski B, Nogradi A, Babetto E, Garcia-Alias G, Coleman MP (2010) Mechanisms of axonal spheroid formation in central nervous system Wallerian degeneration. J Neuropathol Exp Neurol 69:455-472.

Bennett JL, Owens GP (2017) Neuromyelitis Optica: Deciphering a Complex Immune-Mediated Astrocytopathy. J Neuroophthalmol 37:291-299.

Bennett JL, Lam C, Kalluri SR, Saikali P, Bautista K, Dupree C, Glogowska M, Case D, Antel JP, Owens GP, Gilden D, Nessler S, Stadelmann C, Hemmer B (2009) Intrathecal pathogenic anti-aquaporin-4 antibodies in early neuromyelitis optica. Ann Neurol 66:617-629.

Berger DR, Seung HS, Lichtman JW (2018) VAST (Volume Annotation and Segmentation Tool): Efficient Manual and Semi-Automatic Labeling of Large 3D Image Stacks. Front Neural Circuits 12:88.

Booth HDE, Hirst WD, Wade-Martins R (2017) The Role of Astrocyte Dysfunction in Parkinson's Disease Pathogenesis. Trends Neurosci 40:358-370.

Brill MS, Lichtman JW, Thompson W, Zuo Y, Misgeld T (2011) Spatial constraints dictate glial territories at murine neuromuscular junctions. J Cell Biol 195:293-305.

Brill MS, Kleele T, Ruschkies L, Wang M, Marahori NA, Reuter MS, Hausrat TJ, Weigand E, Fisher M, Ahles A, Engelhardt S, Bishop DL, Kneussel M, Misgeld T (2016) Branch-Specific Microtubule Destabilization Mediates Axon Branch Loss during Neuromuscular Synapse Elimination. Neuron 92:845-856.

Brosnan CF, Raine CS (2013) The astrocyte in multiple sclerosis revisited. Glia 61:453-465.

Bruck W, Bruck Y, Diederich U, Piddlesden SJ (1995a) The membrane attack complex of complement mediates peripheral nervous system demyelination in vitro. Acta Neuropathol 90:601-607.

Bruck W, Porada P, Poser S, Rieckmann P, Hanefeld F, Kretzschmar HA, Lassmann H (1995b) Monocyte/macrophage differentiation in early multiple sclerosis lesions. Ann Neurol 38:788-796.

Bruck W, Popescu B, Lucchinetti CF, Markovic-Plese S, Gold R, Thal DR, Metz I (2012) Neuromyelitis optica lesions may inform multiple sclerosis heterogeneity debate. Ann Neurol 72:385-394.

Cai H, Zhu J, Zhang N, Wang Q, Zhang C, Yang C, Sun J, Sun X, Yang L, Yu C (2017) Subregional structural and connectivity damage in the visual cortex in neuromyelitis optica. Sci Rep 7:41914.

Chen T, Lennon VA, Liu YU, Bosco DB, Li Y, Yi MH, Zhu J, Wei S, Wu LJ (2020) Astrocyte-microglia interaction drives evolving neuromyelitis optica lesion. J Clin Invest 130:4025-4038.

Coleman M (2005) Axon degeneration mechanisms: commonality amid diversity. Nat Rev Neurosci 6:889-898.

Coleman MP, Perry VH (2002) Axon pathology in neurological disease: a neglected therapeutic target. Trends Neurosci 25:532-537.

Coleman MP, Freeman MR (2010) Wallerian degeneration, wld(s), and nmnat. Annu Rev Neurosci 33:245-267.

Coleman MP, Hoke A (2020) Programmed axon degeneration: from mouse to mechanism to medicine. Nat Rev Neurosci 21:183-196.

Combes AJE, Matthews L, Lee JS, Li DKB, Carruthers R, Traboulsee AL, Barker GJ, Palace J, Kolind S (2017) Cervical cord myelin water imaging shows degenerative changes over one year in multiple sclerosis but not neuromyelitis optica spectrum disorder. Neuroimage Clin 16:17-22.

Court FA, Coleman MP (2012) Mitochondria as a central sensor for axonal degenerative stimuli. Trends Neurosci 35:364-372.

Curcio M, Bradke F (2018) Axon Regeneration in the Central Nervous System: Facing the Challenges from the Inside. Annu Rev Cell Dev Biol 34:495-521.

Datar A, Ameeramja J, Bhat A, Srivastava R, Mishra A, Bernal R, Prost J, Callan-Jones A, Pullarkat PA (2019) The Roles of Microtubules and Membrane Tension in Axonal Beading, Retraction, and Atrophy. Biophys J 117:880-891.

Davalos D, Lee JK, Smith WB, Brinkman B, Ellisman MH, Zheng B, Akassoglou K (2008) Stable in vivo imaging of densely populated glia, axons and blood vessels in the mouse spinal cord using two-photon microscopy. J Neurosci Methods 169:1-7.

Duan T, Smith AJ, Verkman AS (2018) Complement-dependent bystander injury to neurons in AQP4-IgG seropositive neuromyelitis optica. J Neuroinflammation 15:294.

Erturk A, Hellal F, Enes J, Bradke F (2007) Disorganized microtubules underlie the formation of retraction bulbs and the failure of axonal regeneration. J Neurosci 27:9169-9180.

Fernandez-Valenzuela JJ, Sanchez-Varo R, Munoz-Castro C, De Castro V, Sanchez-Mejias E, Navarro V, Jimenez S, Nunez-Diaz C, Gomez-Arboledas A, Moreno-Gonzalez I, Vizuete M, Davila JC, Vitorica J, Gutierrez A (2020) Enhancing microtubule stabilization rescues cognitive deficits and ameliorates pathological phenotype in an amyloidogenic Alzheimer's disease model. Sci Rep 10:14776.

Friese MA, Schattling B, Fugger L (2014) Mechanisms of neurodegeneration and axonal dysfunction in multiple sclerosis. Nat Rev Neurol 10:225-238.

Friese MA, Craner MJ, Etzensperger R, Vergo S, Wemmie JA, Welsh MJ, Vincent A, Fugger L (2007) Acid-sensing ion channel-1 contributes to axonal degeneration in autoimmune inflammation of the central nervous system. Nat Med 13:1483-1489.

Fujihara K (2019) Neuromyelitis optica spectrum disorders: still evolving and broadening. Curr Opin Neurol 32:385-394.

Greenberg MM, Leitao C, Trogadis J, Stevens JK (1990) Irregular geometries in normal unmyelinated axons: a 3D serial EM analysis. J Neurocytol 19:978-988.

Griffin JM, Bradke F (2020) Therapeutic repair for spinal cord injury: combinatory approaches to address a multifaceted problem. EMBO Mol Med 12:e11505.

Hellal F, Hurtado A, Ruschel J, Flynn KC, Laskowski CJ, Umlauf M, Kapitein LC, Strikis D, Lemmon V, Bixby J, Hoogenraad CC, Bradke F (2011) Microtubule stabilization reduces scarring and causes axon regeneration after spinal cord injury. Science 331:928-931.

Herwerth M, Kalluri SR, Srivastava R, Kleele T, Kenet S, Illes Z, Merkler D, Bennett JL, Misgeld T, Hemmer B (2016) In vivo imaging reveals rapid astrocyte depletion and axon damage in a model of neuromyelitis optica-related pathology. Ann Neurol 79:794-805.

Hildebrand DGC et al. (2017) Whole-brain serial-section electron microscopy in larval zebrafish. Nature 545:345-349.

Hinson SR, Pittock SJ, Lucchinetti CF, Roemer SF, Fryer JP, Kryzer TJ, Lennon VA (2007) Pathogenic potential of IgG binding to water channel extracellular domain in neuromyelitis optica. Neurology 69:2221-2231.

Hokari M, Yokoseki A, Arakawa M, Saji E, Yanagawa K, Yanagimura F, Toyoshima Y, Okamoto K, Ueki S, Hatase T, Ohashi R, Fukuchi T, Akazawa K, Yamada M, Kakita A, Takahashi H, Nishizawa M, Kawachi I (2016) Clinicopathological features in anterior visual pathway in neuromyelitis optica. Ann Neurol 79:605-624.

Jarius S, Paul F, Weinshenker BG, Levy M, Kim HJ, Wildemann B (2020) Neuromyelitis optica. Nat Rev Dis Primers 6:85.

Kasthuri N et al. (2015) Saturated Reconstruction of a Volume of Neocortex. Cell 162:648-661.

Kawachi I, Lassmann H (2017) Neurodegeneration in multiple sclerosis and neuromyelitis optica. J Neurol Neurosurg Psychiatry 88:137-145.

Kerschensteiner M, Schwab ME, Lichtman JW, Misgeld T (2005) In vivo imaging of axonal degeneration and regeneration in the injured spinal cord. Nat Med 11:572-577.

Knoferle J, Koch JC, Ostendorf T, Michel U, Planchamp V, Vutova P, Tonges L, Stadelmann C, Bruck W, Bahr M, Lingor P (2010) Mechanisms of acute axonal degeneration in the optic nerve in vivo. Proc Natl Acad Sci U S A 107:6064-6069.

Lennon VA, Kryzer TJ, Pittock SJ, Verkman AS, Hinson SR (2005) IgG marker of optic-spinal multiple sclerosis binds to the aquaporin-4 water channel. J Exp Med 202:473-477.

Lennon VA, Wingerchuk DM, Kryzer TJ, Pittock SJ, Lucchinetti CF, Fujihara K, Nakashima I, Weinshenker BG (2004) A serum autoantibody marker of neuromyelitis optica: distinction from multiple sclerosis. Lancet 364:2106-2112.

Levy M, Fujihara K, Palace J (2021) New therapies for neuromyelitis optica spectrum disorder. Lancet Neurol 20:60-67.

Liddelow SA et al. (2017) Neurotoxic reactive astrocytes are induced by activated microglia. Nature 541:481-487.

Linnerbauer M, Wheeler MA, Quintana FJ (2020) Astrocyte Crosstalk in CNS Inflammation. Neuron 108:608-622.

Lucchinetti CF, Guo Y, Popescu BF, Fujihara K, Itoyama Y, Misu T (2014) The pathology of an autoimmune astrocytopathy: lessons learned from neuromyelitis optica. Brain Pathol 24:83-97.

Maday S, Twelvetrees AE, Moughamian AJ, Holzbaur EL (2014) Axonal transport: cargo-specific mechanisms of motility and regulation. Neuron 84:292-309.

Mank M, Santos AF, Direnberger S, Mrsic-Flogel TD, Hofer SB, Stein V, Hendel T, Reiff DF, Levelt C, Borst A, Bonhoeffer T, Hubener M, Griesbeck O (2008) A genetically encoded calcium indicator for chronic in vivo two-photon imaging. Nat Methods 5:805-811.

Misu T, Hoftberger R, Fujihara K, Wimmer I, Takai Y, Nishiyama S, Nakashima I, Konno H, Bradl M, Garzuly F, Itoyama Y, Aoki M, Lassmann H (2013) Presence of six different lesion types suggests diverse mechanisms of tissue injury in neuromyelitis optica. Acta Neuropathol 125:815-827.

Nikic I, Merkler D, Sorbara C, Brinkoetter M, Kreutzfeldt M, Bareyre FM, Bruck W, Bishop D, Misgeld T, Kerschensteiner M (2011) A reversible form of axon damage in experimental autoimmune encephalomyelitis and multiple sclerosis. Nat Med 17:495-499.

Nitsch R, Pohl EE, Smorodchenko A, Infante-Duarte C, Aktas O, Zipp F (2004) Direct impact of T cells on neurons revealed by two-photon microscopy in living brain tissue. J Neurosci 24:2458-2464.

O'Sullivan D, Miller JH, Northcote PT, La Flamme AC (2013) Microtubule-stabilizing agents delay the onset of EAE through inhibition of migration. Immunol Cell Biol 91:583-592.

Ochs S, Jersild RA, Jr. (1987) Cytoskeletal organelles and myelin structure of beaded nerve fibers. Neuroscience 22:1041-1056.

Ochs S, Pourmand R, Jersild RA, Jr., Friedman RN (1997) The origin and nature of beading: a reversible transformation of the shape of nerve fibers. Prog Neurobiol 52:391-426.

Orem BC, Rajaee A, Stirling DP (2020) IP3R-mediated intra-axonal Ca(2+) release contributes to secondary axonal degeneration following contusive spinal cord injury. Neurobiol Dis 146:105123.

Osterloh JM et al. (2012) dSarm/Sarm1 is required for activation of an injury-induced axon death pathway. Science 337:481-484.

Ouardouz M, Nikolaeva MA, Coderre E, Zamponi GW, McRory JE, Trapp BD, Yin X, Wang W, Woulfe J, Stys PK (2003) Depolarization-induced Ca2+ release in ischemic spinal cord white matter involves L-type Ca2+ channel activation of ryanodine receptors. Neuron 40:53-63.

Papadopoulos MC, Verkman AS (2013) Aquaporin water channels in the nervous system. Nat Rev Neurosci 14:265-277.

Parratt JD, Prineas JW (2010) Neuromyelitis optica: a demyelinating disease characterized by acute destruction and regeneration of perivascular astrocytes. Mult Scler 16:1156-1172.

Pekny M, Pekna M, Messing A, Steinhauser C, Lee JM, Parpura V, Hol EM, Sofroniew MV, Verkhratsky A (2016) Astrocytes: a central element in neurological diseases. Acta Neuropathol 131:323-345.

Prineas JW, Lee S (2019) Multiple Sclerosis: Destruction and Regeneration of Astrocytes in Acute Lesions. J Neuropathol Exp Neurol 78:140-156.

Pullarkat PA, Dommersnes P, Fernandez P, Joanny JF, Ott A (2006) Osmotically driven shape transformations in axons. Phys Rev Lett 96:048104.

Raff MC, Whitmore AV, Finn JT (2002) Axonal self-destruction and neurodegeneration. Science 296:868-871.

Roemer SF, Parisi JE, Lennon VA, Benarroch EE, Lassmann H, Bruck W, Mandler RN, Weinshenker BG, Pittock SJ, Wingerchuk DM, Lucchinetti CF (2007) Pattern-specific loss of aquaporin-4 immunoreactivity distinguishes neuromyelitis optica from multiple sclerosis. Brain 130:1194-1205.

Romanelli E, Sorbara CD, Nikic I, Dagkalis A, Misgeld T, Kerschensteiner M (2013) Cellular, subcellular and functional in vivo labeling of the spinal cord using vital dyes. Nat Protoc 8:481-490.

Rothhammer V et al. (2018) Microglial control of astrocytes in response to microbial metabolites. Nature 557:724-728.

Ruschel J, Hellal F, Flynn KC, Dupraz S, Elliott DA, Tedeschi A, Bates M, Sliwinski C, Brook G, Dobrindt K, Peitz M, Brustle O, Norenberg MD, Blesch A, Weidner N, Bunge MB, Bixby JL, Bradke F (2015) Axonal regeneration. Systemic administration of epothilone B promotes axon regeneration after spinal cord injury. Science 348:347-352.

Schattling B, Steinbach K, Thies E, Kruse M, Menigoz A, Ufer F, Flockerzi V, Bruck W, Pongs O, Vennekens R, Kneussel M, Freichel M, Merkler D, Friese MA (2012) TRPM4 cation channel mediates

axonal and neuronal degeneration in experimental autoimmune encephalomyelitis and multiple sclerosis. Nat Med 18:1805-1811.

Schindelin J, Arganda-Carreras I, Frise E, Kaynig V, Longair M, Pietzsch T, Preibisch S, Rueden C, Saalfeld S, Schmid B, Tinevez JY, White DJ, Hartenstein V, Eliceiri K, Tomancak P, Cardona A (2012) Fiji: an open-source platform for biological-image analysis. Nat Methods 9:676-682.

Schneider CA, Rasband WS, Eliceiri KW (2012) NIH Image to ImageJ: 25 years of image analysis. Nat Methods 9:671-675.

Serna M, Giles JL, Morgan BP, Bubeck D (2016) Structural basis of complement membrane attack complex formation. Nat Commun 7:10587.

Shriver LP, Dittel BN (2006) T-cell-mediated disruption of the neuronal microtubule network: correlation with early reversible axonal dysfunction in acute experimental autoimmune encephalomyelitis. Am J Pathol 169:999-1011.

Singh S, Dallenga T, Winkler A, Roemer S, Maruschak B, Siebert H, Bruck W, Stadelmann C (2017) Relationship of acute axonal damage, Wallerian degeneration, and clinical disability in multiple sclerosis. J Neuroinflammation 14:57.

Sorbara CD, Wagner NE, Ladwig A, Nikic I, Merkler D, Kleele T, Marinkovic P, Naumann R, Godinho L, Bareyre FM, Bishop D, Misgeld T, Kerschensteiner M (2014) Pervasive axonal transport deficits in multiple sclerosis models. Neuron 84:1183-1190.

Stirling DP, Stys PK (2010) Mechanisms of axonal injury: internodal nanocomplexes and calcium deregulation. Trends Mol Med 16:160-170.

Stirling DP, Cummins K, Wayne Chen SR, Stys P (2014) Axoplasmic reticulum Ca(2+) release causes secondary degeneration of spinal axons. Ann Neurol 75:220-229.

Stys PK (1998) Anoxic and ischemic injury of myelinated axons in CNS white matter: from mechanistic concepts to therapeutics. J Cereb Blood Flow Metab 18:2-25.

Tradtrantip L, Asavapanumas N, Verkman AS (2020) Emerging therapeutic targets for neuromyelitis optica spectrum disorder. Expert Opin Ther Targets 24:219-229.

Tradtrantip L, Yao X, Su T, Smith AJ, Verkman AS (2017) Bystander mechanism for complement-initiated early oligodendrocyte injury in neuromyelitis optica. Acta Neuropathol 134:35-44.

Trapp BD, Stys PK (2009) Virtual hypoxia and chronic necrosis of demyelinated axons in multiple sclerosis. Lancet Neurol 8:280-291.

Vargas ME, Yamagishi Y, Tessier-Lavigne M, Sagasti A (2015) Live Imaging of Calcium Dynamics during Axon Degeneration Reveals Two Functionally Distinct Phases of Calcium Influx. J Neurosci 35:15026-15038.

Verkhratsky A, Sofroniew MV, Messing A, deLanerolle NC, Rempe D, Rodriguez JJ, Nedergaard M (2012) Neurological diseases as primary gliopathies: a reassessment of neurocentrism. ASN Neuro 4.

Waxman SG (2006) Axonal conduction and injury in multiple sclerosis: the role of sodium channels. Nat Rev Neurosci 7:932-941.

Waxman SG, Bennett MV (1972) Relative conduction velocities of small myelinated and non-myelinated fibres in the central nervous system. Nat New Biol 238:217-219.

Weil MT, Mobius W, Winkler A, Ruhwedel T, Wrzos C, Romanelli E, Bennett JL, Enz L, Goebels N, Nave KA, Kerschensteiner M, Schaeren-Wiemers N, Stadelmann C, Simons M (2016) Loss of Myelin

Basic Protein Function Triggers Myelin Breakdown in Models of Demyelinating Diseases. Cell Rep 16:314-322.

Williams PR, Marincu BN, Sorbara CD, Mahler CF, Schumacher AM, Griesbeck O, Kerschensteiner M, Misgeld T (2014) A recoverable state of axon injury persists for hours after spinal cord contusion in vivo. Nat Commun 5:5683.

Wingerchuk DM, Pittock SJ, Lucchinetti CF, Lennon VA, Weinshenker BG (2007) A secondary progressive clinical course is uncommon in neuromyelitis optica. Neurology 68:603-605.

Wingerchuk DM, Banwell B, Bennett JL, Cabre P, Carroll W, Chitnis T, de Seze J, Fujihara K, Greenberg B, Jacob A, Jarius S, Lana-Peixoto M, Levy M, Simon JH, Tenembaum S, Traboulsee AL, Waters P, Wellik KE, Weinshenker BG, International Panel for NMOD (2015) International consensus diagnostic criteria for neuromyelitis optica spectrum disorders. Neurology 85:177-189.

Winkler A, Wrzos C, Haberl M, Weil MT, Gao M, Mobius W, Odoardi F, Thal DR, Chang M, Opdenakker G, Bennett JL, Nessler S, Stadelmann C (2021) Blood-brain barrier resealing in neuromyelitis optica occurs independently of astrocyte regeneration. J Clin Invest 131.

Witte ME, Schumacher AM, Mahler CF, Bewersdorf JP, Lehmitz J, Scheiter A, Sanchez P, Williams PR, Griesbeck O, Naumann R, Misgeld T, Kerschensteiner M (2019) Calcium Influx through Plasma-Membrane Nanoruptures Drives Axon Degeneration in a Model of Multiple Sclerosis. Neuron 101:615-624 e615.

Wolf JA, Stys PK, Lusardi T, Meaney D, Smith DH (2001) Traumatic axonal injury induces calcium influx modulated by tetrodotoxin-sensitive sodium channels. J Neurosci 21:1923-1930.

Yang J, Weimer RM, Kallop D, Olsen O, Wu Z, Renier N, Uryu K, Tessier-Lavigne M (2013) Regulation of axon degeneration after injury and in development by the endogenous calpain inhibitor calpastatin. Neuron 80:1175-1189.

Yun SP et al. (2018) Block of A1 astrocyte conversion by microglia is neuroprotective in models of Parkinson's disease. Nat Med 24:931-938.

Zhang B, Carroll J, Trojanowski JQ, Yao Y, Iba M, Potuzak JS, Hogan AM, Xie SX, Ballatore C, Smith AB, 3rd, Lee VM, Brunden KR (2012) The microtubule-stabilizing agent, epothilone D, reduces axonal dysfunction, neurotoxicity, cognitive deficits, and Alzheimer-like pathology in an interventional study with aged tau transgenic mice. J Neurosci 32:3601-3611.

Acknowledgements

We thank M. Budak, N. Budak, P. Apostolopoulos and S. Taskin for animal husbandry and Y. Hufnagel, K. Wullimann, M. Schetterer, V. Grummel, K. Schulz and O. Kowatsch for technical and administrative support. We thank G. Kislinger for rendering and reconstruction and K. Heise for support with the analysis of EM data. The *Aldh1l1*:GFP mouse strain used for this project (STOCK Tg(Aldh1l1-EGFP)OFC789Gsat/Mmucd; identification no.: 011015-UCD) was obtained from the Mutant Mouse Regional Resource Center, a NCRR-NIH-funded strain repository, and was donated to the MMRRC by the NINDS funded GENSAT BAC transgenic project.

Funding

This project was supported by the Deutsche Forschungsgemeinschaft (DFG) grant TRR 274/1 2020 (B03 to MH, CS and TM; Z01 to MS – ID 408885537), as well as under Germany's Excellence Strategy within the framework of the Munich Cluster for Systems Neurology (EXC 2145 SyNergy – ID 390857198; to TM, BH, MS) and by the Gemeinnützige Hertie foundation (P1150064 to MH, BH and TM; Hertie Network of Excellence in Clinical Neuroscience grant to NS). BH's laboratory was further by the EU consortium MultipleMS and the BMBF funded Clinspect-M project. TM is supported by European Research Council under the European Union's Seventh Framework Program (grant no. FP/2007-2013; ERC Grant Agreement no.: 616791), the German Center for Neurodegenerative Disease (DZNE) and the DFG (CRC870 A11 – ID 118803580, Mi 694/7-1 – ID 299370739, Mi 694/8-1 – ID 323061152, Mi 694/9-1 A03 – ID 428663564). CS was further supported by the DFG (CRC 43, STA 1389/2-1, STA 1389/5-1, and under Germany's Excellence Strategy, EXC 2067/1 – ID 390729940), the Gemeinnützige Hertie Foundation, the Deutsche Multiple Sklerose Gesellschaft (DMSG), and the National MS Society (USA). NS's research is supported by a DFG research (426715780) and by the Hertie Network of Excellence in Clinical Neuroscience (P1200019). SK received support from the DFG-funded Graduate School of Systemic Neurosciences (GSC 82 – ID 24184143). JLB is supported by the National Institutes of Health (EY022936).

Author Contributions

MH, SK, BH and TM are responsible for the concept and study design. MH, SK, AW, CS, MW, MS, NS, JLB were involved in sample/data acquisition and analysis. MH, SK, BH and TM drafted the manuscript and figures with input from all the authors. MH and SK contributed equally as first authors. BH and TM contributed equally as senior authors.

Competing Interests

TM, SK, NS, MS, AW: No competing interests. MH received speaker honoraria from Alexion Company (outside of the submitted work). CS served on scientific advisory boards for Roche, Merck, and Novartis; she received speaker's honoraria from Roche, Merck, and Novartis; her institution received research grants from Novartis, Roche, and medDay. BH has served on scientific advisory boards for Novartis; he has served as DMSC member for AllergyCare, Polpharma and TG therapeutics; he or his institution have received speaker honoraria from Desitin; his institution received research grants from Regeneron for MS research. He holds part of two patents; one for the detection of antibodies against KIR4.1 in a subpopulation of patients with MS and one for genetic determinants of neutralizing antibodies to interferon. None of these activities causes a conflict of interest relevant to the topic of the study.

Data and Material Availability

All data are available in the main text or the supplementary materials. Primary data tables will be made available by the authors on reasonable request. Mouse lines can be requested from the providing investigators and are protected by standard MTAs.

Figure 1

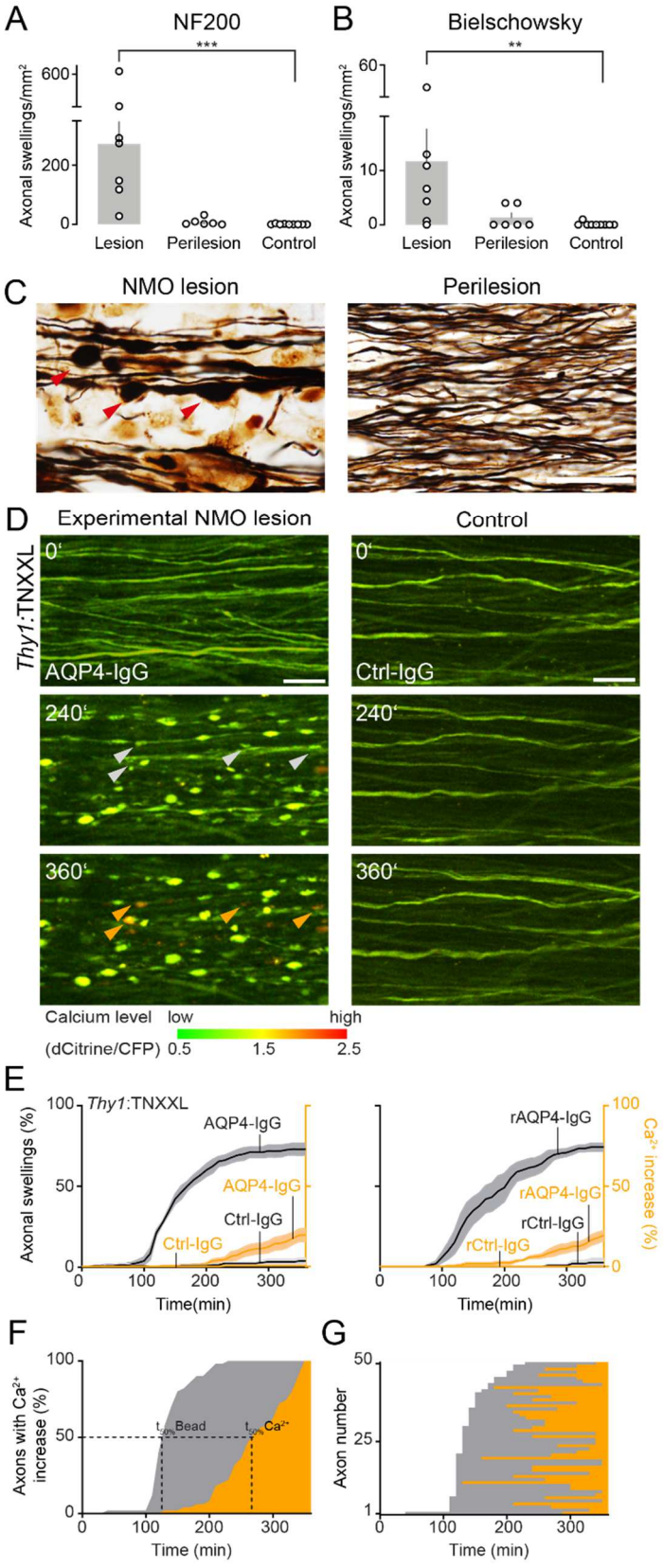
A
NF200
***
Axonal swellings/mm²
600
200
0
Lesion
Perilesion
Control
B
Bielschowsky
**
60
10
C
NMO lesion
Perilesion
D
Experimental NMO lesion
Control
Thy1:TNXXL
0'
AQP4-IgG
Ctrl-IgG
240'
360'
Calcium level
low
high
(dCitrine/CFP) 0.5
1.5
2.5
E
Axonal swellings (%)
Thy1:TNXXL
AQP4-IgG
Ctrl-IgG
rAQP4-IgG
rCtrl-IgG
Ca²⁺ increase (%)
Time(min)
F
Axons with Ca²⁺ increase (%)
Bead
Ca²⁺
Time (min)
G
Axon number
Time (min)

Figure 1: *Axonal beading occurs in NMO lesions and precedes calcium rise.*

(**A**) Density of beaded axons quantified in NF200 staining and (**B**) Bielschowsky silver impregnations. NMO lesions (beaded axons/ μm^2: Bielschowsky: 11.7 ± 6.0, NF200: 271.1 ± 75.6; n = 7 patients), perilesion (Bielschowsky: 1.3 ± 0.8, NF200: 8.3 ± 4.9; n = 6), control white matter (Bielschowsky: 0.1 ± 0.1, NF200: 0.7 ± 0.5; n = 9). Data represent mean ± SEM; NMO lesions vs control ** p = 0.004 (left), *** p = 0.0002 (right); Kruskal-Wallis test followed by Dunn's multiple comparisons test

(**C**) Representative "pearls-on-string" axonal beading (red arrowheads) morphology in a Bielschowsky silver impregnation of an early NMO lesions (left). Very few beadings were observed in perilesional white matter (right). Scale bar: 20 µm.

(**D**) *In vivo* two-photon time-lapse imaging showing development of axonal beadings (white arrowheads) and intracellular calcium rise (orange arrowheads) at the indicated times (minutes) after AQP4-Ig/complement application. Axons remain unaffected in control experiments (Ctrl-IgG/complement). Calcium levels pseudo-color coded as indicated; scale bar: 20 µm.

(**E**) Increase of beaded (gray) and high calcium-containing axons (orange) in *Thy1*:TNXXL mice over 6h after experimental NMO lesion induction. The majority of labeled axons showed beading (Left, AQP4-IgG: 73.0 ± 3.7%, n = 5 mice vs. control: Ctrl-IgG: 3.4 ± 1.7%, n = 4. Right, rAQP4-IgG: 74.3 ± 2.4%, n = 4;; rCtrl-IgG 2.5 ± 2.5%, n = 3), Mann Whitney test, * p (AQP4-IgG vs Ctrl-IgG) = 0.015. Some beadings followed by calcium rise (threshold: dCitrine/CFP ≥ 1.5. Left, NMO AQP4-IgG: 19.6 ± 3.9% vs. control Ctrl-IgG: 0.5 ± 0.5%. Right, rAQP4-IgG: 19.4 ± 3.1% vs. rCtrl-IgG 0 ± 0%). Data represent mean ± SEM. n >200 axons were analyzed for each condition.

(**F**) Population and (**G**) axon individual (ordered by time of beading onset) data showing the relative time-course of beading (gray) and calcium elevation (orange) in the subset of axons that lost calcium homeostasis. While on average, the calcium rise was delayed by 136 ± 9 min ($t_{50\%}$[beading] – $t_{50\%}$[calcium rise]; mean ± SEM), on an axon-to-axon there is no consistent temporal relationship between the time of beading and of calcium rise. n = 50 high-calcium axons from 5 experiments.

Figure 2

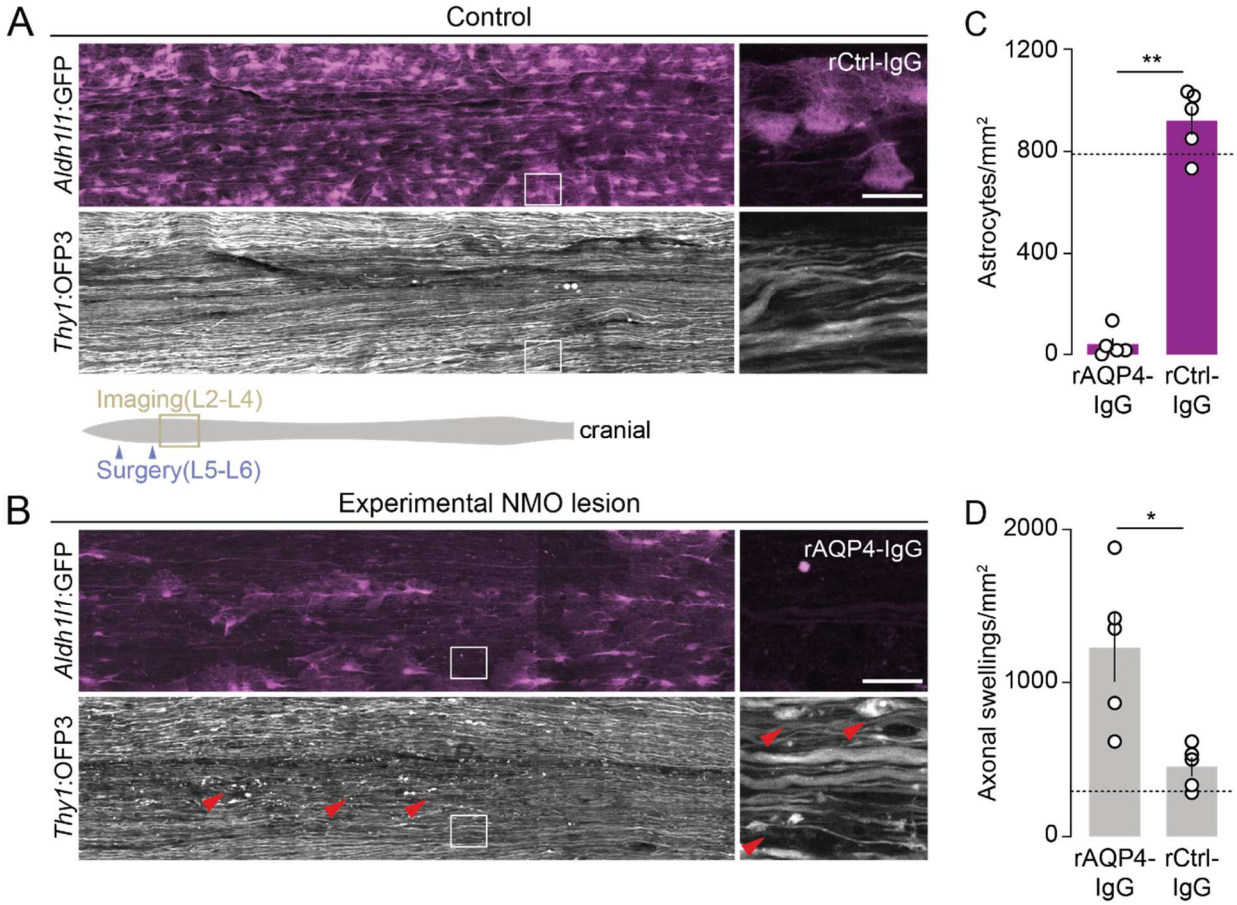
A
Control
Aldh1l1:GFP
Thy1:OFP3
rCtrl-IgG
Imaging(L2-L4)
cranial
Surgery(L5-L6)
B
Experimental NMO lesion
rAQP4-IgG
C
Astrocytes/mm²
1200
800
400
0
**
rAQP4-IgG
rCtrl-IgG
D
Axonal swellings/mm²
2000
1000
0
*
rAQP4-IgG
rCtrl-IgG

Figure 2: *Astrocyte depletion leads to persistent axonal beading in experimental NMO lesions.*

(**A-B**) Representative overview confocal images of spinal cord whole-mounts of *Aldh1l1*:GFP x *Thy1*:OFP3 mice. In control tissue (**A**), astrocytes (*Aldh1l1:*GFP, magenta) remained mostly unaffected 24h after superfusion with rCtrl-IgG/complement (90 min) with only a small number of axon showing swellings (*Thy1:*OFP3, grey; arrowhead) in control tissue, possibly due to surgery. In experimental NMO lesions 24h after superfusion with rAQP4-IgG/complement (for 90 min; **B**), astrocyte loss and axonal beadings (arrowheads) were apparent. Note patchy astrocyte loss likely due to the non-homogenous distribution of rAQP4-IgG/complement in subdural space, only substantially astrocyte-depleted areas were included in analysis.

(**C**) Astrocyte density within analyzed areas of chronic lesions and control treated spinal tissue (rCtrl-IgG: 920 ± 57 vs. rAQP4-IgG: 40 ± 24 mm^{-2}, n = 5 mice each).

(**D**) Density of beaded axons in experimental NMO lesions vs. control-treated spinal tissue (rCtrl-IgG: 453 ± 63 vs. rAQP4-IgG: 1227 ± 222 mm^{-2}, n = 5 mice each). Only astrocyte depleted regions were included in the analysis for the rAQP4-IgG group.

Dashed lines indicate the average density of astrocytes (C) and swollen axons (D) quantified in mice without any surgical interventions (n = 3 mice). Schematic representation of spinal cord (gray) with surgery (purple arrowheads) and imaging (yellow box) areas is shown between A and B. Boxed areas are magnified on the right. $n \geq 48$ axons were analyzed per animal. Data represented as mean ± SEM. Mann Whitney test; **p = 0.0079 in C, *p = 0.0159 in D. Scale bars: 40 µm.

Figure 3

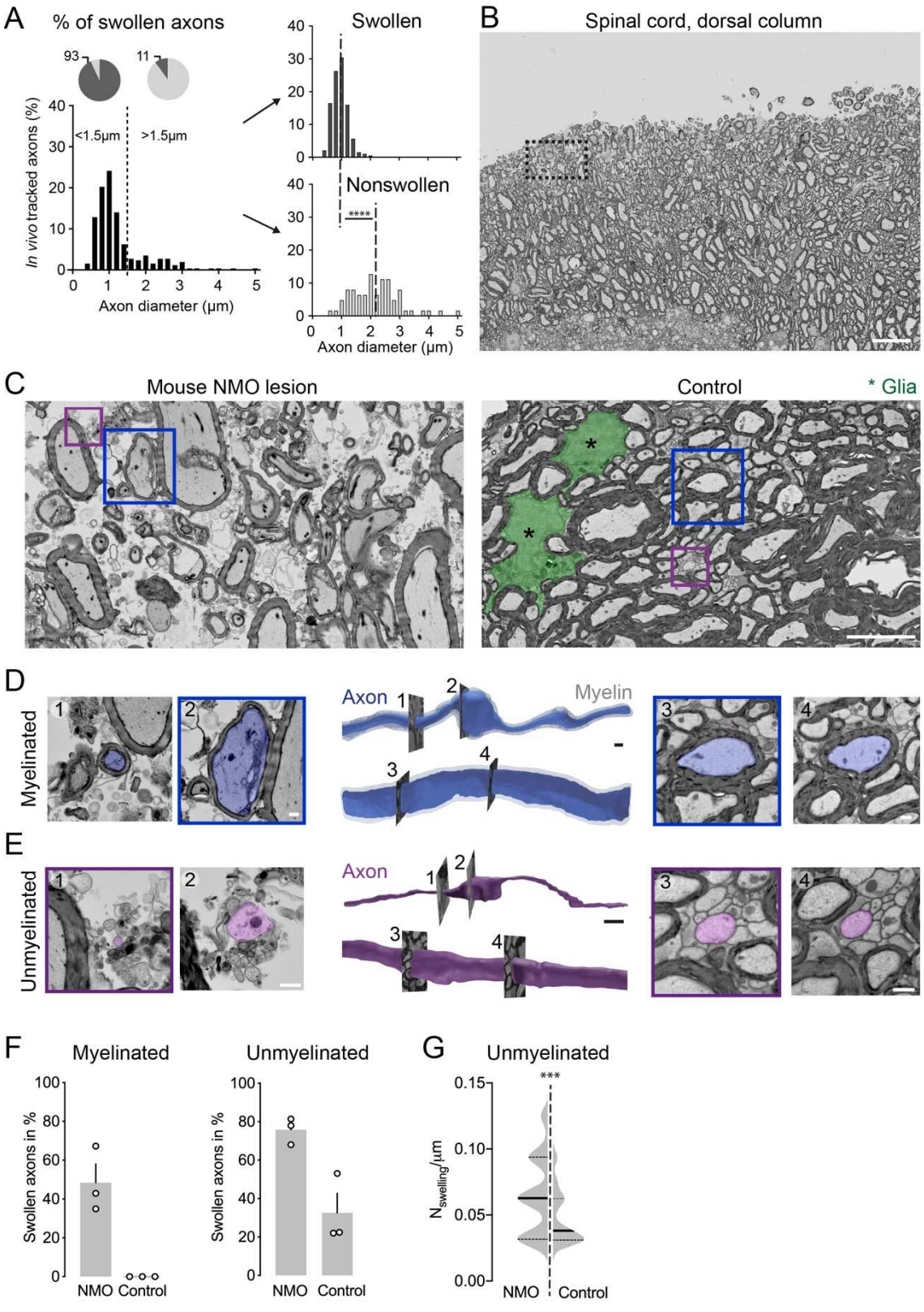
A
% of swollen axons
93
11
<1.5µm
>1.5µm
In vivo tracked axons (%)
Axon diameter (µm)
Swollen
Nonswollen
****
B
Spinal cord, dorsal column
C
Mouse NMO lesion
Control
* Glia
D
Myelinated
Axon
Myelin
E
Unmyelinated
F
Myelinated
Unmyelinated
Swollen axons in %
NMO
Control
G
Unmyelinated
***
N swelling/µm

Figure 3: *Electron microscopy (EM) analysis of axonal pathology in experimental NMO lesions.*

(**A**) Histograms of axon caliber distribution of the axon population imaged *in vivo* in *Thy1:*TNXXL mice (>250 axons from n = 5 mice, binning 0.2 µm). Overall population (left) and split into swollen/non-swollen (right) after 6h of AQP4-IgG/complement application. Pie charts: Thin axons were more likely to swell (<1.5 µm: 93 ± 1.7% vs. >1.5 µm: 9.1 ± 3.2%; n = 5 mice). Dashed lines in right diagrams represents mean of initial diameter in swollen and non-swollen axon populations. Data represent mean ± SEM. Mann Whitney test, ****p < 0.0001.

(**B-C**) Volume EM analysis by tape-based scanning EM of mouse spinal lesions 6h after NMO induction (resolution: 20x20x200 nm^3). (**B**) shows cross-section image of dorsal spinal column. Boxed area: x-y position of the 3D data series used in C. Scale bar: 20µm. Higher magnification images of experimental NMO lesion (**C**, left) shows edema, glial cell loss and axonal injury. In control tissue (right), tightly packed axons and glial cells (green) were visible without signs of edema or cell loss. Boxes: Axons analyzed in (D) and (E). Scale bar: 5µm.

(**D-E**) 3D surface rendering of myelinated (**D**; axon: blue, myelin: gray) and unmyelinated axons (**E**; purple). Representative cross-sections of non-swollen (1) and swollen (2) axon segments in experimental NMO lesion (left) and of non-swollen axons with comparable diameters (3, 4) in control conditions (right). Scale bar: 1µm.

(**F**) Percentage of swollen axons in myelinated (NMO: 47.4 ± 10.4%; control: 0.00 ± 0.0%) and unmyelinated (NMO: 74.1 ± 4.4% right; control: 30.5 ± 11.3%) axon populations. NMO: n_{myel} = 411, n_{unmyel} = 142; Control: n_{myel} = 319, n_{unmyel} = 148 axons; N=3 mice.

(G) Density plot of beadings of unmyelinated axons in experimental NMO lesions (0.065 ± 0.003, left) vs. control tissue (0.046 ± 0.003, right). Myelinated axons are not plotted, as no swellings were observed in controls (F). Bold lines: median, dashed lines: quartiles. Data represent mean ± SEM. Mann Whitney test, ***p < 0.001.

Figure 4

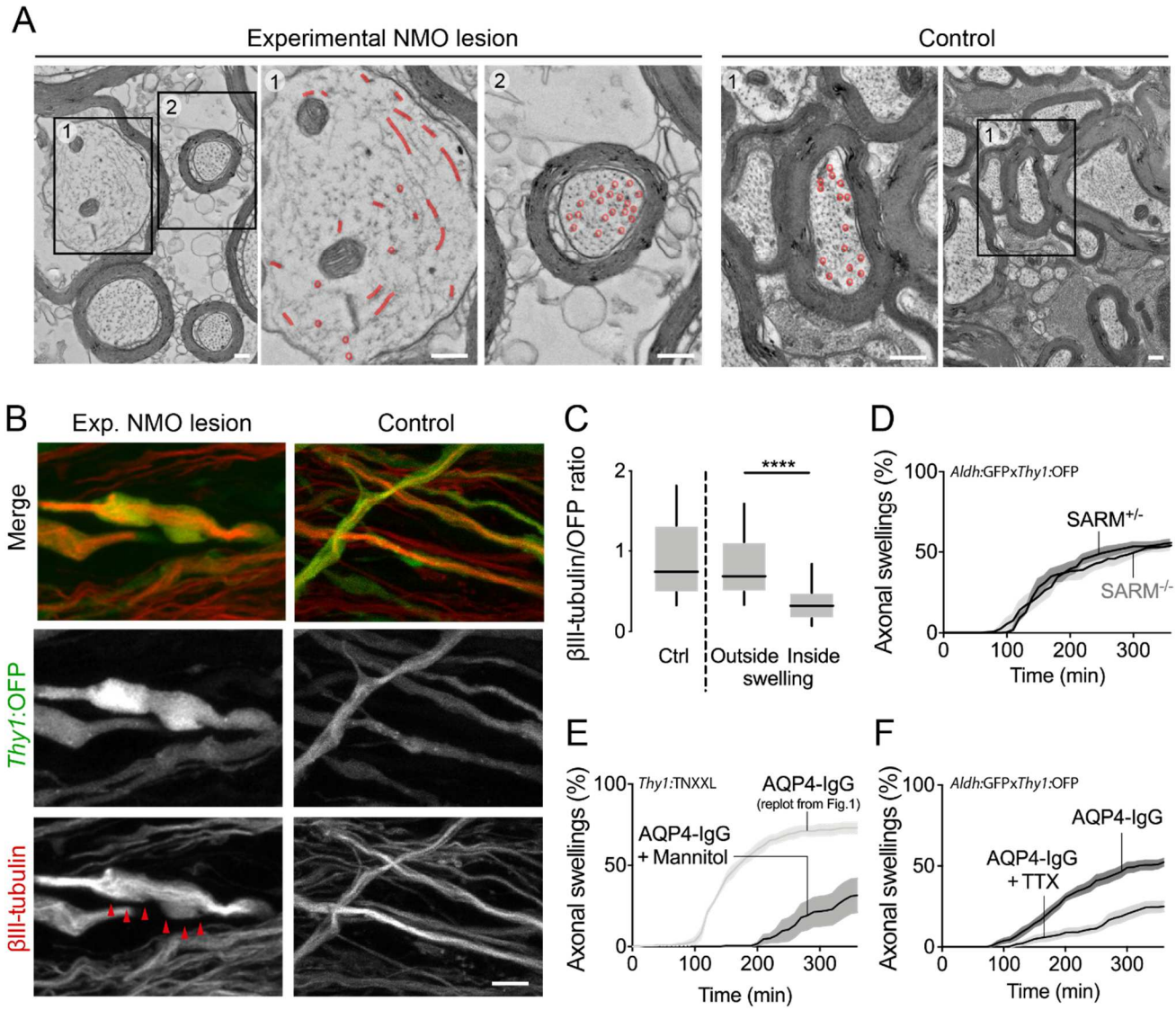
A
Experimental NMO lesion
Control
1
2
B
Exp. NMO lesion
Control
Merge
Thy1:OFP
βIII-tubulin
C
βIII-tubulin/OFP ratio
****
Ctrl
Outside swelling
Inside swelling
D
Aldh:GFPxThy1:OFP
SARM+/-
SARM-/-
Axonal swellings (%)
Time (min)
E
Thy1:TNXXL
AQP4-IgG
(replot from Fig.1)
AQP4-IgG + Mannitol
F
AQP4-IgG
AQP4-IgG + TTX

Figure 4: *Axonal beadings show cytoskeletal disruptions, driven by ionic and osmotic overload.*

(**A**) High-resolution transmission EM analysis of swollen axons in an experimental NMO lesion shows edema and microtubule disorganization (red) within beadings (left, 1). Well-arranged, densely packed microtubules (red) are visible in neighboring non-swollen axon areas (2) and in control tissue (right, 1). Scale bar: 200 nm.

(**B**) Confocal image of *Thy1:*OFP3 spinal cord axons (green), stained with βIII-tubulin antibody (red) after 6h application of AQP4-IgG or Ctrl-IgG/complement. Red arrowheads point to an axon bead containing disorganized microtubules. Scale bar: 5 µm.

(**C**) Quantification of βIII-tubulin mean fluorescent intensity (MFI) normalized to OFP signal of *Thy1:*OFP3 axons in control tissue (median: 0.75, n = 137 axons) and experimental NMO lesions (median, outside: 0.69; inside: 0.32, n = 102 axons; 5 mice for each condition). Box-and-whisker plot: 10-90 percentile. Kruskal-Wallis test followed by Dunn's multiple comparisons test using axons, ***$p < 0.0001$.

(**D**) Percentage of swollen axons within 6h of experimental NMO lesion induction was similar in SARM1-deficient KO vs. heterozygous mice in *Aldh1l1:*GFPx*Thy1:*OFP3 background ($SARM1^{-/-}$: 54.0 ± 3.1%; $SARM^{-/+}$: 55.5 ± 2.7%; from n = 5 mice each), as well as to wild type *Thy1:*OFP3 mice (cf. F, below).

(**E**) Local application of hyperosmolar (200% of the initial osmolarity) mannitol solution delayed and diminished beading in NMO spinal lesions (mean ± SEM: 31.5 ± 10.4%, n = 5 *Thy1:*TNXXL mice). Percentage of swollen axons induced by AQP4-IgG/complement under normal osmotic conditions from Fig.1 re-plotted for comparison (73.0 ± 3.7 %, n = 5). Mann-Whitney test, ** $p = 0.0079$.

(**F**) Local treatment with voltage-gated sodium channel blocker TTX (1 µM) reduced the number of swollen axons (mean ± SEM, TTX: 25.0 ± 3.2%; vehicle: 52.4 ± 2.4%; n = 6 *Aldh1l1:*GFPx*Thy1:*OFP3 mice for each condition). Mann-Whitney test, ** $p = 0.0022$.

Figure 5

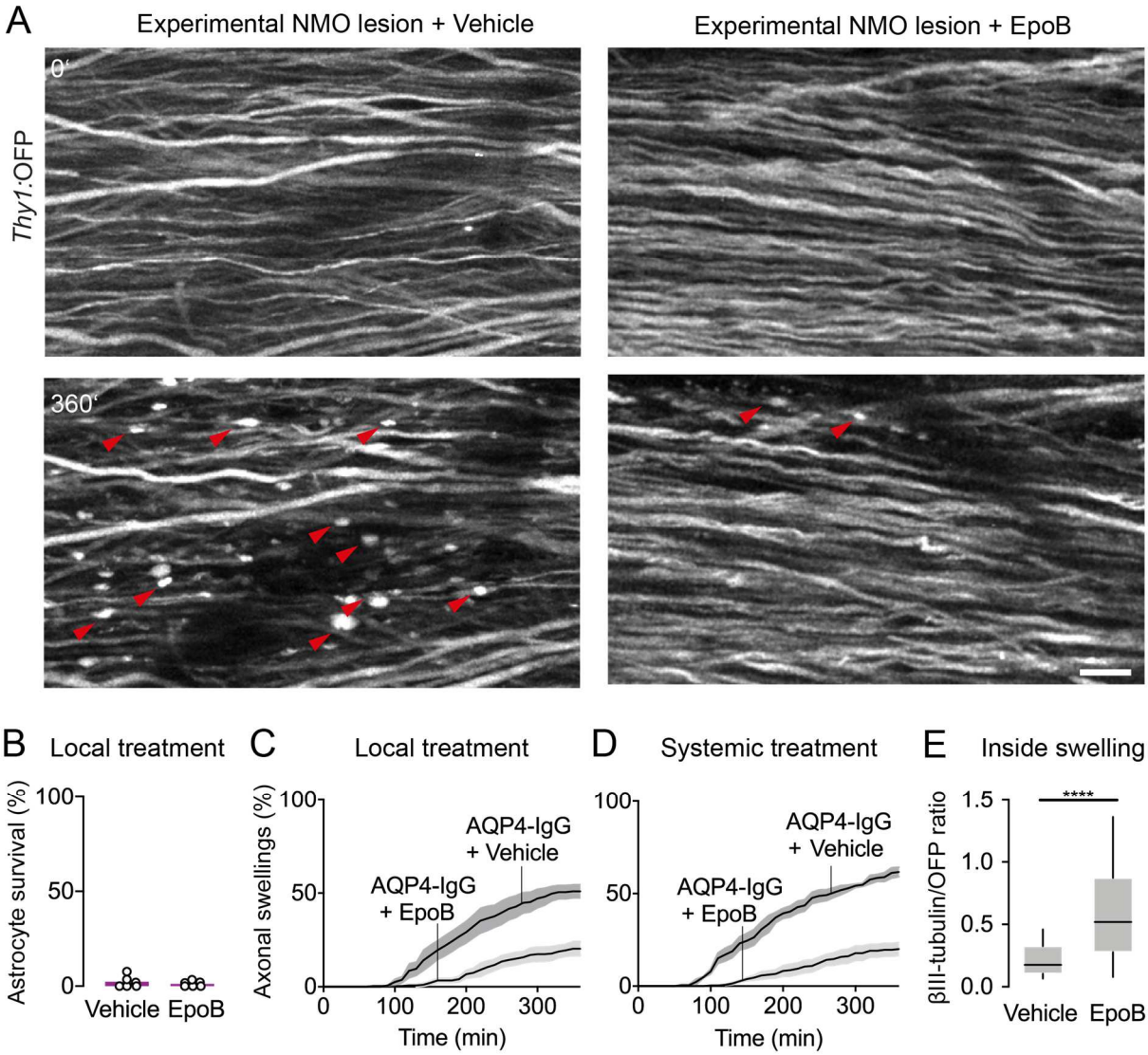
A
Experimental NMO lesion + Vehicle
Experimental NMO lesion + EpoB
Thy1:OFP
0'
360'
B
Local treatment
Astrocyte survival (%)
100
50
0
Vehicle
EpoB
C
Local treatment
Axonal swellings (%)
AQP4-IgG
+ Vehicle
AQP4-IgG
+ EpoB
Time (min)
D
Systemic treatment
E
Inside swelling
βIII-tubulin/OFP ratio
****
1.5
1.0
0.5
0.0

Figure 5: *Microtubule stabilization protects axons from beading.*

(**A**) *In vivo* two photon imaging of *Aldh1l1:*GFPx*Thy1*:OFP mice spinal cord axons within 6h of experimetal NMO lesion induction with local epoB (5µg/ml) or vehicle application. Red arrowheads indicate axonal beading, which is diminished with epoB treatment. Scale bar: 20 µm.

(**B**) Unchanged depletion of spinal cord astrocytes following local epoB or vehicle treatment (survival after 3h, epoB: 2.3 ± 1.3% vs. vehicle: 1.2 ± 0.6%; n = 6 mice each).

(**C**) Quantification of axonal beading after 6h local epoB treatment (epoB: 19.9 ± 3.1%; vehicle: 50.9 ± 3.8%, n = 6 mice each). Mann Whitney test, $p < 0.01$.

(**D**) The fraction of beaded axons was reduced following systemic administration of epoB 24h prior to lesion induction (after 6h: 19.2 ± 3.4% vs. vehicle: 61.6 ± 2.5%, n = 5, 4 mice respectively) Mann Whitney test; $p < 0.05$.

(**E**) Quantification of βIII-tubulin staining mean fluorescent intensity (MFI) normalized to OFP signal in *Thy1*:OFP mice. Local epoB treatment preserved tubulin staining compared to vehicle (median, vehicle: 0.17 vs. epoB: 0.52, n = 188, 65 axons respectively in 5 mice each).

Mann Whitney test; ****$p < 0.0001$. Box-and-whisker plot: 10-90 percentile. Data represent mean ± SEM in B-D.

Manuscript II

Membrane attack complex initiates oligodendrocyte injury in neuromyelitis optica-related mouse model

Selin Kenet[1,2], Marina Herwerth[1,3,*], Jeffrey L. Bennett[4], Bernhard Hemmer[3,5] and Thomas Misgeld[1,5,6]

Manuscript in preparation

Contributions to the paper: I performed all the experiments and the data analysis presented in the manuscript. I drafted the manuscript with the input from Marina Herwerth and Thomas Misgeld.

Membrane attack complex initiates oligodendrocyte injury in neuromyelitis optica-related mouse model

Selin Kenet[1,2], Marina Herwerth[1,3,*], Jeffrey L. Bennett[4], Bernhard Hemmer[3,5] and Thomas Misgeld[1,5,6]

[1]Institute of Neuronal Cell Biology, Technical University of Munich, Munich, Germany.

[2]Graduate School of Systemic Neurosciences, Ludwig-Maximilians University, Munich, Germany.

[3]Department of Neurology, Klinikum rechts der Isar, Technical University of Munich, Germany.

[4]Department of Neurology and Ophthalmology, University of Colorado School of Medicine, Aurora USA.

[5]Munich Cluster of Systems Neurology (SyNergy), Munich, Germany.

[6]German Center for Neurodegenerative Diseases (DZNE), Munich, Germany.

*Present address: Institute of Pharmacology and Toxicology, University of Zurich, Zurich, Switzerland.

Abstract

Neuromyelitis optica spectrum disease (NMOSD) is an autoimmune disease predominantly affecting spinal cord and optic nerve. The majority of NMOSD patients have serum antibodies (IgG) against the water channel protein aquaporin-4 (AQP4), which is in the CNS expressed on astrocytic end-feet and ependymal cells. Despite this primary astrocytic target, demyelination is also prominent in AQP4-IgG seropositive NMO patients, and is regarded as secondary to astrocyte loss. However, it remains unresolved how targeting of an astrocytic antigen drives injury of other cell types, such as oligodendrocytes.

Here, we investigated early signs of oligodendrocyte damage in a mouse model of experimental NMO induced by spinal application of patient-derived AQP4-IgG and human complement followed by in vivo imaging. Morphological assessment and calcium imaging of genetically labeled astrocytes and oligodendrocytes revealed a membrane attack complex (MAC)-mediated fast spread mechanism of NMO pathology. Within an hour of AQP4-IgG application, intracellular calcium levels in astrocytes increased globally and membrane rupture swiftly followed as confirmed by uptake of a cell-impermeable nuclear dye and subsequent cellular fragmentation. Concurrent to the global astrocytic calcium rise, oligodendrocyte processes also showed transient calcium overload, which however reached the somata comparatively later. In contrast to the pervasive and swift lytic cell death of astrocytes, only some oligodendrocytes were lost at later time points. While dye exclusion experiments negated overt membrane rupture, expression of human MAC-inhibitor protein CD59 on oligodendrocytes still protected these cells from secondary damage after AQP4-IgG–mediated astrocyte injury.

These results imply that oligodendrocyte pathology in AQP4-IgG+ NMO is not driven by the loss of astrocytes per se, but rather evolves from MAC-dependent ‘bystander’ targeting of oligodendrocytes. At the same time, our dynamic observations suggest that despite the similar MAC-mediated starting point of glial injury, the executive phase of cell damage might differ and could result in activation of distinct cell death pathways in the two major glial cell targets of NMO.

Introduction

Neuromyelitis optica (NMO) is an autoimmune disease characterized with neuroinflammatory lesions on the optic nerve and spinal cord (Wingerchuk et al., 2015). Serum antibodies (IgG) targeting the water channel protein aquaporin-4 (AQP4) – which is expressed on astrocytic endfeet and ependymal cells in CNS (Papadopoulos and Verkman, 2013) - are specific marker for the disease and present in the majority of patients (Lennon et al., 2004; Lennon et al., 2005; Hinson et al., 2007). Experimental and pathological data support the notion that in the CNS parenchyma cellular injury initiates with AQP4-IgG orchestrated complement attack on astrocytes (Hinson et al., 2007; Misu et al., 2007; Roemer et al., 2007; Ratelade et al., 2013), while complement-independent steps might also contribute to astrocyte dysfunction (Hinson et al., 2008; Hinson et al., 2012) during NMO lesion formation. Although the primary cellular target of NMO pathology are astrocytes, NMO lesions manifests with subsequent neuronal pathology and demyelination (Lucchinetti et al., 2002; Roemer et al., 2007; Parratt and Prineas, 2010; Misu et al., 2013). Despite the well-characterized immunopathological features of NMO, we only have a limited understanding of the mechanisms that drive the secondary injury to other cell types, such as oligodendrocytes.

In addition, considerable number of AQP4-seronegative NMO patients have antibodies against the myelin oligodendrocyte glycoprotein (MOG-IgG), an antigen expressed on the outer surface of CNS myelin (Mader et al., 2011; Kitley et al., 2012; Probstel et al., 2015). AQP4- and MOG-IgG seropositive patients display distinct clinical presentation, therefore gave rise to the term NMO spectrum diseases (NMOSD) (Wingerchuk et al., 2007; Fujihara, 2019). Regardless of the glial cell target of NMOSD autoantibodies, demyelinating lesions is prominent feature among these patients (Wingerchuk et al., 2015) - which is a common hallmark of several neuroinflammatory diseases, in which proposed links between demyelination and astrocyte damage or dysfunction have been implicated (Parratt and Prineas, 2010; Sharma et al., 2010; Ponath et al., 2018). For instance, impairment of extracellular glutamate removal by astrocytes can lead to glutamate excitotoxicity in oligodendrocytes, which has been implicated in myelin damage (Micu et al., 2006; Kostic et al., 2013) and in NMO pathology (Marignier et al., 2010; Wrzos et al., 2014). In addition, astrocyte damage can lead to disruption between glial metabolic coupling, which reduce the provision of essential metabolites to oligodendrocytes and cause secondary demyelination (Sharma et al., 2010; Markoullis et al., 2012; Masaki, 2015). However, an alternative interpretation suggest a direct immune attack on oligodendrocytes, either during the chronic phase of NMO lesion

development, when a local cellular immune response develops at the site of the initial astrocytopathic lesion (Lucchinetti et al., 2002; Misu et al., 2013), or due to the complement attack that lacks cellular specificity ('bystander damage'; (Tradtrantip et al., 2017)).

To study the mechanisms of NMO lesion formation and spread of cellular pathology, a range of rodent models were established. These models supported the pathogenic roles of AQP4-IgG (Bradl and Lassmann, 2014; Duan and Verkman, 2020) and provided insights on complement dependent (Saadoun et al., 2010; Wrzos et al., 2014; Tradtrantip et al., 2017; Duan et al., 2018) and independent (Ratelade et al., 2012; Ratelade et al., 2013; Duan et al., 2019) modes of cellular damage in NMO. However, the models could not reveal the swift dynamics by which secondary oligodendrocyte damage occurs after AQP4-IgG induced injury. To address such questions, in vivo imaging can serve as a useful approach, as it has been used in the past to reveal the mechanisms of oligodendrocyte injury in other models of neuroinflammation, e.g. related to multiple sclerosis (Romanelli et al., 2016).

For this purpose, we previously established a mouse model of AQP4-IgG/complement induced lesions in the dorsal column of the mouse spinal cord, which is accessible to in vivo two-photon imaging (Herwerth et al., 2016). Here, we now used this approach to investigate the dynamics of oligodendrocyte injury that follows AQP4-IgG mediated astrocyte loss. Our results revealed that the initial site of injury appears to occur along on oligodendrocytes' internodes and involves local calcium dyshomeostasis, compatible with previous observations of myelin vesiculation (Weil et al., 2016). With a delay, oligodendrocytes show somatic changes, and die at relatively late time points. Underlying this outside-in pathology appears to be a 'bystander' injury arise during the membrane attack complex (MAC) assembly on astrocytes (Hinson 2007); as oligodendrocyte-specific expression of the MAC inhibitor protein CD59 protected oligodendrocytes from AQP4-IgG mediated damage. Notably, the characteristics of cell death appear to be distinct between astrocytes and oligodendrocytes, given that the former, but not the latter show signs of full-fledged membrane permeabilization – suggesting that further investigations could reveal selective means to rescue oligodendrocytes, even though their initial injury appears to be initiated by a complement attack.

Results

Characterization of glial injury in experimental NMO lesions

Using in vivo imaging, we investigated the early signs of glial damage in an acute spinal model of experimental NMO that we previously established. This approach leads to rapid depletion

of astrocytes within couple of hours by local application of patient-derived or recombinant AQP4-IgGs together with human complement to the dorsal spinal cord of the mouse (Herwerth et al., 2016). Experimental NMO lesions induced in triple transgenic *ALDH1L1*:GFP x *Plp:*CreERT x *CAG*:fl tdTom mice (Doerflinger et al., 2003; Madisen et al., 2010; Yang et al., 2011) allowed simultaneous assessment of astrocyte and oligodendrocyte morphology for up to 8 hours following application of AQP4-IgG/complement. As previously described, in this model AQP4-IgG binding to astrocytes initiates the classical complement cascade (Herwerth et al., 2016) and results in lytic depletion of astrocytes. We observed astrocyte loss mostly within the first 1.5 hours of local AQP4-IgG/complement treatment (mean±SEM: astrocyte loss $t_{50\%}$ = 77 ± 7 min, n=3 mice; **Fig. 1A, D**). Morphological signs of damage to oligodendrocyte cell bodies were noted later (mean±SEM: oligodendrocyte loss $t_{50\%}$ = 332 ± 43 min, n=3 mice) with the emergence of a swollen and more spheroid appearance of the somata (**Fig. 1A, D**). Notably, in the neuropil, where oligodendrocytes support internodes via thin connectors, the appearance of a grainy pattern likely representing the formation of beadings on oligodendrocyte processes and internodes was also apparent (**Fig. 1A**). No glial pathology was detectable under control conditions following application of Ctrl-IgG/complement (**Fig. 1B**).

Putative mechanisms of oligodendrocyte injury involve glutamate excitotoxicity (Wrzos et al., 2014), calcium-mediated myelin vesiculation (Weil et al., 2016) and complement-mediated 'bystander' poration (Tradtrantip et al., 2017); all of which involves intracellular calcium rise in oligodendrocytes albeit with different spatio-temporal and pharmacological profiles. Therefore, we developed and assay to measure glial calcium dynamics in experimental NMO and assess the possible role of calcium in glial pathology. For this purpose, we used a floxed reporter mouse line to express the genetically-encoded calcium sensor, GCaMP5g (Akerboom et al., 2012; Gee et al., 2014), in oligodendrocyte and astrocyte glial population (*Plp*:CreERT or *GFAP*:Cre respectively; (Doerflinger et al., 2003; Gregorian et al., 2009); in our hands, *Plp:*CreERT spontaneously recombines floxed alleles without the need for tamoxifen injections). Following application of AQP4-IgG/complement, astrocytes showed global calcium rise (mean±SEM: astrocytic high Ca^{2+} $t_{50\%}$ = 55 ± 3.8 min, n=3 mice; **Fig. 1C, E**) preceding their lytic death (mean±SEM: $t_{50\%}$[astrocyte loss] – $t_{50\%}$[high Ca^{2+}] = 28 ± 4.7, n=3 mice; **Fig. 1D-E**). Similar temporal dynamics of astrocyte loss (mean±SEM: $t_{50\%}$ = 78 ± 16.4 min, n=4, **Fig. 1F**) and increase in intracellular calcium (mean±SEM: astrocytic high Ca^{2+} $t_{50\%}$ = 64 ± 17.4 min n=4; **Fig. 1G**) were observed using recombinant AQP4 antibodies (rAQP4-

IgG) and complement. A recombinant isotype control antibody (rCtrl-IgG) induced no glia changes (**Fig. 1F-G**). This early calcium dyshomeostasis is compatible with the anticipated MAC pores on astrocytic membranes; as such pores would allow largely unhindered extracellular calcium influx (Bayly-Jones et al., 2017). Interestingly, oligodendrocytes showed a similar calcium dyshomeostasis (mean±SEM: oligodendrocyte high Ca^{2+} $t_{50\%}$ = 106 ± 6.9 min, n=2 mice; **Fig. 1C, E**), preceding the onset of morphological alterations observed in oligodendrocyte somata and processes (**Fig. 1D-E**). Thus, we demonstrated that despite astrocytes are being the apparent target of NMO-related cytotoxicity in vivo, oligodendrocytes appear to undergo similar ionic and morphological changes albeit with later onset and slower cellular spread.

MAC-inhibitor protein CD59 protects oligodendrocytes from AQP4-IgG-mediated injury

There are various possible mechanisms to explain calcium influx into oligodendrocytes observed after AQP4-IgG targeted complement lysis of astrocytes. One that has been championed in vitro, and is also supported by some in situ staining evidence, is a spill-over of activated complement proteins to oligodendrocytes ('bystander injury'; (Tradtrantip et al., 2017; Duan et al., 2018)). AQP4-IgG-mediated complement targeting of astrocytes involves enzymatic activation of complement proteins and sequential insertion of soluble C5b to C9 proteins into the plasma membrane to form an osmolytic pore, called membrane attack complex (MAC, C5b-9). Such pores drive ion and water influx to antibody-targeted cells (Bayly-Jones et al., 2017) and cause rapid necrotic lysis. In order to test whether in our in vivo model complement-mediated bystander injury might also contribute, we established a system of cell type-specific transgenic overexpression of the human (h) MAC-inhibitor protein CD59, by taking advantage of a previously developed floxed knock-in allele of this protein (Feng et al., 2016). CD59 is a glycosylphosphatidylinositol-linked membrane protein, which blocks MAC pore formation by interfering with the oligomerization and incorporation of C9 protein in preassembly complexes of MAC (Farkas et al., 2002; Kimberley et al., 2007).

As expected, if overexpressed on astrocytes (*GFAP:*Cre x *CAG:*fl tdTom x *CAG:*fl hCD59), even heterozygote hCD59 expression protected against the direct complement attack mediated by AQP4-IgG for up to 6 hours of lesion induction (astrocyte survival %, mean ± SEM: $hCD59_{HE}$ 90 ± 3.3% n=5; $hCD59_{HO}$ 93 ± 3, n=3; **Fig. 2A-C**). Whereas, hCD59 negative littermate controls showed complete astrocyte depletion after 3 hours (mean ± SEM: WT 1.4 ± 0.9 %, n=5; **Fig. 2A-C**). Remarkably, when hCD59 was selectively overexpressed in oligodendrocytes (*MOG:*Cre (Hovelmeyer et al., 2005) crossed with *CAG:*fl tdTom x *CAG:*fl

hCD59), secondary injury following AQP4-IgG/complement was also blocked (oligodendrocyte survival %, mean ± SEM: WT 33 ± 4.9, n=3; $hCD59_{HE}$ 96 ± 0.7, n=4; $hCD59_{HO}$ 100 ± 0, n= 3; **Fig. 2D-E**). We confirmed the unaltered depletion of astrocytes under these conditions (mean ± SEM 1.1 ± 1.1 %, n=3), by parallel transgenic labeling of both the astro- and oligodendroglial cell population (*ALDH1L1*:GFP x *MOG:*Cre x *CAG:*fl tdTom x *CAG:*fl hCD59; **Fig. 2F-G**).

Overall, our results revealed that at least acute oligodendrocyte injury in our model is MAC-mediated and allows a number of conclusions: First, bystander attack appears to be the core mechanisms of oligodendrocyte injury in our model, which corroborates earlier predictions based on in vitro models and MAC immunostainings (Tradtrantip et al., 2017). Second, astrocyte lysis and the resulting changes in the extracellular milieu are not sufficient to cause the oligodendrocyte pathology that we detected in our model. Finally, the spurious presence of MAC pores on oligodendrocytes provides a plausible route for calcium entry as detected in our calcium imaging experiments (**Fig. 1E)**. Further experiments are required to determine the role of spurious MAC pores, or alternative calcium sources (such as activation of additional voltage-gated channels or calcium release from internal stores) on oligodendrocyte calcium dyshomeostasis e.g. using specific blockers (Witte et al., 2019).

MAC-mediated oligodendrocyte injury initiates in processes and partially porates membranes

Despite an apparently similar mechanism of MAC-mediated glial injury, oligodendrocyte loss occurs with a delay after astrocytes die (**Fig. 1D-E**). In order to understand this delay and define possible divergence points in cell death mechanisms between astrocytes and oligodendrocytes, we investigated the spatio-temporal characteristics of oligodendrocyte injury in more detail. For this purpose, we used transgenic mice (*Plp:*CreERT mice crossed to reporter GCaMP5g line without tamoxifen delivery; leaky recombinase expression of this Cre reporter line results in sparse labeling of cells in mice that are heterozygous for both alleles), in which only some oligodendrocytes express the GCaMP5g calcium sensor. Individual oligodendrocytes were imaged for the first 2 hours following lesion induction with AQP4-IgG/complement. Typically, we observed local transient calcium elevation in the oligodendrocyte processes, which sometimes briefly invaded the soma (mean±SEM: t_{local} Ca^{2+}= 53.5 ± 8.6 min, n=4, N=3 mice), before a global and steady state of calcium dyshomeostasis of the entire cell was apparent (mean±SEM: t_{global} Ca^{2+}= 75 ± 6 min, n=4, N=3 mice; **Fig. 3A**). Such calcium rise preceded the morphological changes described above – a granular appearance in oligodendrocyte processes was detected and the cell body became more spheroid (**Fig. 3A**). Oligodendrocytes

in Ctrl-IgG/complement treated mice lack calcium changes and morphological signs of cellular damage (**Fig. 3B**). These observations suggest that the site of complement spill over might be located in the oligodendrocyte's periphery, e.g. at nodes of Ranvier, where oligodendrocyte processes and astrocytic endfeet, where MAC is primarily deposited, are in close proximity (Hinson et al., 2007). This could explain some of the spatio-temporal differences in morphological changes and patterns of calcium influx that we observe comparing astrocytes and oligodendrocytes, and importantly also activate different pathways of cellular demise.

We next explored the degree of membrane disruption in astrocytes and oligodendrocytes under AQP4-IgG/complement attack. For this purpose, we used the well-established cell death indicator, ethidium homodimer (EtHD). This nuclear dye is excluded in the cells with intact membranes, but brightly stains the nuclei of porated cells after intercalating into DNA. The dye uptake assay clearly showed that astrocyte nuclei were labeled in experimental NMO lesions in vivo (*ALDH1L1:*GFP; **Fig. 3C**), suggesting a high degree of membrane disruption, while EtHD staining was not apparent in oligodendrocytes (*Plp:*GFP, (Mallon et al., 2002); **Fig. 3C**). This difference suggests that the primary attack of MAC on astrocytes causes poration of these cells and leads to a necrotic phenomenon, whereas the bystander complement attack on oligodendrocytes is more restricted in extent and it might initiate a relatively delayed cell death mechanism. Identifying the diverging mechanisms of glial cell death is the focus of ongoing follow-up investigations in our lab, with the hope of identifying possible acute intervention points to prevent oligodendrocyte loss in nascent NMO lesions.

Discussion

Demyelination and oligodendrocyte damage is a common hallmark of neuroinflammatory diseases. In MS, myelin is targeted by immune attack, although lacking a defined antigen association; while in NMO the antigen target is known, AQP4 (Lennon et al., 2004; Lennon et al., 2005). How this defined target on astrocytes can result in pathology spread, including oligodendrocytes remains unclear; and it might well involve several parallel pathways that operate during different phases of NMO lesion development. A complement-mediated attack on oligodendrocytes (Tradtrantip et al., 2017), as well as secondary damage mechanisms, where oligodendrocytes and myelin are injured by the absence of astrocytes via various forms of metabolic or ionic coupling (Marignier et al., 2010; Wrzos et al., 2014; Richard et al., 2020), have been invoked. Currently, a variety of experimental models is used to gain insights into

possible mechanisms of spreading cellular pathology in NMO (Saadoun et al., 2010; Wrzos et al., 2014). However, most of these models are geared towards the late phases of lesion development. Our acute model combined with in vivo imaging offers a unique window into the immediate dynamics of how glial damage progresses. Such insights might hint towards intervention points early during the formation of lesions that can swiftly turn highly destructive and disabling.

Our most notable observations were the following:

(1) Within two hours of initiating complement injury at astrocytes with AQP4-IgG, both astrocytes and oligodendrocytes showed a rise in intracellular calcium (**Fig. 1C, E**).

(2) The rapid disruption of the glial calcium homeostasis preceded morphological changes and subsequent cell loss (**Fig. 1D-E**), suggesting that calcium dyshomeostasis could play an early causative role not only in glia cell loss, but also in earlier stages of oligodendrocyte injury; such as myelin vesiculation (Weil et al., 2016).

(3) The antibody-mediated complement attack on astrocytes resulted in MAC pore formation in the astrocytic cell membrane, which can explain the loss of membrane integrity (**Fig. 3C**) and massive calcium influx in astrocytes prior to cell lysis (**Fig. 1C-E**).

(4) Notably, this MAC attack was not restricted to astrocytes, but appeared to affect oligodendrocytes as well, likely in the cells' periphery (**Fig. 3A**), and is responsible for the acute loss of oligodendrocytes observed in our experimental NMO lesions.

(5) Despite this similar starting point of injury involving MAC pores, astrocytes and oligodendrocytes undergo cell death with very distinct spatio-temporal characteristics (e.g. time of onset of injury, pattern of calcium influx, degree of membrane disruption), leaving open the possibility of distinct cell death pathways are activated (Xie et al., 2020). Identifying these cell death mechanisms, and contribution of calcium dyshomeostasis to trigger such cascades, are important next steps in our attempts to understand the dynamics of early NMO lesion formation.

However, this is not to claim that all aspects of the spread of pathology to other cell types in NMO lesions is mediated by 'bystander injury'. Indeed, our own studies of acute axonal pathology show that the mechanism of bystander injury spread is not likely to explain the most obvious axonal pathology (see accompanying manuscript; Herwerth*, Kenet* et al., in submission). However, also for oligodendrocytes, many additional modes of cellular injury following AQP4-IgG/complement-mediated astrocyte lysis are conceivable:

Indeed, the intact interaction between astrocytes and oligodendrocytes is indispensable for the proper function of oligodendrocytes and involves several types of cellular and molecular interaction. For instance, dysfunction of astrocytes impairs the homeostatic regulation of neurotransmitter levels in the CNS (Murphy-Royal et al., 2017), to which oligodendrocytes are vulnerable. When astrocytic uptake of glutamate is disturbed, extracellular glutamate reaches to toxic levels for oligodendrocytes. This has been proposed as a mechanisms of oligodendrocyte and myelin loss in ischemia (Karadottir et al., 2005; Salter and Fern, 2005; Micu et al., 2006) and in models of demyelination related to multiple sclerosis (Pitt et al., 2000; Bannerman et al., 2007). Even without complement-mediated lysis, AQP4-IgG bound to its target on astrocytes could reduce surface expression levels or the function of AQP4 and other interacting membrane proteins. For example, the levels of the astrocyte-enriched glutamate transporter EAAT2 are reduced (Hinson et al., 2008; Geis et al., 2015). This could potentiate glutamate-mediated toxicity in early phases of NMO, even if no overt loss of astrocytes is apparent (Hinson et al., 2008; da Silva et al., 2019). However, there have been contradicting results on EAAT2 and AQP4 internalization following AQP4-IgG treatment (Ratelade et al., 2011; Rossi et al., 2012). Regardless, glutamate excitotoxicity alone seems unlikely to explain oligodendrocyte loss in our model at least within the first 6 hours of the lesion induction, as under cell autonomous hCD59 protection, oligodendrocytes were largely unaffected despite complete astrocyte depletion and hence loss of astrocytic glutamate buffering (**Fig. 2F-G**). At the same time, sublethal excitotoxicity mediated by kainate receptors, calcium influx and reactive oxygen species signaling is known to sensitize oligodendrocytes to complement attack (e.g. via IgG-independent MAC insertion (Alberdi et al., 2006; Matute, 2007)). Our current data cannot rule out such an intersection of toxicity mechanisms, which resembles a pathway previously described for neurons (Xiong and McNamara, 2002) and further studies conducted with glutamate receptor blockers will be needed to elucidate the role of glutamate in experimental lesions. Indeed, other forms of astrocyte-oligodendrocyte coupling, such as syncytial coupling via connexins (Orthmann-Murphy et al., 2007) or osmo-ionic influences that we found to be relevant for early axon injury (see accompanying manuscript; Herwerth*, Kenet* et al., in submission) are also relegated at best to a secondary role based on the hCD59-mediated protection of oligodendrocytes, which would not protect against such non-immunological impact.

CD59 has a well-described mode of action: It acts as a complement regulatory protein and binds the complement proteins C8 and C9 during the assembly of MAC. It thus hinders C9

polymerization and inhibits insertion of the osmo-lytic MAC pore into the plasma membrane, which protects the target cells from complement-mediated lysis (Farkas et al., 2002; Kimberley et al., 2007). A protective role of endogenous CD59 in NMO-related pathology has been described using knockout rodent models, which were more vulnerable to AQP4-IgG mediated injury. These mutants developed demyelinating lesions under conditions when normally minimal pathology is observed (Zhang and Verkman, 2014; Yao and Verkman, 2017b). CD59 knockout animals also develop peripheral organ injury, which is mostly absent in NMO despite high levels of AQP4 expression, e.g. in the kidneys (Yao and Verkman, 2017a).

Thus, our observation of oligodendrocyte protection by cell-type specific expression of hCD59 following AQP4-IgG–mediated astrocyte depletion (**Fig. 2D-G**) strongly supports the notion of an IgG-independent complement attack on oligodendrocytes. This provides direct in vivo evidence for a 'bystander' injury mechanism, where an astrocyte-targeted IgG attack (Lennon et al., 2005; Hinson et al., 2007) result in the terminal complement complex assembly also in nearby cells. This has been proposed based on immune-histochemical detection of MAC components on neurons and oligodendrocytes implicated bystander complement injury (Tradtrantip et al., 2017; Duan et al., 2018).The presence of MAC pores would explain the calcium influx (Tegla et al., 2011) that we observed in oligodendrocytes (**Fig. 1C, E; Fig3A**).

Despite this strong evidence for a similar starting point of toxicity based on membrane-inserted MAC pores, the extent of injury and subsequent fates of astrocytes and oligodendrocytes differed in our experiments. Astrocytes showed signs of overt membrane poration, immediate and global calcium influx, and swiftly swelled before they succumbed to cell lysis (**Fig. 1; Fig. 3C**). In contrast, oligodendrocytes showed globally intact membranes, delayed and local calcium dyshomeostasis and appeared to die slower (**Fig. 1; Fig. 3C**). One important open question from our study is, whether this downstream divergence can be harnessed to rescue oligodendrocytes once a lesion has started to form. In further experiments, different cell death pathways could be explored – while astrocytes die of lytic necrosis, the cell death of oligodendrocytes bears morphological hallmarks of more controlled forms of cell death (e.g. nuclear compaction). In addition to classical apoptosis, several other forms of inflammation- and membrane poration-related cell death cascades have been described (Galluzzi et al., 2018). MAC pores at sublytic density are known to trigger pore-dependent or -independent signaling, which can activate a variety of such cell death pathways (Xie et al., 2020), which could in the future be probed in our model by pharmacological and genetic intervention. Indeed, if cell death signaling is prevented, oligodendrocytes might be capable of surviving a local

complement attack. Nucleated cells have mechanisms to counteract MAC-mediated cell lysis, including MAC removal from the plasma membrane via vesicular shedding and internalization (Scolding et al., 1989b; Moskovich and Fishelson, 2007). Whether this will allow long-term survival of oligodendrocytes, and have additional beneficial effects such as protecting axons, or aiding remyelination (to which surviving oligodendrocytes appear to contribute in certain settings; (Franklin et al., 2020), would require long-term observations, e.g. using a chronic spinal cord imaging approach. Indeed, our data only address the acute phase of NMO lesion development immediately after AQP4-IgG-mediated astrocyte lysis. It is worth noting that during the chronic phases of NMO-related injury, other forms of astrocyte-oligodendrocyte interactions, e.g. involving connexins (Sharma et al., 2010; Richard et al., 2020) or glutamate excitotoxicity (Marignier et al., 2010; Wrzos et al., 2014), might well become highly relevant.

Material and Methods

Animals

We used 2- to 6-month old female and male mice. To visualize astrocyte morphology *ALDH1L1*:GFP ((Yang et al., 2011); MGI:3843271), or *GFAP*:Cre ((Gregorian et al., 2009); JAX: 24098) mice crossed with *Rosa26 CAG*:STOP-flox-tdTom reporter line (tdTom; (Madisen et al., 2010); JAX: 7914) were used. Oligodendrocyte morphology was assessed in the crosses of *PLP*:GFP ((Mallon et al., 2002); JAX: 33357), or *PLP*:CreERT-tdTom transgenic lines (*PLP*:CreERT; (Doerflinger et al., 2003); (JAX: 5975)). Calcium imaging was conducted in the *GFAP*:Cre and *PLP*:CreERT crosses with *Polr2a CAG:*flox GCaMP5g IRES tdTom mice (GCaMP5g; (Gee et al., 2014); JAX: 24477). For glia specific expression of MAC inhibitor protein CD59, *MOG:*Cre-tdTom or *GFAP*:Cre-tdTom mice crossed to *Hipp11 CAG:* STOP-flox-CD59 line (hCD59 mice; Feng et al 2016, courtesy of Prof. Bin Gao, NIAAA – NIH, USA; *MOG:*Cre mice (Hovelmeyer et al., 2005), courtesy of Prof. Ari Waisman, University of Mainz, Germany). Due to constitutive Cre recombines activity observed in the different progenies from *PLP*:CreERT crosses, tamoxifen administration was not necessary. All the animal experiments were conducted in accordance with local regulations and were approved by the responsible regulatory agencies.

Complement and antibody sources

Plasma sample of an AQP4-IgG-positive NMO patient treated in the Department of Neurology, Klinikum rechts der Isar, Technical University of Munich was included to the study. The

patient was fullfiling the NMO diagnostic criteria (Wingerchuk et al., 2015). For control plasma and the complement source, healthy subject plasma and sera of three healthy donors were included to the study (from the Bavarian Red Cross). All subjects gave written informed consent for the use of their samples for research purposes. Plasma and serum samples were collected and treated as previously described (Herwerth et al., 2016). In order to eliminate complement activity of the NMO and control plasma, samples were heat inactivated and only used as IgG sources in the experiments. As complement source, pooled sera of three healthy subjects was supplied in each experiment. Human IgG1 antibody, recombinant AQP4-IgG (rAb7-5-53) was reconstructed from a clonotypic plasma blast obtained from the CSF of an NMO patient (Bennett et al., 2009). Human IgG1 antibody of unknown specificity developed from a chronic meningitis patient, recombinant control-IgG (rAb ICOS-5-2) was used as an isotype control.

Surgical Procedure and In Vivo Imaging

Laminectomy surgeries were performed as previously described (Nikic et al., 2011; Herwerth et al., 2016). In brief, mice were anaesthetized by intraperitoneal injection of medetomidin (0.5 mg/kg), midazolam (5 mg/kg), fentayl (0.05 mg/kg). Anesthesia was re-applied as needed. After a double dorsal laminectomy over the lumbar L4 and L5 segments, mice were suspended using compact spinal cord clamps (Davalos et al., 2008). The dura mater was punctured with the tip of a hypodermic needle and removed by the help of fine forceps to have a dura-free imaging window. 2% agarose well was built around the surgery area to allow application of artificial cerebrospinal fluid, aCSF (in mM: 148.2 NaCL, 3.0 KCl, 0.8 Na2HPO4, 0.2 NaH2PO4, 1.4 CaCl2 and 0.8 MgCl2) or antibody/complement mix over the imaging window.

Diluted recombinant antibodies (rAQP4-IgG vs rCtrl-IgG ICOS-5-2; 1,5µg/ml) or heat-inactivated plasma (AQP4-IgG vs Ctrl-IgG; 150 µg/ml); together with 20% of healthy sera as a complement source was applied every 30 minutes for the first 2 hours, afterwards the solution was re-applied every 60 min for the rest of imaging time window. In some experiments, cell membrane disruption was verified by addition of ethidium homodimer-1 to antibody/complement mix (1:500, 0.56mg/ ml stock; Invitrogen, Carlsbad, CA). We have previously shown that photo-toxicity or transgenic labeling does not influence the health of glial cells under these experimental conditions (Herwerth et al., 2016).

In vivo imaging of the lumbar spinal cord was performed as previously described (Nikic et al., 2011; Romanelli et al., 2013; Herwerth et al., 2016). Briefly, two-photon microscope (Olympus FV1000 MPE or FVMPE-RS) equipped with a X25/1.05 N.A. water-dipping cone objective,

was tuned to 770nm for GFP/EtHD, 920nm for GCaMP5g/tdTom, 950nm for GFP/tdTom to acquire imaging stacks. Emission was filtered through 690 nm short-pass dichroic mirror, and separated with G/R (BA 495-540, BA 570-625) filter set mounted in front of gallium arsenide phosphide photomultiplier tubes.

Time-lapse stacks were acquired at 10-minute intervals for 6-8 hours (glial morphology imaging) or at 5-minute intervals for 6 hours (glial calcium imaging). In sparsely labeled oligodendrocyte imaging experiments, stacks were acquired at 10-min intervals for the first 30min and at every 2 minutes, for 3 hours. Indicated parameters were used while imaging: up to 50 stacks with a z-step of 1.5-2 µm; zoom of 1.5–3.0; pixel size ranging 0.28– 0.38 µm.

Cell survival analysis: While assessing the survival analysis, death cells were defined by a loss of at least 50% intensity of mean gray value, or by the appearance of morphological changes on astrocytes (disintegration of the cell) and oligodendrocytes (swollen somata with process blebbing, appearance of condensed nuclei). Since the difference between control and NMO experiments was obvious to evaluator, scoring was done without blinding.

GCaMP5g Calcium analysis: Time of visually detectable calcium transitions was first assessed from z-projections of image stacks. Each transition was verified in unprocessed three-dimensional image stacks. A cell was scored to have elevated calcium, if the GCaMP5g levels were 50% greater than the baseline obtained at the beginning of each experiment. Mean gray value intensities were measured in Fiji from the unprocessed, singular planes. ROIs were assigned manually within the stacks.

Image Processing and Data Analysis

Images were processed using the open-source image analysis software ImageJ/Fiji (Schindelin et al., 2012) and Adobe Creative Suite. For figure representations, individual channels of imaging series were combined using pseudo-colors. Gamma values were adjusted to enhance visibility of cellular structures in non-quantitative figure panels. Data sets were processed with Excel (Microsoft Corporation, Redmond, WA) and the GraphPad Prism 9 software (GraphPad Software, San Diego, California USA). All results are presented as mean ± SEM. When comparing two experimental groups, nonparametric t-test followed by Mann-Whitney test was performed using GraphPad Prism 9 software. P values < 0.05 were considered to be significant and indicated with "*", p values < 0.01 with "**" and <0.001 with "***".

References

Akerboom J et al. (2012) Optimization of a GCaMP calcium indicator for neural activity imaging. J Neurosci 32:13819-13840.

Alberdi E, Sanchez-Gomez MV, Torre I, Domercq M, Perez-Samartin A, Perez-Cerda F, Matute C (2006) Activation of kainate receptors sensitizes oligodendrocytes to complement attack. J Neurosci 26:3220-3228.

Bannerman P, Horiuchi M, Feldman D, Hahn A, Itoh A, See J, Jia ZP, Itoh T, Pleasure D (2007) GluR2-free alpha-amino-3-hydroxy-5-methyl-4-isoxazolepropionate receptors intensify demyelination in experimental autoimmune encephalomyelitis. J Neurochem 102:1064-1070.

Bayly-Jones C, Bubeck D, Dunstone MA (2017) The mystery behind membrane insertion: a review of the complement membrane attack complex. Philos Trans R Soc Lond B Biol Sci 372.

Bennett JL, Lam C, Kalluri SR, Saikali P, Bautista K, Dupree C, Glogowska M, Case D, Antel JP, Owens GP, Gilden D, Nessler S, Stadelmann C, Hemmer B (2009) Intrathecal pathogenic anti-aquaporin-4 antibodies in early neuromyelitis optica. Ann Neurol 66:617-629.

Bradl M, Lassmann H (2014) Experimental models of neuromyelitis optica. Brain Pathol 24:74-82.

da Silva APB, Souza DG, Souza DO, Machado DC, Sato DK (2019) Role of Glutamatergic Excitotoxicity in Neuromyelitis Optica Spectrum Disorders. Front Cell Neurosci 13:142.

Davalos D, Lee JK, Smith WB, Brinkman B, Ellisman MH, Zheng B, Akassoglou K (2008) Stable in vivo imaging of densely populated glia, axons and blood vessels in the mouse spinal cord using two-photon microscopy. J Neurosci Methods 169:1-7.

Doerflinger NH, Macklin WB, Popko B (2003) Inducible site-specific recombination in myelinating cells. Genesis 35:63-72.

Duan T, Verkman AS (2020) Experimental animal models of aquaporin-4-IgG-seropositive neuromyelitis optica spectrum disorders: progress and shortcomings. Brain Pathol 30:13-25.

Duan T, Smith AJ, Verkman AS (2018) Complement-dependent bystander injury to neurons in AQP4-IgG seropositive neuromyelitis optica. J Neuroinflammation 15:294.

Duan T, Smith AJ, Verkman AS (2019) Complement-independent bystander injury in AQP4-IgG seropositive neuromyelitis optica produced by antibody-dependent cellular cytotoxicity. Acta Neuropathol Commun 7:112.

Farkas I, Baranyi L, Ishikawa Y, Okada N, Bohata C, Budai D, Fukuda A, Imai M, Okada H (2002) CD59 blocks not only the insertion of C9 into MAC but inhibits ion channel formation by homologous C5b-8 as well as C5b-9. J Physiol 539:537-545.

Feng D et al. (2016) Cre-inducible human CD59 mediates rapid cell ablation after intermedilysin administration. J Clin Invest 126:2321-2333.

Franklin RJM, Frisen J, Lyons DA (2020) Revisiting remyelination: Towards a consensus on the regeneration of CNS myelin. Semin Cell Dev Biol.

Fujihara K (2019) Neuromyelitis optica spectrum disorders: still evolving and broadening. Curr Opin Neurol 32:385-394.

Galluzzi L et al. (2018) Molecular mechanisms of cell death: recommendations of the Nomenclature Committee on Cell Death 2018. Cell Death Differ 25:486-541.

Gee JM, Smith NA, Fernandez FR, Economo MN, Brunert D, Rothermel M, Morris SC, Talbot A, Palumbos S, Ichida JM, Shepherd JD, West PJ, Wachowiak M, Capecchi MR, Wilcox KS, White JA, Tvrdik P (2014) Imaging activity in neurons and glia with a Polr2a-based and cre-dependent GCaMP5G-IRES-tdTomato reporter mouse. Neuron 83:1058-1072.

Geis C, Ritter C, Ruschil C, Weishaupt A, Grunewald B, Stoll G, Holmoy T, Misu T, Fujihara K, Hemmer B, Stadelmann C, Bennett JL, Sommer C, Toyka KV (2015) The intrinsic pathogenic role of autoantibodies to aquaporin 4 mediating spinal cord disease in a rat passive-transfer model. Exp Neurol 265:8-21.

Gregorian C, Nakashima J, Le Belle J, Ohab J, Kim R, Liu A, Smith KB, Groszer M, Garcia AD, Sofroniew MV, Carmichael ST, Kornblum HI, Liu X, Wu H (2009) Pten deletion in adult neural stem/progenitor cells enhances constitutive neurogenesis. J Neurosci 29:1874-1886.

Herwerth M, Kalluri SR, Srivastava R, Kleele T, Kenet S, Illes Z, Merkler D, Bennett JL, Misgeld T, Hemmer B (2016) In vivo imaging reveals rapid astrocyte depletion and axon damage in a model of neuromyelitis optica-related pathology. Ann Neurol 79:794-805.

Hinson SR, Pittock SJ, Lucchinetti CF, Roemer SF, Fryer JP, Kryzer TJ, Lennon VA (2007) Pathogenic potential of IgG binding to water channel extracellular domain in neuromyelitis optica. Neurology 69:2221-2231.

Hinson SR, Roemer SF, Lucchinetti CF, Fryer JP, Kryzer TJ, Chamberlain JL, Howe CL, Pittock SJ, Lennon VA (2008) Aquaporin-4-binding autoantibodies in patients with neuromyelitis optica impair glutamate transport by down-regulating EAAT2. J Exp Med 205:2473-2481.

Hinson SR, Romero MF, Popescu BF, Lucchinetti CF, Fryer JP, Wolburg H, Fallier-Becker P, Noell S, Lennon VA (2012) Molecular outcomes of neuromyelitis optica (NMO)-IgG binding to aquaporin-4 in astrocytes. Proc Natl Acad Sci U S A 109:1245-1250.

Hovelmeyer N, Hao Z, Kranidioti K, Kassiotis G, Buch T, Frommer F, von Hoch L, Kramer D, Minichiello L, Kollias G, Lassmann H, Waisman A (2005) Apoptosis of oligodendrocytes via Fas and TNF-R1 is a key event in the induction of experimental autoimmune encephalomyelitis. J Immunol 175:5875-5884.

Karadottir R, Cavelier P, Bergersen LH, Attwell D (2005) NMDA receptors are expressed in oligodendrocytes and activated in ischaemia. Nature 438:1162-1166.

Kimberley FC, Sivasankar B, Paul Morgan B (2007) Alternative roles for CD59. Mol Immunol 44:73-81.

Kitley J, Woodhall M, Waters P, Leite MI, Devenney E, Craig J, Palace J, Vincent A (2012) Myelin-oligodendrocyte glycoprotein antibodies in adults with a neuromyelitis optica phenotype. Neurology 79:1273-1277.

Kostic M, Zivkovic N, Stojanovic I (2013) Multiple sclerosis and glutamate excitotoxicity. Rev Neurosci 24:71-88.

Lennon VA, Kryzer TJ, Pittock SJ, Verkman AS, Hinson SR (2005) IgG marker of optic-spinal multiple sclerosis binds to the aquaporin-4 water channel. J Exp Med 202:473-477.

Lennon VA, Wingerchuk DM, Kryzer TJ, Pittock SJ, Lucchinetti CF, Fujihara K, Nakashima I, Weinshenker BG (2004) A serum autoantibody marker of neuromyelitis optica: distinction from multiple sclerosis. Lancet 364:2106-2112.

Lucchinetti CF, Mandler RN, McGavern D, Bruck W, Gleich G, Ransohoff RM, Trebst C, Weinshenker B, Wingerchuk D, Parisi JE, Lassmann H (2002) A role for humoral mechanisms in the pathogenesis of Devic's neuromyelitis optica. Brain 125:1450-1461.

Mader S, Gredler V, Schanda K, Rostasy K, Dujmovic I, Pfaller K, Lutterotti A, Jarius S, Di Pauli F, Kuenz B, Ehling R, Hegen H, Deisenhammer F, Aboul-Enein F, Storch MK, Koson P, Drulovic J, Kristoferitsch W, Berger T, Reindl M (2011) Complement activating antibodies to myelin oligodendrocyte glycoprotein in neuromyelitis optica and related disorders. J Neuroinflammation 8:184.

Madisen L, Zwingman TA, Sunkin SM, Oh SW, Zariwala HA, Gu H, Ng LL, Palmiter RD, Hawrylycz MJ, Jones AR, Lein ES, Zeng H (2010) A robust and high-throughput Cre reporting and characterization system for the whole mouse brain. Nat Neurosci 13:133-140.

Mallon BS, Shick HE, Kidd GJ, Macklin WB (2002) Proteolipid promoter activity distinguishes two populations of NG2-positive cells throughout neonatal cortical development. J Neurosci 22:876-885.

Marignier R, Nicolle A, Watrin C, Touret M, Cavagna S, Varrin-Doyer M, Cavillon G, Rogemond V, Confavreux C, Honnorat J, Giraudon P (2010) Oligodendrocytes are damaged by neuromyelitis optica immunoglobulin G via astrocyte injury. Brain 133:2578-2591.

Markoullis K, Sargiannidou I, Gardner C, Hadjisavvas A, Reynolds R, Kleopa KA (2012) Disruption of oligodendrocyte gap junctions in experimental autoimmune encephalomyelitis. Glia 60:1053-1066.

Masaki K (2015) Early disruption of glial communication via connexin gap junction in multiple sclerosis, Balo's disease and neuromyelitis optica. Neuropathology 35:469-480.

Matute C (2007) Interaction between glutamate signalling and immune attack in damaging oligodendrocytes. Neuron Glia Biol 3:281-285.

Micu I, Jiang Q, Coderre E, Ridsdale A, Zhang L, Woulfe J, Yin X, Trapp BD, McRory JE, Rehak R, Zamponi GW, Wang W, Stys PK (2006) NMDA receptors mediate calcium accumulation in myelin during chemical ischaemia. Nature 439:988-992.

Misu T, Fujihara K, Kakita A, Konno H, Nakamura M, Watanabe S, Takahashi T, Nakashima I, Takahashi H, Itoyama Y (2007) Loss of aquaporin 4 in lesions of neuromyelitis optica: distinction from multiple sclerosis. Brain 130:1224-1234.

Misu T, Hoftberger R, Fujihara K, Wimmer I, Takai Y, Nishiyama S, Nakashima I, Konno H, Bradl M, Garzuly F, Itoyama Y, Aoki M, Lassmann H (2013) Presence of six different lesion types suggests diverse mechanisms of tissue injury in neuromyelitis optica. Acta Neuropathol 125:815-827.

Moskovich O, Fishelson Z (2007) Live cell imaging of outward and inward vesiculation induced by the complement c5b-9 complex. J Biol Chem 282:29977-29986.

Murphy-Royal C, Dupuis J, Groc L, Oliet SHR (2017) Astroglial glutamate transporters in the brain: Regulating neurotransmitter homeostasis and synaptic transmission. J Neurosci Res 95:2140-2151.

Nikic I, Merkler D, Sorbara C, Brinkoetter M, Kreutzfeldt M, Bareyre FM, Bruck W, Bishop D, Misgeld T, Kerschensteiner M (2011) A reversible form of axon damage in experimental autoimmune encephalomyelitis and multiple sclerosis. Nat Med 17:495-499.

Orthmann-Murphy JL, Freidin M, Fischer E, Scherer SS, Abrams CK (2007) Two distinct heterotypic channels mediate gap junction coupling between astrocyte and oligodendrocyte connexins. J Neurosci 27:13949-13957.

Papadopoulos MC, Verkman AS (2013) Aquaporin water channels in the nervous system. Nat Rev Neurosci 14:265-277.

Parratt JD, Prineas JW (2010) Neuromyelitis optica: a demyelinating disease characterized by acute destruction and regeneration of perivascular astrocytes. Mult Scler 16:1156-1172.

Pitt D, Werner P, Raine CS (2000) Glutamate excitotoxicity in a model of multiple sclerosis. Nat Med 6:67-70.

Ponath G, Park C, Pitt D (2018) The Role of Astrocytes in Multiple Sclerosis. Front Immunol 9:217.

Probstel AK, Rudolf G, Dornmair K, Collongues N, Chanson JB, Sanderson NS, Lindberg RL, Kappos L, de Seze J, Derfuss T (2015) Anti-MOG antibodies are present in a subgroup of patients with a neuromyelitis optica phenotype. J Neuroinflammation 12:46.

Ratelade J, Bennett JL, Verkman AS (2011) Evidence against cellular internalization in vivo of NMO-IgG, aquaporin-4, and excitatory amino acid transporter 2 in neuromyelitis optica. J Biol Chem 286:45156-45164.

Ratelade J, Zhang H, Saadoun S, Bennett JL, Papadopoulos MC, Verkman AS (2012) Neuromyelitis optica IgG and natural killer cells produce NMO lesions in mice without myelin loss. Acta Neuropathol 123:861-872.

Ratelade J, Asavapanumas N, Ritchie AM, Wemlinger S, Bennett JL, Verkman AS (2013) Involvement of antibody-dependent cell-mediated cytotoxicity in inflammatory demyelination in a mouse model of neuromyelitis optica. Acta Neuropathol 126:699-709.

Richard C, Ruiz A, Cavagna S, Bigotte M, Vukusic S, Masaki K, Suenaga T, Kira JI, Giraudon P, Marignier R (2020) Connexins in neuromyelitis optica: a link between astrocytopathy and demyelination. Brain 143:2721-2732.

Roemer SF, Parisi JE, Lennon VA, Benarroch EE, Lassmann H, Bruck W, Mandler RN, Weinshenker BG, Pittock SJ, Wingerchuk DM, Lucchinetti CF (2007) Pattern-specific loss of aquaporin-4 immunoreactivity distinguishes neuromyelitis optica from multiple sclerosis. Brain 130:1194-1205.

Romanelli E, Sorbara CD, Nikic I, Dagkalis A, Misgeld T, Kerschensteiner M (2013) Cellular, subcellular and functional in vivo labeling of the spinal cord using vital dyes. Nat Protoc 8:481-490.

Romanelli E, Merkler D, Mezydlo A, Weil MT, Weber MS, Nikic I, Potz S, Meinl E, Matznick FE, Kreutzfeldt M, Ghanem A, Conzelmann KK, Metz I, Bruck W, Routh M, Simons M, Bishop D, Misgeld T, Kerschensteiner M (2016) Myelinosome formation represents an early stage of oligodendrocyte damage in multiple sclerosis and its animal model. Nat Commun 7:13275.

Rossi A, Ratelade J, Papadopoulos MC, Bennett JL, Verkman AS (2012) Neuromyelitis optica IgG does not alter aquaporin-4 water permeability, plasma membrane M1/M23 isoform content, or supramolecular assembly. Glia 60:2027-2039.

Saadoun S, Waters P, Bell BA, Vincent A, Verkman AS, Papadopoulos MC (2010) Intra-cerebral injection of neuromyelitis optica immunoglobulin G and human complement produces neuromyelitis optica lesions in mice. Brain 133:349-361.

Salter MG, Fern R (2005) NMDA receptors are expressed in developing oligodendrocyte processes and mediate injury. Nature 438:1167-1171.

Schindelin J, Arganda-Carreras I, Frise E, Kaynig V, Longair M, Pietzsch T, Preibisch S, Rueden C, Saalfeld S, Schmid B, Tinevez JY, White DJ, Hartenstein V, Eliceiri K, Tomancak P, Cardona A (2012) Fiji: an open-source platform for biological-image analysis. Nat Methods 9:676-682.

Scolding NJ, Morgan BP, Houston WA, Linington C, Campbell AK, Compston DA (1989) Vesicular removal by oligodendrocytes of membrane attack complexes formed by activated complement. Nature 339:620-622.

Sharma R, Fischer MT, Bauer J, Felts PA, Smith KJ, Misu T, Fujihara K, Bradl M, Lassmann H (2010) Inflammation induced by innate immunity in the central nervous system leads to primary astrocyte dysfunction followed by demyelination. Acta Neuropathol 120:223-236.

Tegla CA, Cudrici C, Patel S, Trippe R, 3rd, Rus V, Niculescu F, Rus H (2011) Membrane attack by complement: the assembly and biology of terminal complement complexes. Immunol Res 51:45-60.

Tradtrantip L, Yao X, Su T, Smith AJ, Verkman AS (2017) Bystander mechanism for complement-initiated early oligodendrocyte injury in neuromyelitis optica. Acta Neuropathol 134:35-44.

Weil MT, Mobius W, Winkler A, Ruhwedel T, Wrzos C, Romanelli E, Bennett JL, Enz L, Goebels N, Nave KA, Kerschensteiner M, Schaeren-Wiemers N, Stadelmann C, Simons M (2016) Loss of Myelin Basic Protein Function Triggers Myelin Breakdown in Models of Demyelinating Diseases. Cell Rep 16:314-322.

Wingerchuk DM, Pittock SJ, Lucchinetti CF, Lennon VA, Weinshenker BG (2007) A secondary progressive clinical course is uncommon in neuromyelitis optica. Neurology 68:603-605.

Wingerchuk DM, Banwell B, Bennett JL, Cabre P, Carroll W, Chitnis T, de Seze J, Fujihara K, Greenberg B, Jacob A, Jarius S, Lana-Peixoto M, Levy M, Simon JH, Tenembaum S, Traboulsee AL, Waters P, Wellik KE, Weinshenker BG, International Panel for NMOD (2015) International consensus diagnostic criteria for neuromyelitis optica spectrum disorders. Neurology 85:177-189.

Witte ME, Schumacher AM, Mahler CF, Bewersdorf JP, Lehmitz J, Scheiter A, Sanchez P, Williams PR, Griesbeck O, Naumann R, Misgeld T, Kerschensteiner M (2019) Calcium Influx through Plasma-Membrane Nanoruptures Drives Axon Degeneration in a Model of Multiple Sclerosis. Neuron 101:615-624 e615.

Wrzos C, Winkler A, Metz I, Kayser DM, Thal DR, Wegner C, Bruck W, Nessler S, Bennett JL, Stadelmann C (2014) Early loss of oligodendrocytes in human and experimental neuromyelitis optica lesions. Acta Neuropathol 127:523-538.

Xie CB, Jane-Wit D, Pober JS (2020) Complement Membrane Attack Complex: New Roles, Mechanisms of Action, and Therapeutic Targets. Am J Pathol 190:1138-1150.

Xiong ZQ, McNamara JO (2002) Fleeting activation of ionotropic glutamate receptors sensitizes cortical neurons to complement attack. Neuron 36:363-374.

Yang Y, Vidensky S, Jin L, Jie C, Lorenzini I, Frankl M, Rothstein JD (2011) Molecular comparison of GLT1+ and ALDH1L1+ astrocytes in vivo in astroglial reporter mice. Glia 59:200-207.

Yao X, Verkman AS (2017a) Marked central nervous system pathology in CD59 knockout rats following passive transfer of Neuromyelitis optica immunoglobulin G. Acta Neuropathol Commun 5:15.

Yao X, Verkman AS (2017b) Complement regulator CD59 prevents peripheral organ injury in rats made seropositive for neuromyelitis optica immunoglobulin G. Acta Neuropathol Commun 5:57.

Zhang H, Verkman AS (2014) Longitudinally extensive NMO spinal cord pathology produced by passive transfer of NMO-IgG in mice lacking complement inhibitor CD59. J Autoimmun 53:67-77.

Acknowledgements

We thank M. Budak, N. Budak, and S. Taskin for animal husbandry and Y. Hufnagel, K. Wullimann, M. Schetterer for technical and administrative support. The *Aldh1l1*:GFP mouse strain used for this project (STOCK Tg(Aldh1l1-EGFP)OFC789Gsat/Mmucd; identification no.: 011015-UCD) was obtained from the Mutant Mouse Regional Resource Center, a NCRR-NIH-funded strain repository, and was donated to the MMRRC by the NINDS funded GENSAT BAC transgenic project.

Funding

This project was supported by the Deutsche Forschungsgemeinschaft (DFG) grant TRR 274/1 2020 (B03 to MH and TM; ID 408885537), as well as under Germany's Excellence Strategy within the framework of the Munich Cluster for Systems Neurology (EXC 2145 SyNergy – ID 390857198; to TM, BH) and by the Gemeinnützige Hertie foundation (P1150064 to MH, BH and TM). BH's laboratory was further by the EU consortium MultipleMS and the BMBF funded Clinspect-M project. TM is supported by European Research Council under the European Union's Seventh Framework Program (grant no. FP/2007-2013; ERC Grant Agreement no.: 616791), the German Center for Neurodegenerative Disease (DZNE) and the DFG (CRC870 A11 – ID 118803580, Mi 694/7-1 – ID 299370739, Mi 694/8-1 – ID 323061152, Mi 694/9-1 A03 – ID 428663564). SK received support from the DFG-funded Graduate School of Systemic Neurosciences (GSC 82 – ID 24184143). JLB is supported by the National Institutes of Health (EY022936).

Author Contributions

SK, MH, BH and TM are responsible for the concept and study design. SK acquired and analyzed glial morphology/calcium imaging data, and characterization of CD59 overexpression experiments. JLB provided recombinant antibodies. SK drafted the manuscript and figures with the input from MH and TM.

Competing Interests

TM, SK: No competing interests. MH received speaker honoraria from Alexion Company (outside of the submitted work). BH has served on scientific advisory boards for Novartis; he has served as DMSC member for AllergyCare, Polpharma and TG therapeutics; he or his institution have received speaker honoraria from Desitin; his institution received research grants from Regeneron for MS research. He holds part of two patents; one for the detection of antibodies against KIR4.1 in a subpopulation of patients with MS and one for genetic

determinants of neutralizing antibodies to interferon. None of these activities causes a conflict of interest relevant to the topic of the study. None of these activities causes a conflict of interest relevant to the topic of the study.

Figure 1

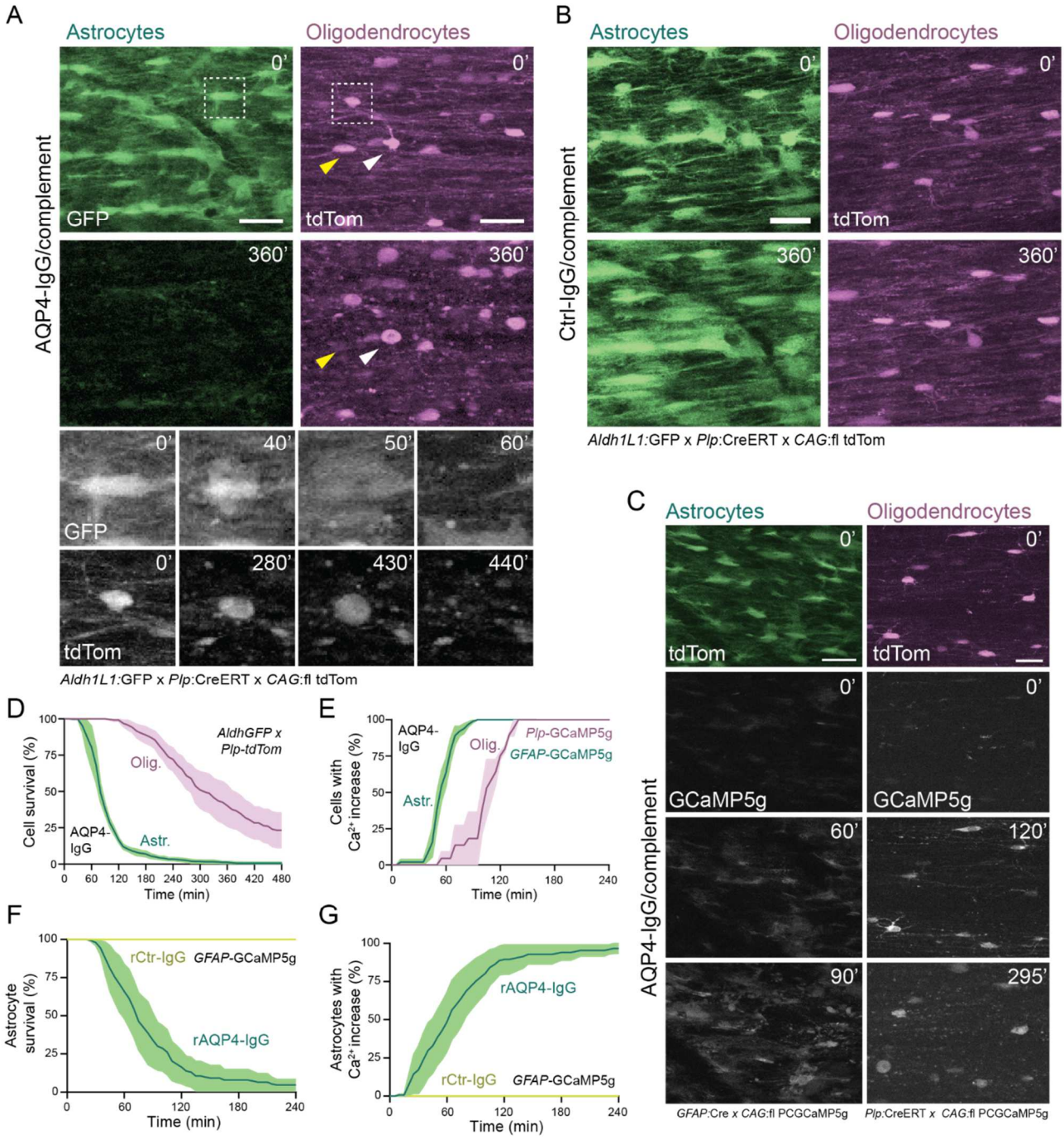
A
Astrocytes
Oligodendrocytes
AQP4-IgG/complement
GFP
tdTom
Aldh1L1:GFP x Plp:CreERT x CAG:fl tdTom
B
Astrocytes
Oligodendrocytes
Ctrl-IgG/complement
tdTom
Aldh1L1:GFP x Plp:CreERT x CAG:fl tdTom
C
Astrocytes
Oligodendrocytes
AQP4-IgG/complement
tdTom
GCaMP5g
GFAP:Cre x CAG:fl PCGCaMP5g
Plp:CreERT x CAG:fl PCGCaMP5g
D
Cell survival (%)
AldhGFP x Plp-tdTom
Olig.
AQP4-IgG
Astr.
Time (min)
E
Cells with Ca2+ increase (%)
AQP4-IgG
Olig.
Plp-GCaMP5g
GFAP-GCaMP5g
Astr.
Time (min)
F
Astrocyte survival (%)
rCtr-IgG GFAP-GCaMP5g
rAQP4-IgG
Time (min)
G
Astrocytes with Ca2+ increase (%)
rAQP4-IgG
rCtr-IgG GFAP-GCaMP5g
Time (min)

Figure 1. *Glial calcium rise preceded AQP4-IgG mediated astrocyte loss and subsequent oligodendrocyte injury*

(A) Representative in vivo time-lapse images in acute spinal experimental NMO lesions showing the astrocyte depletion (green) and oligodendrocyte morphological changes (magenta); swollen somata with condensed nuclei (white arrowhead, 360min). Swollen oligodendrocytes were lost in later time points (yellow arrowhead, 360min). Boxed areas are magnified below and depicting the morphological alterations at indicated time points. GFP: swollen astrocyte (40´), cell lysis (50´); tdTom: swollen oligodendrocyte with process beadings and condensed nuclei (280´, 430´), cell loss (440´). Both astrocytes and oligodendrocytes were imaged simultaneously in a triple transgenic *ALDH1L1*:GFP x *Plp:*CreERT x *CAG*:fl tdTom mouse. Scale bars 30 µm.

(B) After 6h application of Ctrl-IgG/complement, no glial cell loss was observed in spinal cord of *ALDH1L1*:GFP x *Plp:*CreERT x *CAG*:fl tdTom mouse. Scale bar 30 µm.

(C) Glial calcium elevation in experimental NMO lesions. GCaMP5g expressing astrocytes (*GFAP*:Cre x *CAG*:fl PCGCaMP5g IRES tdTom, green) and oligodendrocytes (*Plp*:CreERT x *CAG*:fl PCGCaMP5g IRES tdTom, magenta) showed calcium rise in vivo. Scale bars: 20 µm (left), 30 µm (right).

(D) Survival plot of glial cells following application of AQP4-IgG/complement for 8hours. Oligodendrocyte injury (purple) was observed in relatively later time points compared to astrocytic depletion (green). Astrocytes $t_{50\%}$ survival= 77 ± 7 min; oligodendrocytes $t_{50\%}$ survival = 332 ± 43 min (*ALDH1L1*:GFP x *Plp:*CreERT x *CAG*:fl tdTom mice, n=3).

(E) Percentage of glial cells with high calcium levels (>1.5x to baseline GCaMP5) after AQP4-IgG/complement application. Astrocytes $t_{50\%}$High-Ca = 55 ± 3.8 min, oligodendrocytes $t_{50\%}$High-Ca = 106 ± 6.9 min. *GFAP*:Cre x *CAG*:fl PCGCaMP5g IRES tdTom (green, n=3) and *Plp*:CreERT x *CAG*:fl PCGCaMP5g IRES tdTom (purple, n=2) mice.

(F) Astrocyte survival plot and **(G)** percentage of high-Ca^{2+} cells following application of rAQP4-IgG or rCtrl-IgG/complement. Temporal dynamics of the cell survival and calcium elevation in astrocytes with rAQP4-IgG (green, n=4) was similar to AQP4-IgG treated experimental lesions (D-E; in green). rAQP4-IgG: Astrocytes $t_{50\%}$ High-Ca = 64 ± 17.4 min; $t_{50\%}$ survival= 78 ± 16.4 min. No astrocytic loss or calcium elevation was observed after rCtrl-IgG treatments (yellow, n=3).

Data represent mean ± SEM in D-G.

Figure 2

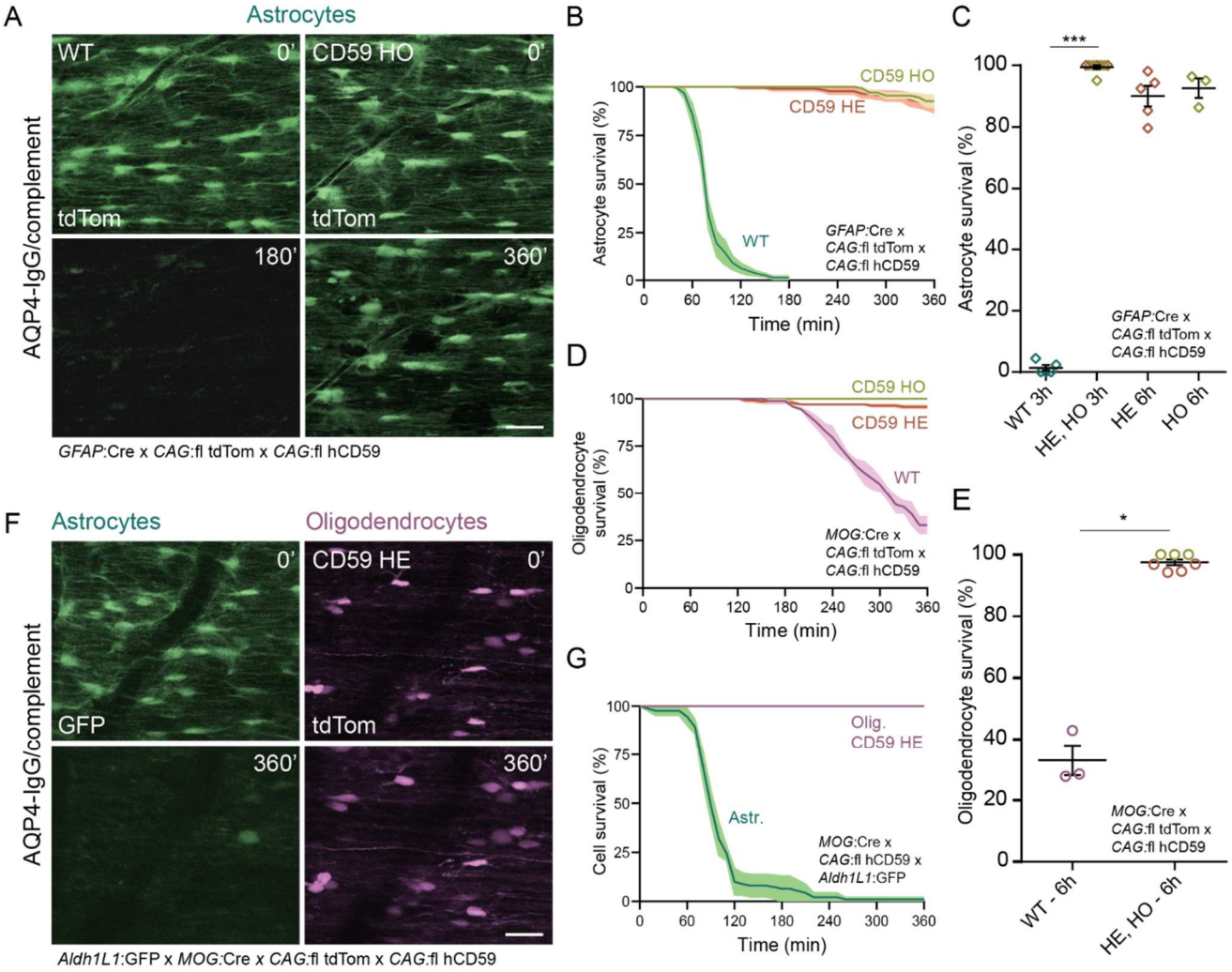
A
Astrocytes
WT
0'
CD59 HO
0'
tdTom
tdTom
180'
360'
AQP4-IgG/complement
GFAP:Cre x CAG:fl tdTom x CAG:fl hCD59
B
CD59 HO
CD59 HE
WT
GFAP:Cre x CAG:fl tdTom x CAG:fl hCD59
Astrocyte survival (%)
Time (min)
C
***
Astrocyte survival (%)
GFAP:Cre x CAG:fl tdTom x CAG:fl hCD59
WT 3h
HE, HO 3h
HE 6h
HO 6h
D
CD59 HO
CD59 HE
WT
MOG:Cre x CAG:fl tdTom x CAG:fl hCD59
Oligodendrocyte survival (%)
Time (min)
E
*
Oligodendrocyte survival (%)
MOG:Cre x CAG:fl tdTom x CAG:fl hCD59
WT - 6h
HE, HO - 6h
F
Astrocytes
Oligodendrocytes
0'
CD59 HE
0'
GFP
tdTom
360'
360'
AQP4-IgG/complement
Aldh1L1:GFP x MOG:Cre x CAG:fl tdTom x CAG:fl hCD59
G
Olig.
CD59 HE
Astr.
MOG:Cre x CAG:fl hCD59 x Aldh1L1:GFP
Cell survival (%)
Time (min)

Figure 2. *Expression of MAC inhibitor protein hCD59 protected the glial cells from AQP4-IgG mediated injury*

(A) Following 6hour treatment with AQP4-IgG/complement, astrocytes expressing the hCD59 protein was protected from a direct complement attack and subsequent cell lysis in *GFAP:*Cre x *CAG*:fl tdTom x *CAG*:fl hCD59 mice (CD59 homozygous, HO and heterozygous, HE). Only minor levels of astrocyte loss was observed in these mice after 6hour of lesion induction. In contrast, astrocytes without hCD59 expression died after 3hours of AQP4-IgG/complement application in littermate controls (CD59 negative, WT). Scale bar: 30 µm

(B) Astrocyte survival plot and **(C)** fraction of live hCD59 expressing astrocytes following treatment with AQP4-IgG/complement: in hCD59 homozygous (CD59 HO, after 6h, mean ± SEM: 93 ± 3, n=3), heterozygous (CD59 HE, after 6h, mean ± SEM: 90 ± 3.3, n=5) mice and littermate controls (WT, after 3h, mean ± SEM: 1.4 ± 0.9 %, n=5). Mann Whitney test, ***p (astrocyte survival after 3h, WT vs $CD59_{HE,HO}$)=0.0008.

(D) Oligodendrocyte survival plot and **(E)** fraction of live oligodendrocytes. Oligodendrocytes expressing hCD59 was protected from AQP4-IgG/complement mediated injury in *MOG:*Cre x *CAG:*fl tdTom x *CAG:*fl hCD59 mice (CD59 HE: 96 ± 0.7, n=4; CD59 HO: 100 ± 0, n=3), compared to hCD59 negative triple transgenic littermates (WT: 33 ± 4.9, n=3). Mann Whitney test, *p (oligodendrocyte survival after 6h, WT vs $CD59_{HE,HO}$)=0.0167.

(F) hCD59 expressing oligodendrocytes were imaged simultaneously with astrocytes in *ALDH1L1:*GFP x *MOG:*Cre x *CAG:*fl tdTom x *CAG*:fl hCD59 mice, during formation of AQP4-IgG/complement mediated experimental NMO lesions. Oligodendrocytes remain protected without any sign of process beading and cell loss, even after complete depletion of astrocytes (after 6h, mean ± SEM: 1.1 ± 1.1 %, n=3). Scale bar: 30 µm

(G) Glial cell survival plot of *ALDH1L1:*GFP x *MOG:*Cre x *CAG:*fl tdTom x *CAG*:fl hCD59 (n=3).

Figure 3

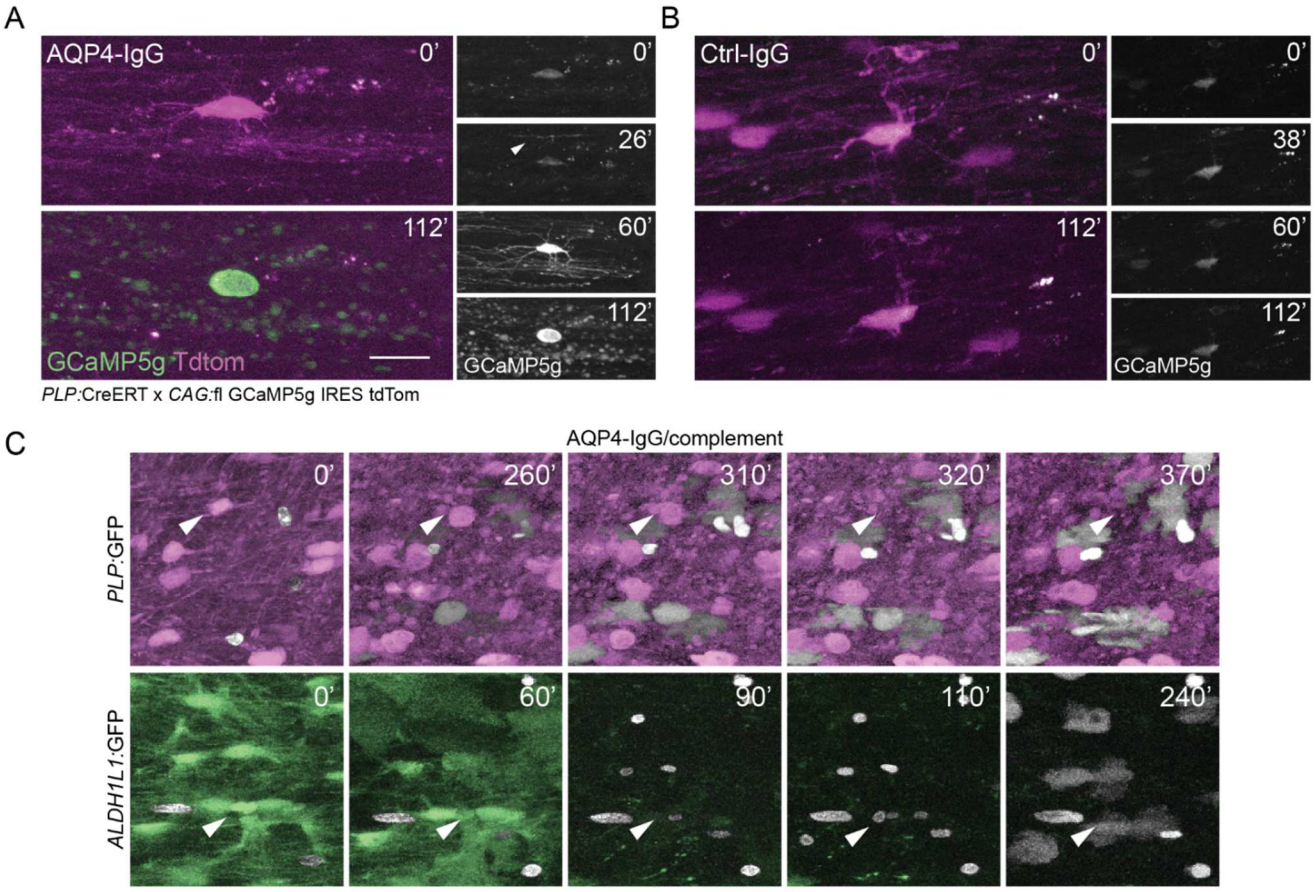
A
AQP4-IgG
0'
0'
26'
112'
60'
112'
GCaMP5g Tdtom
GCaMP5g
B
Ctrl-IgG
0'
0'
38'
112'
60'
112'
GCaMP5g
PLP:CreERT x CAG:fl GCaMP5g IRES tdTom
C
AQP4-IgG/complement
PLP:GFP
0'
260'
310'
320'
370'
ALDH1L1:GFP
0'
60'
90'
110'
240'

Figure 3. *Oligodendrocyte injury initiates in the processes with calcium rise*

(A) Sparsely labeled oligodendrocytes (magenta) expressing GCaMP5g (gray) in *Plp*:CreERT x *CAG*:fl PCGCaMP5g IRES tdTom tg mice. AQP4-IgG/complement mediated injury preceded with transient calcium elevations in oligodendrocyte processes (26'). Global, steady calcium rise was observed at later time points (60') and followed by morphological changes (112'), such as swollen soma and process beadings. Scale bar: 30 µm.

(B) Treatment with Ctrl-IgG/complement did not lead to oligodendrocyte injury and calcium elevation.

(C) Cell-impermeable nuclear dye, EthD uptake assay of oligodendrocytes (magenta) and astrocytes (green). Astrocyte nuclei were labeled and traced with EtHD following the lytic cell death, whereas oligodendrocytes remained negative to such labeling suggesting comparatively preserved membrane integrity of cells.

3 Discussion

Various NMO models have been useful to study the contribution of NMOSD antibodies (AQP4-IgG or MOG-IgG), complement activation and immune cell infiltration into CNS, to the progression of NMO pathogenesis (Bradl et al., 2009; Kinoshita et al., 2009; Saadoun et al., 2010; Saadoun et al., 2014; Wrzos et al., 2014). Although these models could mimic certain hallmarks of NMO and reproduce secondary demyelination and axon injury following astrocyte depletion, these studies were mostly representative for the late phases of NMO lesions (Saadoun et al., 2010; Ratelade et al., 2013).

Therefore, we previously established a mouse model of NMO-related pathology, which allows in vivo imaging during the induction phase of experimental lesions in the spinal cord (Herwerth et al., 2016). This model involves local application of human-derived or recombinant NMO-IgGs together with human complement to the dorsal spinal cord in transgenic mice, which initiates acute astrocyte loss and emergence of NMO-like lesions in optically accessible parts of the mouse spinal cord. This approach allowed us to determine the immediate dynamic changes in cellular morphology and intracellular signaling likely to contribute to NMO lesion formation, which could not be assayed in previous NMO models.

The experiments presented in my thesis were devised to understand how astrocyte loss in our NMO model causes secondary injury in neurons and oligodendrocytes. We found that this primary astrocytopathic attack resulted in antibody-independent, ‘off target’ MAC-mediated oligodendrocyte damage (Kenet et al., in preparation), and acute axonal beading due to cytoskeletal disruptions (Herwerth, Kenet et al., in submission). I also established an NMO survival surgery approach to study the fate of injured axons on the day following the induction of astrocyte loss. Here we found no overt signs of axon degeneration, supporting the notion that a time window for providing acute therapeutic interventions to prevent permanent neurological damage from initial NMO attack might exist.

3.1 MAC-mediated glial injury in experimental NMO lesions

Complement activation was the main mediator of glial cell damage in our NMO model (Herwerth et al., 2016). This is in line with most studies on NMO, despite the notion that also AQ4-IgG alone could have some detrimental effects via direct AQP4 modulation (Hinson et al., 2008; Hinson et al., 2012). Indeed, the complement-dependent pathogenicity of AQP4-

IgGs has been confirmed in various experimental NMO models (Saadoun et al., 2010; Wrzos et al., 2014). Complement activation follows a well-defined pathway, which initiates with antibody binding to target cells, and leads to insertion of the terminal complement complex - the MAC pore - into the plasma membrane that eventually causes the osmolytic death of cells (Tegla et al., 2011). Accordingly, in our model, when the complement regulator protein CD59, which interferes with MAC pore formation (Farkas et al., 2002; Kimberley et al., 2007), was expressed on astrocytes, cell depletion was halted even in the presence of AQP4-IgG and active complement (**Fig. 3**, Kenet et al., in preparation). This is expected and confirming the dual IgG/classical complement requirements of our model that we had demonstrated earlier (Herwerth et al., 2016). However, mechanisms on how cells other than astrocytes are damaged in NMO lesions remains to be less well understood. The previously formulated models implicated alternatives including off-target complement attack (Tradtrantip et al., 2017; Duan et al., 2018), immune cell-mediated toxicity (e.g. depending on the granulocytes that characteristically infiltrate more advanced NMO lesions (Saadoun et al., 2010; Asavapanumas et al., 2014; Asavapanumas and Verkman, 2014)) or non-specific secondary necrosis. While for NMO itself a combination of these factors is likely, our acute NMO model provided the unique opportunity to watch the earliest phases of the cellular spread of pathology. Indeed, despite initial sparing from cell death (Herwerth et al., 2016), oligodendrocytes were also vulnerable to the MAC-mediated complement targeting even though there was no direct antibody attack to oligodendrocytes (Kenet et al., in preparation). Notably, compared to astrocytes, oligodendrocyte injury was slower and seemed to show a more sustained phase of injury to the cell's periphery, before overt somatic shape changes and finally apparent lysis occurred. This proximate secondary injury of oligodendrocytes might be due to an unusually high vulnerability of oligodendrocytes to complement as suggested previously (Alberdi et al., 2006). Macroglial cells in general appear to share this vulnerability compared to many other cells in the body (e.g. AQP4-positive cells in the kidney, which are not typically damaged in NMO (Jarius et al., 2020)), perhaps due to CNS cells are normally shielded from complement by the BBB. Many nucleated cells have mechanisms to protect themselves from complement attack, e.g. based on expression of complement regulatory proteins such as CD46, CD55 and CD59, which protect them from eventual cell lysis (Dunkelberger and Song, 2010). Indeed, oligodendrocytes express low levels of complement regulatory proteins (Wing et al., 1992; Piddlesden and Morgan, 1993; Scolding et al., 1998), which render them vulnerable to the presence of activated complement without the need of a primary antibody attack (Wood et al., 1993). Based on such arguments, antibody-independent bystander complement targeting has

been implicated in NMO-related secondary injury of oligodendrocytes and neurons following AQP4-IgG/complement-mediated injury (Tradtrantip et al., 2017; Duan et al., 2018). In these studies, in situ light microscopy revealed the presence of soluble complement proteins and MAC on oligodendrocytes, but also on neurons, suggesting MAC-mediated spread of experimental NMO pathology from astrocytes to neighboring cells (Tradtrantip et al., 2017; Duan et al., 2018).

For oligodendrocytes, we could corroborate this notion by demonstrating in vivo that oligodendrocyte-specific overexpression of hCD59 protected oligodendrocytes during AQP4-IgG/complement-mediated astrocyte loss in experimental NMO lesions (**Fig. 2D-F**, Kenet et al., in preparation). In vivo observation of the astrocyte-depleted lesions in which CD59-protected oligodendrocytes survived confirmed that the change in extracellular milieu after necrotic death of astrocytes (e.g. dysregulation of water, ion or neurotransmitter levels; (Parpura and Verkhratsky, 2012; Verkhratsky et al., 2012)), the spread of pathology via gap junctions dysfunction (Sharma et al., 2010; Richard et al., 2020) or the loss of astrocytic support e.g. provision of metabolites (Murphy-Royal et al., 2017) was not sufficient to induce acute oligodendrocyte injury (Kenet et al., in preparation). Overall, our findings revealed that antibody-independent MAC-deposition initiates the oligodendrocyte injury in experimental NMO – and provides seminal in vivo support for the 'bystander' model that thus far was mostly based on indirect or in vitro observations.

3.2 Calcium dyshomeostasis and mechanisms of glial cell death

Complement-mediated MAC-driven glial injury first emerged with rapid calcium elevations in astrocytes and oligodendrocytes, preceding any morphological alterations or cell loss (**Fig. 1D-E**, Kenet et al., in preparation). MAC is a transmembrane pore with 11 nm inner diameter that allows ion and water flux (Tegla et al., 2011), which can provide an entry route for extracellular calcium influx into glial cells. In our model, astrocyte calcium elevations were very rapid, possibly mediated by abundant and global MAC deposition on the membrane of astrocytes, perhaps amplified by secondary osmotic membrane rupture (**Fig. 3C**, Kenet et al., in preparation). Oligodendrocytes apparently lacked a similar extent of membrane damage (**Fig. 3C**, Kenet et al., in preparation); still, transient calcium elevations were observed on oligodendrocyte processes soon after AQP4-IgG/complement-mediated targeting of astrocytes (**Fig. 2A**, Kenet et al., in preparation). It is plausible that these early calcium changes might

arise from MAC insertion on oligodendrocyte processes, presumably those that are in close proximity to astrocytes, e.g. near node of Ranvier. Such sites would serve as predilection sites for the unspecific 'bystander' complement attack that spills over from astrocytes to oligodendrocytes (for a summary of oligodendrocyte injury, see Figure 2). However, we currently lack the resolution to pinpoint the exact site of initial oligodendrocyte injury, leaving this notion in the realm of speculation. In any case, it has been previously shown that a complement attack on oligodendrocytes can induce transient calcium oscillations (Wood et al., 1993), which were ascribed to the intrinsically transitory pore opening of MAC or perhaps also the vesicular removal of MAC pores by cell repair mechanisms (Scolding et al., 1989a; Wood et al., 1993). Following the phase of transient calcium rise on processes, oligodendrocytes entered a later phase of global and stable calcium elevation (**Fig. 3A**, Kenet et al., in preparation). These findings suggest the involvement of additional calcium sources to promote sustained calcium elevation in oligodendrocytes, such as calcium release from internal stores or activation of gated calcium channels in the plasma membrane (Wood et al., 1993). Such a secondary amplification, which we have not addressed in our model yet, could be approached using biosensors and pharmacological interventions used previously in the lab to study neuroinflammatory or traumatic axon degeneration (Williams et al., 2014; Witte et al., 2019).

Alternatively, calcium dyshomeostasis in oligodendrocytes might be mediated via gap-junction coupling between astrocytes and oligodendrocytes (Giaume et al., 2013). When calcium rises in an astrocyte's cytoplasm (via ion influx through MAC pores), calcium ions might propagate swiftly to oligodendrocyte processes that are in continuity with astrocytes via connexin channels. However, it should be noted that gap junctions can be gated by intracellular concentration of calcium - at higher concentrations inhibiting the hemi-channel function - providing a potential counterbalance (Giaume et al., 2013). Such transcellular calcium flow from injured astrocytes may explain the short-lasting nature of low intensity calcium elevation observed on oligodendrocyte processes, since this source may dwindle following the swift necrotic death of astrocytes or by inhibition of hemichannels (Kenet et al., in preparation).

Moreover, despite an apparently similar starting point of MAC-mediated injury, several observations in our model provide hints that the eventual fate of oligodendrocytes might differ from the lytic necrosis of astrocytes. For instance, preliminary experiments using dye exclusion failed to detect overt breakdown of membrane integrity in oligodendrocytes – which was apparent in astrocytes. The interplay between the number of MAC pores and cellular mechanisms to resist MAC-deposition (such as vesicular internalization or the shedding of

MAC) would define whether a cell undergoes the osmolytic death (Moskovich and Fishelson, 2007; Xie et al., 2020). In conditions that MAC density does not suffice to exert its lytic effects, additional downstream players were implicated to activate cell death (Ziporen et al., 2009; Lusthaus et al., 2018), pro-inflammatory (Triantafilou et al., 2013) or pro-survival pathways (Soane et al., 1999; Cudrici et al., 2006), most of which involve calcium influx through MAC pores (Xie et al., 2020). This chimes with the spatial and temporal differences we observed in glial morphological changes and calcium dyshomeostasis, which in astrocytes tended to be fast and global while oligodendrocytes showed a slow 'outside-in' pattern of cellular pathology (Kenet et al., in preparation). In future experiments, we plan to explore whether this difference is also reflected in different cell death pathways that mediate final cellular demise – in the hope to define possible intervention points to rescue oligodendrocytes, especially in light of the results that suggest that surviving oligodendrocytes could indeed contribute to subsequent remyelination, e.g. in MS (Yeung et al., 2019).

Moreover, additional factors might differentially regulate complement susceptibility between astrocytes and oligodendrocytes, such as sub-lethal glutamate excitotoxicity, which could modulate MAC insertion or add a 'second hit' to oligodendrocytes (Alberdi et al., 2006; Wrzos et al., 2014) – aspects that we will be able to test by monitoring and modulating glutamate release and signaling. Additionally, our in vivo CD59-overexpression approach allows restricting cellular injury to individual cell types and study long-term consequences, e.g. by moving antibody/complement injury to chronic cortical or spinal window preparations. Here, we have started developing the required preparations, but also employing antibodies that primarily target oligodendrocytes – in an attempt to mimic some aspects of non-AQP4-dependent NMOSD and explain the convergence of such lesions to a similar final state of multi cellular injury, despite the increasingly appreciated differences in lesion pathology between NMO and MOGAD.

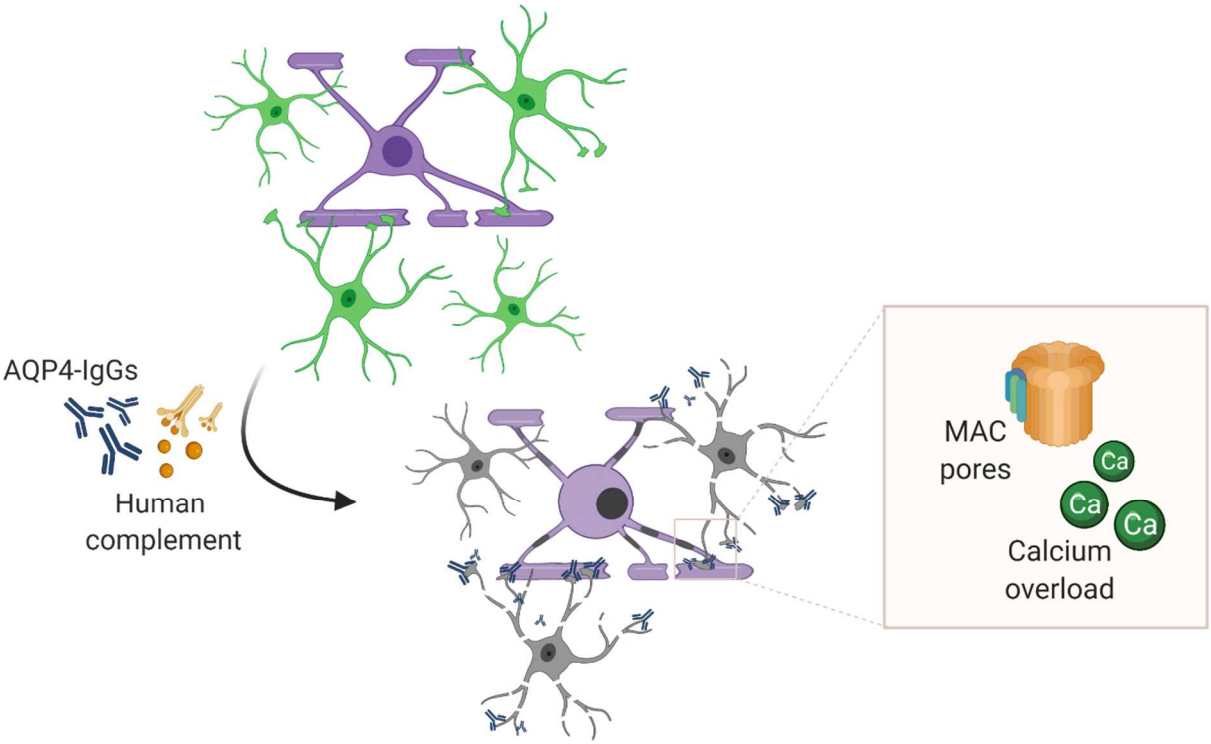

Figure 2. Antibody independent, MAC-mediated oligodendrocyte injury in experimental NMO

Following AQP4-IgG binding to astrocytes (green), classical complement cascade is activated and lead to lytic death of astrocytes (gray). Activated, soluble complement proteins such as components of MAC pore (C5b-9), can spill over and target unspecific cells in close contact with astrocytes; for example oligodendrocytes (purple). MAC deposition allow calcium influx, which can further activate downstream pro-inflammatory or cell death cascades, leading eventual cell loss. (Figure was created with BioRender.com)

3.3 Distinctive features of axonal injury in experimental NMO

In addition to exploring the mechanisms of spreading injury amongst glial cells and hence the emergence of demyelination, I also addressed the question of how axons might get injured in the aftermath of an astrocytopathic attack, as axonal injury is another hallmark of NMO (Lucchinetti et al., 2002; Misu et al., 2013). As opposed to the early and global calcium dyshomeostasis that precedes morphological signs of glial injury, axons in our model showed only inconsistent calcium elevations (**Fig. 1D**, Herwerth*, Kenet* et al., in submission). This was apparent only hours after axons had undergone a dramatic shape change, which we named acute axonal beading. Therefore, our results argue against the presence of membrane pores on axons, which can underlie calcium influx into axons during trauma or MS-related spinal

pathology (Williams et al., 2014; Witte et al., 2019). This result also rules out MAC-pores and hence the previously proposed involvement of a 'bystander' effect in NMO-related axonal injury (Duan et al., 2018). However, our current conclusion is based limited by the possibility that MAC-mediated calcium influx below the detection level of our imaging might still contribute to the beading process. While this is unlikely, given the high sensitivity of the calcium sensor we used (Mank et al., 2008; Williams et al., 2014), a more direct assessment of MAC involvement in acute axonal beading will be desirable for the future. For this, we can investigate the presence of terminal complement proteins on axons in experimental NMO lesions, e.g. using enhanced resolution light microscopy techniques or even immune-electron microscopy. As a 'negative' result with these methods however, will still remain contentious, we also plan to study the axonal injury responses of CD59-expressing neurons to AQP4-IgG/complement-mediated astrocyte loss, in analogy to how we explored the 'bystander' mechanism in oligodendrocytes. Currently, the challenge is to identify a suitable viral promotor or transgenic line to express Cre-recombinase in the thin-caliber dorsal column axon population that we found to be especially vulnerable to acute axonal beading.

In addition to arguing against a bystander attack on axons, our data also refute the involvement of another prominent axon degeneration pathway that has been implicated in neuroinflammation (Singh et al., 2017) namely Wallerian-like degeneration. First, Wallerian-like degeneration is also typically triggered by a calcium-dependent initiation event (Vargas et al., 2015; Coleman and Hoke, 2020). Second, Wallerian-like degeneration can now be defined by the involvement of a core set of endogenous mediators, most prominently SARM (Osterloh et al., 2012). Deletion of the SARM gene did not alter acute axonal beading in our experimental NMO lesions, effectively ruling out this pathway as an early mediator of axon injury (**Fig. 4D**, Herwerth*, Kenet* et al., in submission).

Hence, we turned to alternative explanations of axonal beading. One widely implicated process in axon injury, e.g. after ischemia (Stys, 1998; Stirling and Stys, 2010), but also in neuroinflammatory settings (Waxman, 2006; Friese et al., 2014), is ionic overload – which typically involves sodium initially, but later can also result in secondary calcium influx, e.g. due to bioenergetics failure or pump reversals. Indeed, when we used TTX to reduce sodium load in axons after AQP4-IgG/complement-mediated astrocyte loss, we observed a reduction in axon swellings (**Fig. 4F**, Herwerth*, Kenet* et al., in submission). However, as we did not observe calcium influx into axons before they swelled, we sought an alternative explanation for shape changes – and focused on osmotic effects, as astrocytes and AQP4 are core regulators

of CNS water homeostasis. Indeed, hyperosmotic intervention diminished the axonal beadings (and even the late emergence of a high calcium axons; not shown), suggesting that axonal beading might be driven by an osmotic and hence mechanical process. Previous in vitro and biophysical work (Pullarkat et al., 2006; Datar et al., 2019) has indeed tied the formation of 'string-of-pearl' patterns of axon swelling to a mechanical disruption of the interplay between cytoskeleton and plasma membrane. Both ultrastructural and immunohistochemical data showed that the core of NMO-related axonal beadings showed cytoskeletal arrangements with local microtubule loss (for a summary of axonal injury, see Figure 3). Stabilizing microtubules with pharmacological intervention (as proposed previously for promoting axonal growth; (Hellal et al., 2011; Ruschel et al., 2015)) indeed rescued the beading phenotype (**Fig. 5A**, Herwerth*, Kenet* et al., in submission). Thus, loss of microtubule stability seems to be a promoting factor of acute axonal beading, possibly by altering the threshold tension for beading formation as previously described in pearling-instability models (Datar et al., 2019). Expansion of the tubular volume of an axon within the beaded area can lead to higher surface tension and membrane stretch at the later phases of acute axonal beading. In a vicious cycle, such mechanical stress might irreversibly change the kinetics of voltage gated sodium channels (Shcherbatko et al., 1999), further increasing the local sodium load and perhaps eventually activating the reserve mode of Na^+/Ca^{2+} exchangers (Wolf et al., 2001) and lead calcium influx observed in some of the beaded axons (**Fig. 1D**, Herwerth*, Kenet* et al., in submission). Alternatively, membrane stretch could activate mechanoreceptors and induce calcium influx (Song et al., 2019). In our NMO model, thin axons were more vulnerable to acute axonal beading (**Fig. 3A**, Herwerth*, Kenet* et al., in submission), which might be more sensitive to mechanical stress e.g. due to their expression of Piezo1, a mechano-nociceptive cation channel primarily present in small diameter DRG neurons (Wang et al., 2019). However, also simple geometrical or cytoskeletal characteristics of these axons might explain their pronounced vulnerability; future experiments using pharmacological intervention or a combination of gene deletion and overexpression would allow us to address these open questions.

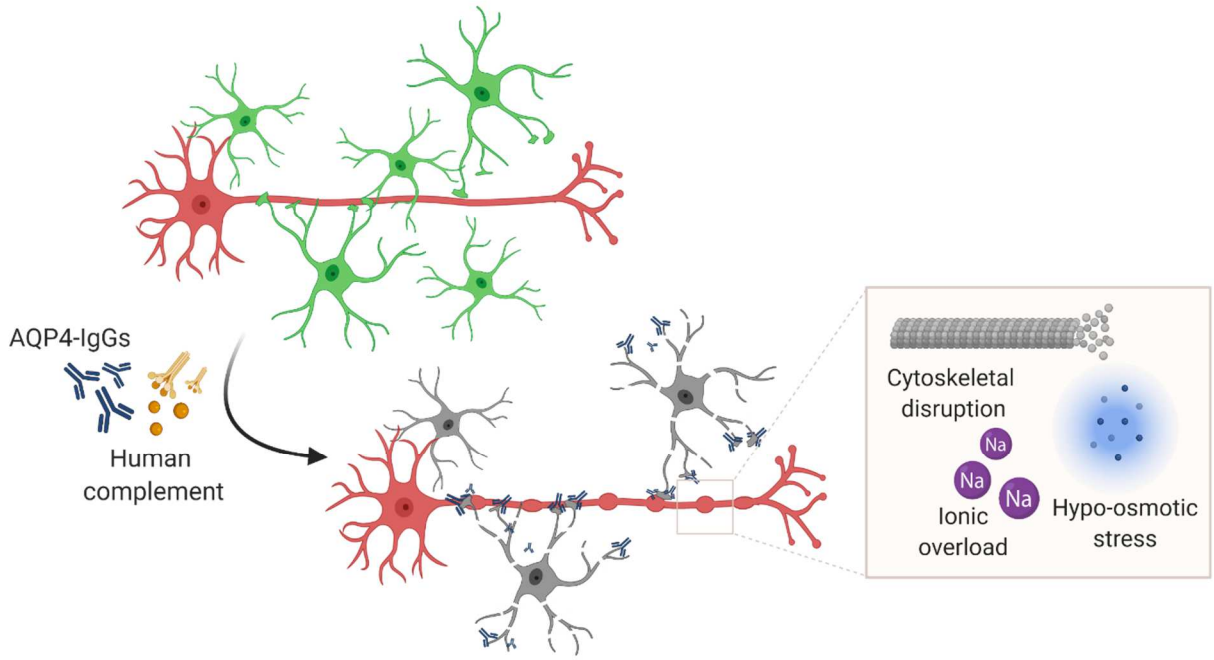

Figure 3. Ionic-osmotic stress and cytoskeletal disruption drive axonal injury in experimental NMO

Following AQP4-IgG binding to astrocytes (green), classical complement cascade is activated and lead to lytic death of astrocytes (gray), which alters homeostasis of extracellular milieu. In the presence of such osmotic stress and ionic overload (e.g. sodium influx to axons), subsequent microtubule loss impairs the cytoskeletal integrity and promotes acute axonal beading (red). (Figure was created with BioRender.com)

3.4 Limitations of NMO-related mouse model

Although our in vivo NMO-related mouse model is unique to allow following the induction and development of experimental lesions, it has certain limitations. First, low activity of mouse complement (Ratelade and Verkman, 2014) made the necessity of providing human complement source together with AQP4-IgGs to induce experimental NMO lesions. Although this is not uncommon, and human complement have been supplemented in various NMO models (Saadoun et al., 2010; Ratelade et al., 2013; Wrzos et al., 2014), this may lead to certain variability in the dynamics of cellular injury progression we have observed in our model when compared to human pathology.

One of the distinctive immunopathological features of NMO is the perivascular deposition of antibodies and complement, which suggests leaky (e.g. area postrema) or disrupted (e.g. due to astrocyte loss, local inflammation or immune cell infiltration (Takeshita et al., 2017; Winkler

et al., 2021)) BBB regions as the primary access sites for peripheral antibodies entry to CNS (Lucchinetti et al., 2002; Misu et al., 2007; Roemer et al., 2007). Our spinal model of NMO employs the local application of antibody/complement over the pial surface; therefore would not mimic vasculocentric nature of initial NMO pathology. Additionally, pial surface delivery is restrictive in terms of lesion localization and spread of experimental NMO, since the pathogenic impact of antibody/complement only applies within the range of tissue penetration of these components.

Lastly, my PhD project focused on elucidating early cellular injury responses underlying development of experimental NMO lesions, but we have not yet explored the later events involved in aggravation of the local inflammatory responses; such as immune cell infiltration, cytokine release or subsequent gliosis, all of which have been implicated in different stages of NMO lesions (Misu et al., 2013). However, presence of complement inhibitors in mouse serum (Ratelade and Verkman, 2014) might hinder secondary amplification steps of neuroinflammatory responses in the absence of supplementary complement source. Therefore, rat models of NMO may be more suitable to investigate chronic stages of experimental lesions – a recent study on systemic antibody transfer model already implicated experimental lesions and behavioral phenotype without the need of additional complement delivery (Hillebrand et al., 2019).

3.5 Conclusion and outlook

The aim of my thesis was to understand the cellular mechanisms involved in the formation and transcellular spread of experimental NMO pathology. While NMO relapses can increasingly be prevented by immunomodulation, including targeting of the complement system (Levy et al., 2021), the first episode of NMO – which is typically the initial manifestation of the disease – is often highly destructive and can cause lasting disability (Wingerchuk et al., 2007; Wingerchuk et al., 2015). Hence, this episode poses a therapeutic challenge akin to other acute forms of CNS injury, such as ischemia or trauma. In analogy to these acute forms of pathology, neuro- or glio-protective interventions could be a first line of treatment before initiating long-term immunomodulation, in order to constrain initial damage and improve the potential for recovery. My hope is that the line of investigation initiated in this thesis work might provide mechanistic understanding of how pathology spreads between cell types in NMO lesions,

which might be of relevance to identify potential intervention points to break the chain of events before irreversible damage occurs.

4 References

Abbott NJ, Ronnback L, Hansson E (2006) Astrocyte-endothelial interactions at the blood-brain barrier. Nat Rev Neurosci 7:41-53.

Akassoglou K, Merlini M, Rafalski VA, Real R, Liang L, Jin Y, Dougherty SE, De Paola V, Linden DJ, Misgeld T, Zheng B (2017) In Vivo Imaging of CNS Injury and Disease. J Neurosci 37:10808-10816.

Akerboom J et al. (2012) Optimization of a GCaMP calcium indicator for neural activity imaging. J Neurosci 32:13819-13840.

Alberdi E, Sanchez-Gomez MV, Torre I, Domercq M, Perez-Samartin A, Perez-Cerda F, Matute C (2006) Activation of kainate receptors sensitizes oligodendrocytes to complement attack. J Neurosci 26:3220-3228.

Allen NJ, Lyons DA (2018) Glia as architects of central nervous system formation and function. Science 362:181-185.

Anderson CM, Swanson RA (2000) Astrocyte glutamate transport: review of properties, regulation, and physiological functions. Glia 32:1-14.

Asavapanumas N, Verkman AS (2014) Neuromyelitis optica pathology in rats following intraperitoneal injection of NMO-IgG and intracerebral needle injury. Acta Neuropathol Commun 2:48.

Asavapanumas N, Ratelade J, Verkman AS (2014) Unique neuromyelitis optica pathology produced in naive rats by intracerebral administration of NMO-IgG. Acta Neuropathol 127:539-551.

Attwell D, Buchan AM, Charpak S, Lauritzen M, Macvicar BA, Newman EA (2010) Glial and neuronal control of brain blood flow. Nature 468:232-243.

Ballatore C, Brunden KR, Huryn DM, Trojanowski JQ, Lee VM, Smith AB, 3rd (2012) Microtubule stabilizing agents as potential treatment for Alzheimer's disease and related neurodegenerative tauopathies. J Med Chem 55:8979-8996.

Bannerman P, Horiuchi M, Feldman D, Hahn A, Itoh A, See J, Jia ZP, Itoh T, Pleasure D (2007) GluR2-free alpha-amino-3-hydroxy-5-methyl-4-isoxazolepropionate receptors intensify demyelination in experimental autoimmune encephalomyelitis. J Neurochem 102:1064-1070.

Bayly-Jones C, Bubeck D, Dunstone MA (2017) The mystery behind membrane insertion: a review of the complement membrane attack complex. Philos Trans R Soc Lond B Biol Sci 372.

Beirowski B, Nogradi A, Babetto E, Garcia-Alias G, Coleman MP (2010) Mechanisms of axonal spheroid formation in central nervous system Wallerian degeneration. J Neuropathol Exp Neurol 69:455-472.

Bennett JL, Owens GP (2017) Neuromyelitis Optica: Deciphering a Complex Immune-Mediated Astrocytopathy. J Neuroophthalmol 37:291-299.

Bennett JL, Lam C, Kalluri SR, Saikali P, Bautista K, Dupree C, Glogowska M, Case D, Antel JP, Owens GP, Gilden D, Nessler S, Stadelmann C, Hemmer B (2009) Intrathecal pathogenic anti-aquaporin-4 antibodies in early neuromyelitis optica. Ann Neurol 66:617-629.

Benoit ME, Tenner AJ (2011) Complement protein C1q-mediated neuroprotection is correlated with regulation of neuronal gene and microRNA expression. J Neurosci 31:3459-3469.

Berger DR, Seung HS, Lichtman JW (2018) VAST (Volume Annotation and Segmentation Tool): Efficient Manual and Semi-Automatic Labeling of Large 3D Image Stacks. Front Neural Circuits 12:88.

Bialas AR, Stevens B (2013) TGF-beta signaling regulates neuronal C1q expression and developmental synaptic refinement. Nat Neurosci 16:1773-1782.
Booth HDE, Hirst WD, Wade-Martins R (2017) The Role of Astrocyte Dysfunction in Parkinson's Disease Pathogenesis. Trends Neurosci 40:358-370.
Bradl M, Lassmann H (2014) Experimental models of neuromyelitis optica. Brain Pathol 24:74-82.
Bradl M, Misu T, Takahashi T, Watanabe M, Mader S, Reindl M, Adzemovic M, Bauer J, Berger T, Fujihara K, Itoyama Y, Lassmann H (2009) Neuromyelitis optica: pathogenicity of patient immunoglobulin in vivo. Ann Neurol 66:630-643.
Brill MS, Lichtman JW, Thompson W, Zuo Y, Misgeld T (2011) Spatial constraints dictate glial territories at murine neuromuscular junctions. J Cell Biol 195:293-305.
Brill MS, Kleele T, Ruschkies L, Wang M, Marahori NA, Reuter MS, Hausrat TJ, Weigand E, Fisher M, Ahles A, Engelhardt S, Bishop DL, Kneussel M, Misgeld T (2016) Branch-Specific Microtubule Destabilization Mediates Axon Branch Loss during Neuromuscular Synapse Elimination. Neuron 92:845-856.
Brosnan CF, Raine CS (2013) The astrocyte in multiple sclerosis revisited. Glia 61:453-465.
Bruck W, Bruck Y, Diederich U, Piddlesden SJ (1995a) The membrane attack complex of complement mediates peripheral nervous system demyelination in vitro. Acta Neuropathol 90:601-607.
Bruck W, Porada P, Poser S, Rieckmann P, Hanefeld F, Kretzschmar HA, Lassmann H (1995b) Monocyte/macrophage differentiation in early multiple sclerosis lesions. Ann Neurol 38:788-796.
Bruck W, Popescu B, Lucchinetti CF, Markovic-Plese S, Gold R, Thal DR, Metz I (2012) Neuromyelitis optica lesions may inform multiple sclerosis heterogeneity debate. Ann Neurol 72:385-394.
Cai H, Zhu J, Zhang N, Wang Q, Zhang C, Yang C, Sun J, Sun X, Yang L, Yu C (2017) Subregional structural and connectivity damage in the visual cortex in neuromyelitis optica. Sci Rep 7:41914.
Chan KY, Jang MJ, Yoo BB, Greenbaum A, Ravi N, Wu WL, Sanchez-Guardado L, Lois C, Mazmanian SK, Deverman BE, Gradinaru V (2017) Engineered AAVs for efficient noninvasive gene delivery to the central and peripheral nervous systems. Nat Neurosci 20:1172-1179.
Chen T, Lennon VA, Liu YU, Bosco DB, Li Y, Yi MH, Zhu J, Wei S, Wu LJ (2020) Astrocyte-microglia interaction drives evolving neuromyelitis optica lesion. J Clin Invest 130:4025-4038.
Chen T, Taniguchi W, Chen QY, Tozaki-Saitoh H, Song Q, Liu RH, Koga K, Matsuda T, Kaito-Sugimura Y, Wang J, Li ZH, Lu YC, Inoue K, Tsuda M, Li YQ, Nakatsuka T, Zhuo M (2018) Top-down descending facilitation of spinal sensory excitatory transmission from the anterior cingulate cortex. Nat Commun 9:1886.
Chung WS, Allen NJ, Eroglu C (2015) Astrocytes Control Synapse Formation, Function, and Elimination. Cold Spring Harb Perspect Biol 7:a020370.
Clarke LE, Liddelow SA, Chakraborty C, Munch AE, Heiman M, Barres BA (2018) Normal aging induces A1-like astrocyte reactivity. Proc Natl Acad Sci U S A 115:E1896-E1905.
Coleman M (2005) Axon degeneration mechanisms: commonality amid diversity. Nat Rev Neurosci 6:889-898.
Coleman MP, Perry VH (2002) Axon pathology in neurological disease: a neglected therapeutic target. Trends Neurosci 25:532-537.
Coleman MP, Freeman MR (2010) Wallerian degeneration, wld(s), and nmnat. Annu Rev Neurosci 33:245-267.

Coleman MP, Hoke A (2020) Programmed axon degeneration: from mouse to mechanism to medicine. Nat Rev Neurosci 21:183-196.
Combes AJE, Matthews L, Lee JS, Li DKB, Carruthers R, Traboulsee AL, Barker GJ, Palace J, Kolind S (2017) Cervical cord myelin water imaging shows degenerative changes over one year in multiple sclerosis but not neuromyelitis optica spectrum disorder. Neuroimage Clin 16:17-22.
Court FA, Coleman MP (2012) Mitochondria as a central sensor for axonal degenerative stimuli. Trends Neurosci 35:364-372.
Cudrici C, Niculescu F, Jensen T, Zafranskaia E, Fosbrink M, Rus V, Shin ML, Rus H (2006) C5b-9 terminal complex protects oligodendrocytes from apoptotic cell death by inhibiting caspase-8 processing and up-regulating FLIP. J Immunol 176:3173-3180.
Curcio M, Bradke F (2018) Axon Regeneration in the Central Nervous System: Facing the Challenges from the Inside. Annu Rev Cell Dev Biol 34:495-521.
da Silva APB, Souza DG, Souza DO, Machado DC, Sato DK (2019) Role of Glutamatergic Excitotoxicity in Neuromyelitis Optica Spectrum Disorders. Front Cell Neurosci 13:142.
Dalakas MC, Alexopoulos H, Spaeth PJ (2020) Complement in neurological disorders and emerging complement-targeted therapeutics. Nat Rev Neurol 16:601-617.
Daneman R, Prat A (2015) The blood-brain barrier. Cold Spring Harb Perspect Biol 7:a020412.
Datar A, Ameeramja J, Bhat A, Srivastava R, Mishra A, Bernal R, Prost J, Callan-Jones A, Pullarkat PA (2019) The Roles of Microtubules and Membrane Tension in Axonal Beading, Retraction, and Atrophy. Biophys J 117:880-891.
Davalos D, Lee JK, Smith WB, Brinkman B, Ellisman MH, Zheng B, Akassoglou K (2008) Stable in vivo imaging of densely populated glia, axons and blood vessels in the mouse spinal cord using two-photon microscopy. J Neurosci Methods 169:1-7.
Davalos D, Grutzendler J, Yang G, Kim JV, Zuo Y, Jung S, Littman DR, Dustin ML, Gan WB (2005) ATP mediates rapid microglial response to local brain injury in vivo. Nat Neurosci 8:752-758.
Deverman BE, Pravdo PL, Simpson BP, Kumar SR, Chan KY, Banerjee A, Wu WL, Yang B, Huber N, Pasca SP, Gradinaru V (2016) Cre-dependent selection yields AAV variants for widespread gene transfer to the adult brain. Nat Biotechnol 34:204-209.
Doerflinger NH, Macklin WB, Popko B (2003) Inducible site-specific recombination in myelinating cells. Genesis 35:63-72.
Duan T, Verkman AS (2020) Experimental animal models of aquaporin-4-IgG-seropositive neuromyelitis optica spectrum disorders: progress and shortcomings. Brain Pathol 30:13-25.
Duan T, Smith AJ, Verkman AS (2018) Complement-dependent bystander injury to neurons in AQP4-IgG seropositive neuromyelitis optica. J Neuroinflammation 15:294.
Duan T, Smith AJ, Verkman AS (2019) Complement-independent bystander injury in AQP4-IgG seropositive neuromyelitis optica produced by antibody-dependent cellular cytotoxicity. Acta Neuropathol Commun 7:112.
Dunkelberger JR, Song WC (2010) Complement and its role in innate and adaptive immune responses. Cell Res 20:34-50.
Erturk A, Hellal F, Enes J, Bradke F (2007) Disorganized microtubules underlie the formation of retraction bulbs and the failure of axonal regeneration. J Neurosci 27:9169-9180.
Escartin C et al. (2021) Reactive astrocyte nomenclature, definitions, and future directions. Nat Neurosci 24:312-325.
Farkas I, Baranyi L, Ishikawa Y, Okada N, Bohata C, Budai D, Fukuda A, Imai M, Okada H (2002) CD59 blocks not only the insertion of C9 into MAC but inhibits ion channel formation by homologous C5b-8 as well as C5b-9. J Physiol 539:537-545.

Farrar MJ, Bernstein IM, Schlafer DH, Cleland TA, Fetcho JR, Schaffer CB (2012) Chronic in vivo imaging in the mouse spinal cord using an implanted chamber. Nat Methods 9:297-302.
Feng D et al. (2016) Cre-inducible human CD59 mediates rapid cell ablation after intermedilysin administration. J Clin Invest 126:2321-2333.
Fenrich KK, Weber P, Hocine M, Zalc M, Rougon G, Debarbieux F (2012) Long-term in vivo imaging of normal and pathological mouse spinal cord with subcellular resolution using implanted glass windows. J Physiol 590:3665-3675.
Fernandez-Valenzuela JJ, Sanchez-Varo R, Munoz-Castro C, De Castro V, Sanchez-Mejias E, Navarro V, Jimenez S, Nunez-Diaz C, Gomez-Arboledas A, Moreno-Gonzalez I, Vizuete M, Davila JC, Vitorica J, Gutierrez A (2020) Enhancing microtubule stabilization rescues cognitive deficits and ameliorates pathological phenotype in an amyloidogenic Alzheimer's disease model. Sci Rep 10:14776.
Franklin RJM, Frisen J, Lyons DA (2020) Revisiting remyelination: Towards a consensus on the regeneration of CNS myelin. Semin Cell Dev Biol.
Friese MA, Schattling B, Fugger L (2014) Mechanisms of neurodegeneration and axonal dysfunction in multiple sclerosis. Nat Rev Neurol 10:225-238.
Friese MA, Craner MJ, Etzensperger R, Vergo S, Wemmie JA, Welsh MJ, Vincent A, Fugger L (2007) Acid-sensing ion channel-1 contributes to axonal degeneration in autoimmune inflammation of the central nervous system. Nat Med 13:1483-1489.
Frigeri A, Nicchia GP, Verbavatz JM, Valenti G, Svelto M (1998) Expression of aquaporin-4 in fast-twitch fibers of mammalian skeletal muscle. J Clin Invest 102:695-703.
Frigeri A, Gropper MA, Umenishi F, Kawashima M, Brown D, Verkman AS (1995) Localization of MIWC and GLIP water channel homologs in neuromuscular, epithelial and glandular tissues. J Cell Sci 108 (Pt 9):2993-3002.
Fujihara K (2019) Neuromyelitis optica spectrum disorders: still evolving and broadening. Curr Opin Neurol 32:385-394.
Galluzzi L et al. (2018) Molecular mechanisms of cell death: recommendations of the Nomenclature Committee on Cell Death 2018. Cell Death Differ 25:486-541.
Gee JM, Smith NA, Fernandez FR, Economo MN, Brunert D, Rothermel M, Morris SC, Talbot A, Palumbos S, Ichida JM, Shepherd JD, West PJ, Wachowiak M, Capecchi MR, Wilcox KS, White JA, Tvrdik P (2014) Imaging activity in neurons and glia with a Polr2a-based and cre-dependent GCaMP5G-IRES-tdTomato reporter mouse. Neuron 83:1058-1072.
Geis C, Ritter C, Ruschil C, Weishaupt A, Grunewald B, Stoll G, Holmoy T, Misu T, Fujihara K, Hemmer B, Stadelmann C, Bennett JL, Sommer C, Toyka KV (2015) The intrinsic pathogenic role of autoantibodies to aquaporin 4 mediating spinal cord disease in a rat passive-transfer model. Exp Neurol 265:8-21.
Giaume C, Leybaert L, Naus CC, Saez JC (2013) Connexin and pannexin hemichannels in brain glial cells: properties, pharmacology, and roles. Front Pharmacol 4:88.
Greenberg MM, Leitao C, Trogadis J, Stevens JK (1990) Irregular geometries in normal unmyelinated axons: a 3D serial EM analysis. J Neurocytol 19:978-988.
Gregorian C, Nakashima J, Le Belle J, Ohab J, Kim R, Liu A, Smith KB, Groszer M, Garcia AD, Sofroniew MV, Carmichael ST, Kornblum HI, Liu X, Wu H (2009) Pten deletion in adult neural stem/progenitor cells enhances constitutive neurogenesis. J Neurosci 29:1874-1886.
Griffin JM, Bradke F (2020) Therapeutic repair for spinal cord injury: combinatory approaches to address a multifaceted problem. EMBO Mol Med 12:e11505.

Guo Y, Weigand SD, Popescu BF, Lennon VA, Parisi JE, Pittock SJ, Parks NE, Clardy SL, Howe CL, Lucchinetti CF (2017) Pathogenic implications of cerebrospinal fluid barrier pathology in neuromyelitis optica. Acta Neuropathol 133:597-612.

Han RT, Kim RD, Molofsky AV, Liddelow SA (2021) Astrocyte-immune cell interactions in physiology and pathology. Immunity 54:211-224.

Hellal F, Hurtado A, Ruschel J, Flynn KC, Laskowski CJ, Umlauf M, Kapitein LC, Strikis D, Lemmon V, Bixby J, Hoogenraad CC, Bradke F (2011) Microtubule stabilization reduces scarring and causes axon regeneration after spinal cord injury. Science 331:928-931.

Herwerth M, Kalluri SR, Srivastava R, Kleele T, Kenet S, Illes Z, Merkler D, Bennett JL, Misgeld T, Hemmer B (2016) In vivo imaging reveals rapid astrocyte depletion and axon damage in a model of neuromyelitis optica-related pathology. Ann Neurol 79:794-805.

Hildebrand DGC et al. (2017) Whole-brain serial-section electron microscopy in larval zebrafish. Nature 545:345-349.

Hillebrand S, Schanda K, Nigritinou M, Tsymala I, Bohm D, Peschl P, Takai Y, Fujihara K, Nakashima I, Misu T, Reindl M, Lassmann H, Bradl M (2019) Circulating AQP4-specific auto-antibodies alone can induce neuromyelitis optica spectrum disorder in the rat. Acta Neuropathol 137:467-485.

Hinson SR, Pittock SJ, Lucchinetti CF, Roemer SF, Fryer JP, Kryzer TJ, Lennon VA (2007) Pathogenic potential of IgG binding to water channel extracellular domain in neuromyelitis optica. Neurology 69:2221-2231.

Hinson SR, Roemer SF, Lucchinetti CF, Fryer JP, Kryzer TJ, Chamberlain JL, Howe CL, Pittock SJ, Lennon VA (2008) Aquaporin-4-binding autoantibodies in patients with neuromyelitis optica impair glutamate transport by down-regulating EAAT2. J Exp Med 205:2473-2481.

Hinson SR, Romero MF, Popescu BF, Lucchinetti CF, Fryer JP, Wolburg H, Fallier-Becker P, Noell S, Lennon VA (2012) Molecular outcomes of neuromyelitis optica (NMO)-IgG binding to aquaporin-4 in astrocytes. Proc Natl Acad Sci U S A 109:1245-1250.

Hoftberger R, Guo Y, Flanagan EP, Lopez-Chiriboga AS, Endmayr V, Hochmeister S, Joldic D, Pittock SJ, Tillema JM, Gorman M, Lassmann H, Lucchinetti CF (2020) The pathology of central nervous system inflammatory demyelinating disease accompanying myelin oligodendrocyte glycoprotein autoantibody. Acta Neuropathol 139:875-892.

Hokari M, Yokoseki A, Arakawa M, Saji E, Yanagawa K, Yanagimura F, Toyoshima Y, Okamoto K, Ueki S, Hatase T, Ohashi R, Fukuchi T, Akazawa K, Yamada M, Kakita A, Takahashi H, Nishizawa M, Kawachi I (2016) Clinicopathological features in anterior visual pathway in neuromyelitis optica. Ann Neurol 79:605-624.

Hor JY, Asgari N, Nakashima I, Broadley SA, Leite MI, Kissani N, Jacob A, Marignier R, Weinshenker BG, Paul F, Pittock SJ, Palace J, Wingerchuk DM, Behne JM, Yeaman MR, Fujihara K (2020) Epidemiology of Neuromyelitis Optica Spectrum Disorder and Its Prevalence and Incidence Worldwide. Front Neurol 11:501.

Hovelmeyer N, Hao Z, Kranidioti K, Kassiotis G, Buch T, Frommer F, von Hoch L, Kramer D, Minichiello L, Kollias G, Lassmann H, Waisman A (2005) Apoptosis of oligodendrocytes via Fas and TNF-R1 is a key event in the induction of experimental autoimmune encephalomyelitis. J Immunol 175:5875-5884.

Jarius S, Wildemann B (2013) The history of neuromyelitis optica. J Neuroinflammation 10:8.

Jarius S, Paul F, Weinshenker BG, Levy M, Kim HJ, Wildemann B (2020) Neuromyelitis optica. Nat Rev Dis Primers 6:85.

Johannssen HC, Helmchen F (2010) In vivo Ca2+ imaging of dorsal horn neuronal populations in mouse spinal cord. J Physiol 588:3397-3402.
Kanmogne M, Klein RS (2021) Neuroprotective versus Neuroinflammatory Roles of Complement: From Development to Disease. Trends Neurosci 44:97-109.
Karadottir R, Cavelier P, Bergersen LH, Attwell D (2005) NMDA receptors are expressed in oligodendrocytes and activated in ischaemia. Nature 438:1162-1166.
Kasthuri N et al. (2015) Saturated Reconstruction of a Volume of Neocortex. Cell 162:648-661.
Kawachi I, Lassmann H (2017) Neurodegeneration in multiple sclerosis and neuromyelitis optica. J Neurol Neurosurg Psychiatry 88:137-145.
Kerschensteiner M, Schwab ME, Lichtman JW, Misgeld T (2005) In vivo imaging of axonal degeneration and regeneration in the injured spinal cord. Nat Med 11:572-577.
Kimberley FC, Sivasankar B, Paul Morgan B (2007) Alternative roles for CD59. Mol Immunol 44:73-81.
Kinoshita M, Nakatsuji Y, Kimura T, Moriya M, Takata K, Okuno T, Kumanogoh A, Kajiyama K, Yoshikawa H, Sakoda S (2009) Neuromyelitis optica: Passive transfer to rats by human immunoglobulin. Biochem Biophys Res Commun 386:623-627.
Kitley J, Woodhall M, Waters P, Leite MI, Devenney E, Craig J, Palace J, Vincent A (2012) Myelin-oligodendrocyte glycoprotein antibodies in adults with a neuromyelitis optica phenotype. Neurology 79:1273-1277.
Kitley J, Waters P, Woodhall M, Leite MI, Murchison A, George J, Kuker W, Chandratre S, Vincent A, Palace J (2014) Neuromyelitis optica spectrum disorders with aquaporin-4 and myelin-oligodendrocyte glycoprotein antibodies: a comparative study. JAMA Neurol 71:276-283.
Knoferle J, Koch JC, Ostendorf T, Michel U, Planchamp V, Vutova P, Tonges L, Stadelmann C, Bruck W, Bahr M, Lingor P (2010) Mechanisms of acute axonal degeneration in the optic nerve in vivo. Proc Natl Acad Sci U S A 107:6064-6069.
Kostic M, Zivkovic N, Stojanovic I (2013) Multiple sclerosis and glutamate excitotoxicity. Rev Neurosci 24:71-88.
Lemke G (2001) Glial control of neuronal development. Annu Rev Neurosci 24:87-105.
Lennon VA, Kryzer TJ, Pittock SJ, Verkman AS, Hinson SR (2005) IgG marker of optic-spinal multiple sclerosis binds to the aquaporin-4 water channel. J Exp Med 202:473-477.
Lennon VA, Wingerchuk DM, Kryzer TJ, Pittock SJ, Lucchinetti CF, Fujihara K, Nakashima I, Weinshenker BG (2004) A serum autoantibody marker of neuromyelitis optica: distinction from multiple sclerosis. Lancet 364:2106-2112.
Levy M, Fujihara K, Palace J (2021) New therapies for neuromyelitis optica spectrum disorder. Lancet Neurol 20:60-67.
Liddelow SA, Barres BA (2017) Reactive Astrocytes: Production, Function, and Therapeutic Potential. Immunity 46:957-967.
Liddelow SA et al. (2017) Neurotoxic reactive astrocytes are induced by activated microglia. Nature 541:481-487.
Lin MZ, Schnitzer MJ (2016) Genetically encoded indicators of neuronal activity. Nat Neurosci 19:1142-1153.
Linnerbauer M, Wheeler MA, Quintana FJ (2020) Astrocyte Crosstalk in CNS Inflammation. Neuron 108:608-622.
Liu X, Zhang Z, Guo W, Burnstock G, He C, Xiang Z (2013) The superficial glia limitans of mouse and monkey brain and spinal cord. Anat Rec (Hoboken) 296:995-1007.
Lorenzana AO, Lee JK, Mui M, Chang A, Zheng B (2015) A surviving intact branch stabilizes remaining axon architecture after injury as revealed by in vivo imaging in the mouse spinal cord. Neuron 86:947-954.

Lucchinetti CF, Guo Y, Popescu BF, Fujihara K, Itoyama Y, Misu T (2014) The pathology of an autoimmune astrocytopathy: lessons learned from neuromyelitis optica. Brain Pathol 24:83-97.

Lucchinetti CF, Mandler RN, McGavern D, Bruck W, Gleich G, Ransohoff RM, Trebst C, Weinshenker B, Wingerchuk D, Parisi JE, Lassmann H (2002) A role for humoral mechanisms in the pathogenesis of Devic's neuromyelitis optica. Brain 125:1450-1461.

Lusthaus M, Mazkereth N, Donin N, Fishelson Z (2018) Receptor-Interacting Protein Kinases 1 and 3, and Mixed Lineage Kinase Domain-Like Protein Are Activated by Sublytic Complement and Participate in Complement-Dependent Cytotoxicity. Front Immunol 9:306.

Maday S, Twelvetrees AE, Moughamian AJ, Holzbaur EL (2014) Axonal transport: cargo-specific mechanisms of motility and regulation. Neuron 84:292-309.

Mader S, Gredler V, Schanda K, Rostasy K, Dujmovic I, Pfaller K, Lutterotti A, Jarius S, Di Pauli F, Kuenz B, Ehling R, Hegen H, Deisenhammer F, Aboul-Enein F, Storch MK, Koson P, Drulovic J, Kristoferitsch W, Berger T, Reindl M (2011) Complement activating antibodies to myelin oligodendrocyte glycoprotein in neuromyelitis optica and related disorders. J Neuroinflammation 8:184.

Madisen L, Zwingman TA, Sunkin SM, Oh SW, Zariwala HA, Gu H, Ng LL, Palmiter RD, Hawrylycz MJ, Jones AR, Lein ES, Zeng H (2010) A robust and high-throughput Cre reporting and characterization system for the whole mouse brain. Nat Neurosci 13:133-140.

Magistretti PJ, Allaman I (2018) Lactate in the brain: from metabolic end-product to signalling molecule. Nat Rev Neurosci 19:235-249.

Mallon BS, Shick HE, Kidd GJ, Macklin WB (2002) Proteolipid promoter activity distinguishes two populations of NG2-positive cells throughout neonatal cortical development. J Neurosci 22:876-885.

Mank M, Santos AF, Direnberger S, Mrsic-Flogel TD, Hofer SB, Stein V, Hendel T, Reiff DF, Levelt C, Borst A, Bonhoeffer T, Hubener M, Griesbeck O (2008) A genetically encoded calcium indicator for chronic in vivo two-photon imaging. Nat Methods 5:805-811.

Marignier R, Nicolle A, Watrin C, Touret M, Cavagna S, Varrin-Doyer M, Cavillon G, Rogemond V, Confavreux C, Honnorat J, Giraudon P (2010) Oligodendrocytes are damaged by neuromyelitis optica immunoglobulin G via astrocyte injury. Brain 133:2578-2591.

Marignier R, Ruiz A, Cavagna S, Nicole A, Watrin C, Touret M, Parrot S, Malleret G, Peyron C, Benetollo C, Auvergnon N, Vukusic S, Giraudon P (2016) Neuromyelitis optica study model based on chronic infusion of autoantibodies in rat cerebrospinal fluid. J Neuroinflammation 13:111.

Markoullis K, Sargiannidou I, Gardner C, Hadjisavvas A, Reynolds R, Kleopa KA (2012) Disruption of oligodendrocyte gap junctions in experimental autoimmune encephalomyelitis. Glia 60:1053-1066.

Masaki K (2015) Early disruption of glial communication via connexin gap junction in multiple sclerosis, Balo's disease and neuromyelitis optica. Neuropathology 35:469-480.

Matute C (2007) Interaction between glutamate signalling and immune attack in damaging oligodendrocytes. Neuron Glia Biol 3:281-285.

Micu I, Jiang Q, Coderre E, Ridsdale A, Zhang L, Woulfe J, Yin X, Trapp BD, McRory JE, Rehak R, Zamponi GW, Wang W, Stys PK (2006) NMDA receptors mediate calcium accumulation in myelin during chemical ischaemia. Nature 439:988-992.

Misgeld T, Nikic I, Kerschensteiner M (2007) In vivo imaging of single axons in the mouse spinal cord. Nat Protoc 2:263-268.

Misu T, Fujihara K, Kakita A, Konno H, Nakamura M, Watanabe S, Takahashi T, Nakashima I, Takahashi H, Itoyama Y (2007) Loss of aquaporin 4 in lesions of neuromyelitis optica: distinction from multiple sclerosis. Brain 130:1224-1234.

Misu T, Hoftberger R, Fujihara K, Wimmer I, Takai Y, Nishiyama S, Nakashima I, Konno H, Bradl M, Garzuly F, Itoyama Y, Aoki M, Lassmann H (2013) Presence of six different lesion types suggests diverse mechanisms of tissue injury in neuromyelitis optica. Acta Neuropathol 125:815-827.

Moskovich O, Fishelson Z (2007) Live cell imaging of outward and inward vesiculation induced by the complement c5b-9 complex. J Biol Chem 282:29977-29986.

Murphy-Royal C, Dupuis J, Groc L, Oliet SHR (2017) Astroglial glutamate transporters in the brain: Regulating neurotransmitter homeostasis and synaptic transmission. J Neurosci Res 95:2140-2151.

Nelson NA, Wang X, Cook D, Carey EM, Nimmerjahn A (2019) Imaging spinal cord activity in behaving animals. Exp Neurol 320:112974.

Nicchia GP, Mastrototaro M, Rossi A, Pisani F, Tortorella C, Ruggieri M, Lia A, Trojano M, Frigeri A, Svelto M (2009) Aquaporin-4 orthogonal arrays of particles are the target for neuromyelitis optica autoantibodies. Glia 57:1363-1373.

Nikic I, Merkler D, Sorbara C, Brinkoetter M, Kreutzfeldt M, Bareyre FM, Bruck W, Bishop D, Misgeld T, Kerschensteiner M (2011) A reversible form of axon damage in experimental autoimmune encephalomyelitis and multiple sclerosis. Nat Med 17:495-499.

Nimmerjahn A, Kirchhoff F, Helmchen F (2005) Resting microglial cells are highly dynamic surveillants of brain parenchyma in vivo. Science 308:1314-1318.

Nitsch R, Pohl EE, Smorodchenko A, Infante-Duarte C, Aktas O, Zipp F (2004) Direct impact of T cells on neurons revealed by two-photon microscopy in living brain tissue. J Neurosci 24:2458-2464.

O'Sullivan D, Miller JH, Northcote PT, La Flamme AC (2013) Microtubule-stabilizing agents delay the onset of EAE through inhibition of migration. Immunol Cell Biol 91:583-592.

Ochs S, Jersild RA, Jr. (1987) Cytoskeletal organelles and myelin structure of beaded nerve fibers. Neuroscience 22:1041-1056.

Ochs S, Pourmand R, Jersild RA, Jr., Friedman RN (1997) The origin and nature of beading: a reversible transformation of the shape of nerve fibers. Prog Neurobiol 52:391-426.

Orem BC, Rajaee A, Stirling DP (2020) IP3R-mediated intra-axonal Ca(2+) release contributes to secondary axonal degeneration following contusive spinal cord injury. Neurobiol Dis 146:105123.

Orthmann-Murphy JL, Freidin M, Fischer E, Scherer SS, Abrams CK (2007) Two distinct heterotypic channels mediate gap junction coupling between astrocyte and oligodendrocyte connexins. J Neurosci 27:13949-13957.

Osterloh JM et al. (2012) dSarm/Sarm1 is required for activation of an injury-induced axon death pathway. Science 337:481-484.

Ouardouz M, Nikolaeva MA, Coderre E, Zamponi GW, McRory JE, Trapp BD, Yin X, Wang W, Woulfe J, Stys PK (2003) Depolarization-induced Ca2+ release in ischemic spinal cord white matter involves L-type Ca2+ channel activation of ryanodine receptors. Neuron 40:53-63.

Papadopoulos MC, Verkman AS (2013) Aquaporin water channels in the nervous system. Nat Rev Neurosci 14:265-277.

Parpura V, Verkhratsky A (2012) Homeostatic function of astrocytes: Ca(2+) and Na(+) signalling. Transl Neurosci 3:334-344.

Parratt JD, Prineas JW (2010) Neuromyelitis optica: a demyelinating disease characterized by acute destruction and regeneration of perivascular astrocytes. Mult Scler 16:1156-1172.

Pekny M, Pekna M (2014) Astrocyte reactivity and reactive astrogliosis: costs and benefits. Physiol Rev 94:1077-1098.
Pekny M, Pekna M, Messing A, Steinhauser C, Lee JM, Parpura V, Hol EM, Sofroniew MV, Verkhratsky A (2016) Astrocytes: a central element in neurological diseases. Acta Neuropathol 131:323-345.
Phatnani H, Maniatis T (2015) Astrocytes in neurodegenerative disease. Cold Spring Harb Perspect Biol 7.
Phuan PW, Ratelade J, Rossi A, Tradtrantip L, Verkman AS (2012) Complement-dependent cytotoxicity in neuromyelitis optica requires aquaporin-4 protein assembly in orthogonal arrays. J Biol Chem 287:13829-13839.
Phuan PW, Zhang H, Asavapanumas N, Leviten M, Rosenthal A, Tradtrantip L, Verkman AS (2013) C1q-targeted monoclonal antibody prevents complement-dependent cytotoxicity and neuropathology in in vitro and mouse models of neuromyelitis optica. Acta Neuropathol 125:829-840.
Piddlesden SJ, Morgan BP (1993) Killing of rat glial cells by complement: deficiency of the rat analogue of CD59 is the cause of oligodendrocyte susceptibility to lysis. J Neuroimmunol 48:169-175.
Pitt D, Werner P, Raine CS (2000) Glutamate excitotoxicity in a model of multiple sclerosis. Nat Med 6:67-70.
Ponath G, Park C, Pitt D (2018) The Role of Astrocytes in Multiple Sclerosis. Front Immunol 9:217.
Popescu BF, Lennon VA, Parisi JE, Howe CL, Weigand SD, Cabrera-Gomez JA, Newell K, Mandler RN, Pittock SJ, Weinshenker BG, Lucchinetti CF (2011) Neuromyelitis optica unique area postrema lesions: nausea, vomiting, and pathogenic implications. Neurology 76:1229-1237.
Prineas JW, Lee S (2019) Multiple Sclerosis: Destruction and Regeneration of Astrocytes in Acute Lesions. J Neuropathol Exp Neurol 78:140-156.
Probstel AK, Rudolf G, Dornmair K, Collongues N, Chanson JB, Sanderson NS, Lindberg RL, Kappos L, de Seze J, Derfuss T (2015) Anti-MOG antibodies are present in a subgroup of patients with a neuromyelitis optica phenotype. J Neuroinflammation 12:46.
Propson NE, Gedam M, Zheng H (2021) Complement in Neurologic Disease. Annu Rev Pathol 16:277-298.
Pullarkat PA, Dommersnes P, Fernandez P, Joanny JF, Ott A (2006) Osmotically driven shape transformations in axons. Phys Rev Lett 96:048104.
Raff MC, Whitmore AV, Finn JT (2002) Axonal self-destruction and neurodegeneration. Science 296:868-871.
Ratelade J, Verkman AS (2014) Inhibitor(s) of the classical complement pathway in mouse serum limit the utility of mice as experimental models of neuromyelitis optica. Mol Immunol 62:104-113.
Ratelade J, Bennett JL, Verkman AS (2011) Evidence against cellular internalization in vivo of NMO-IgG, aquaporin-4, and excitatory amino acid transporter 2 in neuromyelitis optica. J Biol Chem 286:45156-45164.
Ratelade J, Zhang H, Saadoun S, Bennett JL, Papadopoulos MC, Verkman AS (2012) Neuromyelitis optica IgG and natural killer cells produce NMO lesions in mice without myelin loss. Acta Neuropathol 123:861-872.
Ratelade J, Asavapanumas N, Ritchie AM, Wemlinger S, Bennett JL, Verkman AS (2013) Involvement of antibody-dependent cell-mediated cytotoxicity in inflammatory demyelination in a mouse model of neuromyelitis optica. Acta Neuropathol 126:699-709.

Ravindra Kumar S, Miles TF, Chen X, Brown D, Dobreva T, Huang Q, Ding X, Luo Y, Einarsson PH, Greenbaum A, Jang MJ, Deverman BE, Gradinaru V (2020) Multiplexed Cre-dependent selection yields systemic AAVs for targeting distinct brain cell types. Nat Methods 17:541-550.

Richard C, Ruiz A, Cavagna S, Bigotte M, Vukusic S, Masaki K, Suenaga T, Kira JI, Giraudon P, Marignier R (2020) Connexins in neuromyelitis optica: a link between astrocytopathy and demyelination. Brain 143:2721-2732.

Roemer SF, Parisi JE, Lennon VA, Benarroch EE, Lassmann H, Bruck W, Mandler RN, Weinshenker BG, Pittock SJ, Wingerchuk DM, Lucchinetti CF (2007) Pattern-specific loss of aquaporin-4 immunoreactivity distinguishes neuromyelitis optica from multiple sclerosis. Brain 130:1194-1205.

Romanelli E, Sorbara CD, Nikic I, Dagkalis A, Misgeld T, Kerschensteiner M (2013) Cellular, subcellular and functional in vivo labeling of the spinal cord using vital dyes. Nat Protoc 8:481-490.

Romanelli E, Merkler D, Mezydlo A, Weil MT, Weber MS, Nikic I, Potz S, Meinl E, Matznick FE, Kreutzfeldt M, Ghanem A, Conzelmann KK, Metz I, Bruck W, Routh M, Simons M, Bishop D, Misgeld T, Kerschensteiner M (2016) Myelinosome formation represents an early stage of oligodendrocyte damage in multiple sclerosis and its animal model. Nat Commun 7:13275.

Rose T, Goltstein PM, Portugues R, Griesbeck O (2014) Putting a finishing touch on GECIs. Front Mol Neurosci 7:88.

Rosenberg PA, Aizenman E (1989) Hundred-fold increase in neuronal vulnerability to glutamate toxicity in astrocyte-poor cultures of rat cerebral cortex. Neurosci Lett 103:162-168.

Rossi A, Ratelade J, Papadopoulos MC, Bennett JL, Verkman AS (2012) Neuromyelitis optica IgG does not alter aquaporin-4 water permeability, plasma membrane M1/M23 isoform content, or supramolecular assembly. Glia 60:2027-2039.

Rothhammer V, Quintana FJ (2015) Control of autoimmune CNS inflammation by astrocytes. Semin Immunopathol 37:625-638.

Rothhammer V et al. (2018) Microglial control of astrocytes in response to microbial metabolites. Nature 557:724-728.

Ruschel J, Hellal F, Flynn KC, Dupraz S, Elliott DA, Tedeschi A, Bates M, Sliwinski C, Brook G, Dobrindt K, Peitz M, Brustle O, Norenberg MD, Blesch A, Weidner N, Bunge MB, Bixby JL, Bradke F (2015) Axonal regeneration. Systemic administration of epothilone B promotes axon regeneration after spinal cord injury. Science 348:347-352.

Saadoun S, Papadopoulos MC (2015) Role of membrane complement regulators in neuromyelitis optica. Mult Scler 21:1644-1654.

Saadoun S, Waters P, Bell BA, Vincent A, Verkman AS, Papadopoulos MC (2010) Intra-cerebral injection of neuromyelitis optica immunoglobulin G and human complement produces neuromyelitis optica lesions in mice. Brain 133:349-361.

Saadoun S, Waters P, Owens GP, Bennett JL, Vincent A, Papadopoulos MC (2014) Neuromyelitis optica MOG-IgG causes reversible lesions in mouse brain. Acta Neuropathol Commun 2:35.

Salter MG, Fern R (2005) NMDA receptors are expressed in developing oligodendrocyte processes and mediate injury. Nature 438:1167-1171.

Sato DK, Callegaro D, Lana-Peixoto MA, Waters PJ, de Haidar Jorge FM, Takahashi T, Nakashima I, Apostolos-Pereira SL, Talim N, Simm RF, Lino AM, Misu T, Leite MI, Aoki M, Fujihara K (2014) Distinction between MOG antibody-positive and AQP4 antibody-positive NMO spectrum disorders. Neurology 82:474-481.

Schafer DP, Lehrman EK, Kautzman AG, Koyama R, Mardinly AR, Yamasaki R, Ransohoff RM, Greenberg ME, Barres BA, Stevens B (2012) Microglia sculpt postnatal neural circuits in an activity and complement-dependent manner. Neuron 74:691-705.

Schattling B, Steinbach K, Thies E, Kruse M, Menigoz A, Ufer F, Flockerzi V, Bruck W, Pongs O, Vennekens R, Kneussel M, Freichel M, Merkler D, Friese MA (2012) TRPM4 cation channel mediates axonal and neuronal degeneration in experimental autoimmune encephalomyelitis and multiple sclerosis. Nat Med 18:1805-1811.

Schindelin J, Arganda-Carreras I, Frise E, Kaynig V, Longair M, Pietzsch T, Preibisch S, Rueden C, Saalfeld S, Schmid B, Tinevez JY, White DJ, Hartenstein V, Eliceiri K, Tomancak P, Cardona A (2012) Fiji: an open-source platform for biological-image analysis. Nat Methods 9:676-682.

Schneider CA, Rasband WS, Eliceiri KW (2012) NIH Image to ImageJ: 25 years of image analysis. Nat Methods 9:671-675.

Schumacher AM, Misgeld T, Kerschensteiner M, Snaidero N (2019) Imaging the execution phase of neuroinflammatory disease models. Exp Neurol 320:112968.

Scolding NJ, Morgan BP, Compston DA (1998) The expression of complement regulatory proteins by adult human oligodendrocytes. J Neuroimmunol 84:69-75.

Scolding NJ, Houston WA, Morgan BP, Campbell AK, Compston DA (1989a) Reversible injury of cultured rat oligodendrocytes by complement. Immunology 67:441-446.

Scolding NJ, Morgan BP, Houston WA, Linington C, Campbell AK, Compston DA (1989b) Vesicular removal by oligodendrocytes of membrane attack complexes formed by activated complement. Nature 339:620-622.

Sekiguchi KJ, Shekhtmeyster P, Merten K, Arena A, Cook D, Hoffman E, Ngo A, Nimmerjahn A (2016) Imaging large-scale cellular activity in spinal cord of freely behaving mice. Nat Commun 7:11450.

Serna M, Giles JL, Morgan BP, Bubeck D (2016) Structural basis of complement membrane attack complex formation. Nat Commun 7:10587.

Sharma R, Fischer MT, Bauer J, Felts PA, Smith KJ, Misu T, Fujihara K, Bradl M, Lassmann H (2010) Inflammation induced by innate immunity in the central nervous system leads to primary astrocyte dysfunction followed by demyelination. Acta Neuropathol 120:223-236.

Shcherbatko A, Ono F, Mandel G, Brehm P (1999) Voltage-dependent sodium channel function is regulated through membrane mechanics. Biophys J 77:1945-1959.

Shi Q, Colodner KJ, Matousek SB, Merry K, Hong S, Kenison JE, Frost JL, Le KX, Li S, Dodart JC, Caldarone BJ, Stevens B, Lemere CA (2015) Complement C3-Deficient Mice Fail to Display Age-Related Hippocampal Decline. J Neurosci 35:13029-13042.

Shriver LP, Dittel BN (2006) T-cell-mediated disruption of the neuronal microtubule network: correlation with early reversible axonal dysfunction in acute experimental autoimmune encephalomyelitis. Am J Pathol 169:999-1011.

Singh S, Dallenga T, Winkler A, Roemer S, Maruschak B, Siebert H, Bruck W, Stadelmann C (2017) Relationship of acute axonal damage, Wallerian degeneration, and clinical disability in multiple sclerosis. J Neuroinflammation 14:57.

Soane L, Rus H, Niculescu F, Shin ML (1999) Inhibition of oligodendrocyte apoptosis by sublytic C5b-9 is associated with enhanced synthesis of bcl-2 and mediated by inhibition of caspase-3 activation. J Immunol 163:6132-6138.

Sofroniew MV (2015) Astrocyte barriers to neurotoxic inflammation. Nat Rev Neurosci 16:249-263.

Sofroniew MV (2020) Astrocyte Reactivity: Subtypes, States, and Functions in CNS Innate Immunity. Trends Immunol 41:758-770.

Sofroniew MV, Vinters HV (2010) Astrocytes: biology and pathology. Acta Neuropathol 119:7-35.
Song Y, Li D, Farrelly O, Miles L, Li F, Kim SE, Lo TY, Wang F, Li T, Thompson-Peer KL, Gong J, Murthy SE, Coste B, Yakubovich N, Patapoutian A, Xiang Y, Rompolas P, Jan LY, Jan YN (2019) The Mechanosensitive Ion Channel Piezo Inhibits Axon Regeneration. Neuron 102:373-389 e376.
Sorbara CD, Wagner NE, Ladwig A, Nikic I, Merkler D, Kleele T, Marinkovic P, Naumann R, Godinho L, Bareyre FM, Bishop D, Misgeld T, Kerschensteiner M (2014) Pervasive axonal transport deficits in multiple sclerosis models. Neuron 84:1183-1190.
Stephan AH, Barres BA, Stevens B (2012) The complement system: an unexpected role in synaptic pruning during development and disease. Annu Rev Neurosci 35:369-389.
Stephan AH, Madison DV, Mateos JM, Fraser DA, Lovelett EA, Coutellier L, Kim L, Tsai HH, Huang EJ, Rowitch DH, Berns DS, Tenner AJ, Shamloo M, Barres BA (2013) A dramatic increase of C1q protein in the CNS during normal aging. J Neurosci 33:13460-13474.
Stevens B, Allen NJ, Vazquez LE, Howell GR, Christopherson KS, Nouri N, Micheva KD, Mehalow AK, Huberman AD, Stafford B, Sher A, Litke AM, Lambris JD, Smith SJ, John SW, Barres BA (2007) The classical complement cascade mediates CNS synapse elimination. Cell 131:1164-1178.
Stirling DP, Stys PK (2010) Mechanisms of axonal injury: internodal nanocomplexes and calcium deregulation. Trends Mol Med 16:160-170.
Stirling DP, Cummins K, Wayne Chen SR, Stys P (2014) Axoplasmic reticulum Ca(2+) release causes secondary degeneration of spinal axons. Ann Neurol 75:220-229.
Stys PK (1998) Anoxic and ischemic injury of myelinated axons in CNS white matter: from mechanistic concepts to therapeutics. J Cereb Blood Flow Metab 18:2-25.
Takai Y et al. (2020) Myelin oligodendrocyte glycoprotein antibody-associated disease: an immunopathological study. Brain 143:1431-1446.
Takeshita Y, Obermeier B, Cotleur AC, Spampinato SF, Shimizu F, Yamamoto E, Sano Y, Kryzer TJ, Lennon VA, Kanda T, Ransohoff RM (2017) Effects of neuromyelitis optica-IgG at the blood-brain barrier in vitro. Neurol Neuroimmunol Neuroinflamm 4:e311.
Tegla CA, Cudrici C, Patel S, Trippe R, 3rd, Rus V, Niculescu F, Rus H (2011) Membrane attack by complement: the assembly and biology of terminal complement complexes. Immunol Res 51:45-60.
Tradtrantip L, Asavapanumas N, Verkman AS (2020) Emerging therapeutic targets for neuromyelitis optica spectrum disorder. Expert Opin Ther Targets 24:219-229.
Tradtrantip L, Yao X, Su T, Smith AJ, Verkman AS (2017) Bystander mechanism for complement-initiated early oligodendrocyte injury in neuromyelitis optica. Acta Neuropathol 134:35-44.
Trapp BD, Stys PK (2009) Virtual hypoxia and chronic necrosis of demyelinated axons in multiple sclerosis. Lancet Neurol 8:280-291.
Triantafilou K, Hughes TR, Triantafilou M, Morgan BP (2013) The complement membrane attack complex triggers intracellular Ca2+ fluxes leading to NLRP3 inflammasome activation. J Cell Sci 126:2903-2913.
Tsymala I et al. (2020) Induction of aquaporin 4-reactive antibodies in Lewis rats immunized with aquaporin 4 mimotopes. Acta Neuropathol Commun 8:49.
Vargas ME, Yamagishi Y, Tessier-Lavigne M, Sagasti A (2015) Live Imaging of Calcium Dynamics during Axon Degeneration Reveals Two Functionally Distinct Phases of Calcium Influx. J Neurosci 35:15026-15038.
Verkhratsky A, Nedergaard M (2018) Physiology of Astroglia. Physiol Rev 98:239-389.

Verkhratsky A, Sofroniew MV, Messing A, deLanerolle NC, Rempe D, Rodriguez JJ, Nedergaard M (2012) Neurological diseases as primary gliopathies: a reassessment of neurocentrism. ASN Neuro 4.

Vogel AL, Knier B, Lammens K, Kalluri SR, Kuhlmann T, Bennett JL, Korn T (2017) Deletional tolerance prevents AQP4-directed autoimmunity in mice. Eur J Immunol 47:458-469.

Vukojicic A, Delestree N, Fletcher EV, Pagiazitis JG, Sankaranarayanan S, Yednock TA, Barres BA, Mentis GZ (2019) The Classical Complement Pathway Mediates Microglia-Dependent Remodeling of Spinal Motor Circuits during Development and in SMA. Cell Rep 29:3087-3100 e3087.

Wang J, La JH, Hamill OP (2019) PIEZO1 Is Selectively Expressed in Small Diameter Mouse DRG Neurons Distinct From Neurons Strongly Expressing TRPV1. Front Mol Neurosci 12:178.

Wang Z, Guo W, Liu Y, Gong Y, Ding X, Shi K, Thome R, Zhang GX, Shi FD, Yan Y (2017) Low expression of complement inhibitory protein CD59 contributes to humoral autoimmunity against astrocytes. Brain Behav Immun 65:173-182.

Waxman SG (2006) Axonal conduction and injury in multiple sclerosis: the role of sodium channels. Nat Rev Neurosci 7:932-941.

Waxman SG, Bennett MV (1972) Relative conduction velocities of small myelinated and non-myelinated fibres in the central nervous system. Nat New Biol 238:217-219.

Weber MS, Derfuss T, Metz I, Bruck W (2018) Defining distinct features of anti-MOG antibody associated central nervous system demyelination. Ther Adv Neurol Disord 11:1756286418762083.

Weil MT, Mobius W, Winkler A, Ruhwedel T, Wrzos C, Romanelli E, Bennett JL, Enz L, Goebels N, Nave KA, Kerschensteiner M, Schaeren-Wiemers N, Stadelmann C, Simons M (2016) Loss of Myelin Basic Protein Function Triggers Myelin Breakdown in Models of Demyelinating Diseases. Cell Rep 16:314-322.

Williams PR, Marincu BN, Sorbara CD, Mahler CF, Schumacher AM, Griesbeck O, Kerschensteiner M, Misgeld T (2014) A recoverable state of axon injury persists for hours after spinal cord contusion in vivo. Nat Commun 5:5683.

Wing MG, Zajicek J, Seilly DJ, Compston DA, Lachmann PJ (1992) Oligodendrocytes lack glycolipid anchored proteins which protect them against complement lysis. Restoration of resistance to lysis by incorporation of CD59. Immunology 76:140-145.

Wingerchuk DM, Pittock SJ, Lucchinetti CF, Lennon VA, Weinshenker BG (2007) A secondary progressive clinical course is uncommon in neuromyelitis optica. Neurology 68:603-605.

Wingerchuk DM, Banwell B, Bennett JL, Cabre P, Carroll W, Chitnis T, de Seze J, Fujihara K, Greenberg B, Jacob A, Jarius S, Lana-Peixoto M, Levy M, Simon JH, Tenembaum S, Traboulsee AL, Waters P, Wellik KE, Weinshenker BG, International Panel for NMOD (2015) International consensus diagnostic criteria for neuromyelitis optica spectrum disorders. Neurology 85:177-189.

Winkler A, Wrzos C, Haberl M, Weil MT, Gao M, Mobius W, Odoardi F, Thal DR, Chang M, Opdenakker G, Bennett JL, Nessler S, Stadelmann C (2021) Blood-brain barrier resealing in neuromyelitis optica occurs independently of astrocyte regeneration. J Clin Invest 131.

Witte ME, Schumacher AM, Mahler CF, Bewersdorf JP, Lehmitz J, Scheiter A, Sanchez P, Williams PR, Griesbeck O, Naumann R, Misgeld T, Kerschensteiner M (2019) Calcium Influx through Plasma-Membrane Nanoruptures Drives Axon Degeneration in a Model of Multiple Sclerosis. Neuron 101:615-624 e615.

Wolf JA, Stys PK, Lusardi T, Meaney D, Smith DH (2001) Traumatic axonal injury induces calcium influx modulated by tetrodotoxin-sensitive sodium channels. J Neurosci 21:1923-1930.

Wood A, Wing MG, Benham CD, Compston DA (1993) Specific induction of intracellular calcium oscillations by complement membrane attack on oligodendroglia. J Neurosci 13:3319-3332.

Wrzos C, Winkler A, Metz I, Kayser DM, Thal DR, Wegner C, Bruck W, Nessler S, Bennett JL, Stadelmann C (2014) Early loss of oligodendrocytes in human and experimental neuromyelitis optica lesions. Acta Neuropathol 127:523-538.

Xie CB, Jane-Wit D, Pober JS (2020) Complement Membrane Attack Complex: New Roles, Mechanisms of Action, and Therapeutic Targets. Am J Pathol 190:1138-1150.

Xiong ZQ, McNamara JO (2002) Fleeting activation of ionotropic glutamate receptors sensitizes cortical neurons to complement attack. Neuron 36:363-374.

Yang J, Weimer RM, Kallop D, Olsen O, Wu Z, Renier N, Uryu K, Tessier-Lavigne M (2013) Regulation of axon degeneration after injury and in development by the endogenous calpain inhibitor calpastatin. Neuron 80:1175-1189.

Yang Y, Vidensky S, Jin L, Jie C, Lorenzini I, Frankl M, Rothstein JD (2011) Molecular comparison of GLT1+ and ALDH1L1+ astrocytes in vivo in astroglial reporter mice. Glia 59:200-207.

Yao X, Verkman AS (2017a) Complement regulator CD59 prevents peripheral organ injury in rats made seropositive for neuromyelitis optica immunoglobulin G. Acta Neuropathol Commun 5:57.

Yao X, Verkman AS (2017b) Marked central nervous system pathology in CD59 knockout rats following passive transfer of Neuromyelitis optica immunoglobulin G. Acta Neuropathol Commun 5:15.

Yeung MSY, Djelloul M, Steiner E, Bernard S, Salehpour M, Possnert G, Brundin L, Frisen J (2019) Dynamics of oligodendrocyte generation in multiple sclerosis. Nature 566:538-542.

Yoshihara K, Matsuda T, Kohro Y, Tozaki-Saitoh H, Inoue K, Tsuda M (2018) Astrocytic Ca(2+) responses in the spinal dorsal horn by noxious stimuli to the skin. J Pharmacol Sci 137:101-104.

Yun SP et al. (2018) Block of A1 astrocyte conversion by microglia is neuroprotective in models of Parkinson's disease. Nat Med 24:931-938.

Zhang B, Carroll J, Trojanowski JQ, Yao Y, Iba M, Potuzak JS, Hogan AM, Xie SX, Ballatore C, Smith AB, 3rd, Lee VM, Brunden KR (2012) The microtubule-stabilizing agent, epothilone D, reduces axonal dysfunction, neurotoxicity, cognitive deficits, and Alzheimer-like pathology in an interventional study with aged tau transgenic mice. J Neurosci 32:3601-3611.

Zhang H, Verkman AS (2014) Longitudinally extensive NMO spinal cord pathology produced by passive transfer of NMO-IgG in mice lacking complement inhibitor CD59. J Autoimmun 53:67-77.

Ziporen L, Donin N, Shmushkovich T, Gross A, Fishelson Z (2009) Programmed necrotic cell death induced by complement involves a Bid-dependent pathway. J Immunol 182:515-521.

Acknowledgements

I would like to express my gratitude to my supervisor Prof. Thomas Misgeld for all the support, guidance, and encouragement he provided during my PhD. I have learned a lot over the last five years. Thank you, Thomas, for the opportunity to be a part of your research team.

I also would like to thank the members of my thesis advisory committee: Dr. Florence Bareyre, Prof. Thomas Korn, and Dr. Ali Ertürk. I appreciate the time and critical feedback you provided.

I am grateful to the Graduate School of Systemic Neurosciences and SyNergy for the financial support, which allowed me to attend summer schools and workshops.

Special thanks to my colleague Dr. Marina Herwerth for introducing me to the methods and offering support whenever needed. It was a pleasure working with you.

I am grateful to Dr. Philip Williams for sharing his knowledge and experience during his visit to Munich, from which I have benefited immensely since the first months of my PhD.

I would like to thank Kristina, Kristine, Manuela, Monika S., Nebahat and Yvonne for all the help; and to all the members of Misgeld, Godinho, Czopka and Konnerth labs with whom I had a chance to meet and work together. Thank you very much for the fascinating discussions, advice, and help.

Thank you, my friends, Serra and Ceren, for your support, care and kindness; and my aunt, Nesibe, for being a role model to me in life.

Thank you, Umut, for your unconditional support and patience.

I would not have made it this far without the support of my parents. Thank you, Mom and Dad, for everything.

Publications

Hiltensperger M, Beltrán E, Kant R, Tyystjärvi S, Lepennetier G, Moreno HD, Bauer IJ, Grassman S, Jarosch S, Schober K, Buchholz VR, **Kenet S**, Gasperi C, Öllinger R, Rad R, Muschaweckh A, Sie C, Aly L, Knier B, Garg G, Afzali AM, Gerdes LA, Kümpfel T, Franzenburg S, Kawakami N, Hemmer B, Busch DH, Misgeld T, Dornmair K, Korn T (2021) Skin and gut imprinted T helper cell subsets exhibit distinct functional phenotypes in central nervous system autoimmunity. Nat Immunol 22:880-892.

Herwerth M, Kalluri SR, Srivastava R, Kleele T, **Kenet S**, Illes Z, Merkler D, Bennett JL, Misgeld T, Hemmer B (2016) In vivo imaging reveals rapid astrocyte depletion and axon damage in a model of neuromyelitis optica-related pathology. Ann Neurol 79:794-805.

Declaration of Author Contributions

Manuscript 1: A new form of axonal pathology in a spinal model of neuromyelitis optica

Marina Herwerth*, **Selin Kenet***, Martina Schifferer, Anne Winkler, Melanie Weber, Nicolas Snaidero, Jeffrey L. Bennett, Christine Stadelmann, Bernhard Hemmer, Thomas Misgeld. *Manuscript in submission.*

MH, SK, BH and TM are responsible for the concept and study design.
MH conducted and analyzed acute neuromyelitis optica (NMO) experiments; acquired and analyzed immunofluorescence data; analyzed electron microscopy (EM) data.
SK conducted and analyzed survival NMO experiments.
MS and NS acquired and interpreted EM data.
AW and CS provided, acquired and analyzed human NMO lesion data.
MW performed immunofluorescence staining; analyzed acute NMO and EM data.
JLB provided recombinant antibodies.
MH, SK and TM drafted the manuscript and figures with input from all the authors.
MH and SK contributed equally as first authors.

Manuscript 2: Membrane attack complex initiates oligodendrocyte injury in neuromyelitis optica-related mouse model

Selin Kenet, Marina Herwerth, Jeffrey L. Bennett, Bernhard Hemmer, Thomas Misgeld *Manuscript in preparation.*

SK, MH, BH and TM are responsible for the concept and study design.
SK acquired and analyzed glial morphology/calcium imaging data, and characterization of CD59 overexpression experiments.
JLB provided recombinant antibodies.
SK drafted the manuscript and figures with the input from MH and TM.

Place, date

Selin Kenet	**Dr. Marina Herwerth**	**Prof. Thomas Misgeld**